A THESIS REPORT ON

HIGH TEMPERATURE TENSILE PROPERTY OF 316L AUSTENITIC STAINLESS STEEL WELDING

A thesis submitted in partial fulfilment of the requirements for the award of the degree of

Master of Engineering in Metallurgical Engineering

Faculty of Engineering and Technology
Jadavpur University

Submitted by

JASIM MONDAL

Class Roll No. 002211302011
Examination Roll No: M4MET24007
Registration No: 163728 of 2022-23

Under the Guidance of

Dr . Utpal Kumar Maity
Assistant Professor
Dept. of Metallurgical and Material Engineering
Jadavpur University, Kolkata-700032

DEPARTMENT OF METALLURGICAL AND MATERIAL ENGINEERING
FACULTY OF ENGINEERING AND TECHNOLOGY
JADAVPUR UNIVERSITY
KOLKATA
August 2024

CERTIFICATE

This is to certify that **Mr. Jasim Mondal (Class Roll No: 002211302011 and Registration No: 163728 of 2022-2023)** is a student of M.E in Metallurgical Engineering at Jadavpur University, Kolkata– 700032, has been entitled a thesis work and directed to submit the final report for the partial fulfilment of the requirements for award degree of M.E in Metallurgical Engineering Examination at the Department of Metallurgical and Material Engineering of Jadavpur University

During the period of final year, he has been carried out the thesis work on **"High Temperature Tensile Property of 316L Austenitic Stainless Steel Welding"** under the guidance and supervision of Assistant Professor Utpal Kumar Maity and the content of this thesis report have not been submitted earlier by any other Institute by any one for award of any degree.

……..
Supervisor
Dr. Utpal Kumar Maity
Assistant Professor,
Department of Metallurgical and Material Engineering
Jadavpur University,
Kolkata-700032

……..
Head of the Department
Dr. Sathi Banerjee
Department of Metallurgical and Material Engineering
Jadavpur University,
Kolkata-700032

……..
DEAN
Faculty of Engineering and Technology
Jadavpur University,
Kolkata-700032

DECLARATION OF ORIGINALITY AND COMPLIANCE WITH ACADEMIC ETHICS

I hereby declare that the thesis "**High Temperature Tensile Property of 316L Austenitic Stainless Steel Welding**" contains literature survey and original research work that has been carried out by myself, as a part of my Master of Engineering Degree in Metallurgical Engineering during the academic year 2022-2024. All the information in this document has been obtained and presented in accordance with academic rules and ethical conduct. As per the rules and regulations I also declare that, I have fully cited all the reference materials and given due credit to their respective authors for any data or information that are not original to this work.

Name: Jasim Mondal

Class Roll Number: 002211302011

Examination Roll Number: M4MET24007

Registration No: 163728 of 2022-2023

Place: Kolkata ……

Signature of Candidate

Date:

CERTIFICATE OF APPROVAL

The foregoing thesis, entitled as "**High Temperature Tensile Property of 316L Austenitic Stainless Steel Welding**" is hereby approved by the committee of final examination for evaluation of the thesis as a creditable study of an engineering subject and presented by Mr. Jasim Mondal (Registration No: 163728 of 2022-2023) in a manner satisfactory to warrant its acceptance as a prerequisite to the degree M.E in Metallurgical Engineering for which it has been submitted. It is understood that by this approval, the undersigned do not necessarily endorse or approve any statement made, opinion expressed, or conclusion drawn therein, but only the thesis for which it is submitted**.**

Committee of final examination for the evaluation of the thesis –

…….

……

…….

Signature of Examiners

ACKNOWLEDGEMENT

I express myself deepest sense of gratitude and obligation to my Hon'ble thesis guide Dr. Utpal Kumar Maity Assistant Professor, Department of Metallurgical and Material Engineering, Jadavpur University for his outstanding support and inspiration to initiate the thesis work and also scrutinized the report in every stage and stimulating suggestions as well as maintain my progress in track & also guiding me in achieving the objective of the thesis. It was a great experience and privilege for me to work under her in a cordial environment.

I would like to take this opportunity to express my heartfelt gratitude to the people who have supported me throughout this research project. Prof. Pravash Chandra Chakraborti, Professor, Department of Metallurgical and Material Engineering, Jadavpur University , who made his time and resources available for my work and providing me the opportunity for undertaking his laboratory works/testing facility.

I would like to express my profound gratitude to Hon'ble Dr. Sathi Banerjee, Head of the Department, Department of Metallurgical and Material Engineering of Jadavpur University for permitting me to undergo this thesis work.

I am also grateful and acknowledge with much appreciation for the crucial role of the Hon'ble professors & entire team of the Metallurgical and Material Engineering Department, Jadavpur University, who made their time and resources available for my work and providing me the opportunity for undertaking the laboratory works/testing facility.

I am also thankful to big brother Manish Kumar Patel and Sayan Kumar Chandra Research Scholars at the Department of Metallurgical and Material Engineering, Jadavpur University who have provided me their moral support, help and cooperation throughout the duration of this project

I am thankful to all friends, family members and aged father , whose suggestions, encouragement and precious time helping me to coordinate/accomplish this work. A special thanks to all who gave me the possibility to complete this report.

Date:

……..

Jasim Mondal
Department of Metallurgical Engineering
Jadavpur University, Kolkata-700032

CONTENTS

PAGE NO

Chapter 4: EXPERIMENTAL PROCEDURE

Chapter 5 : RESULT AND DISCUSSION

ABSTRACT

The thesis investigates the high-temperature tensile properties of 316 austenitic stainless steel welds, focusing on their mechanical behavior at both ambient and elevated temperatures. Key properties such as tensile strength, strain hardening, ductility, and hardness are evaluated to understand how the material responds under thermal stress. The study aims to provide a comprehensive analysis of the weld's performance, particularly in environments where high-temperature resistance is critical. By examining the material's behavior under various thermal conditions, the research offers valuable insights into the weld ability and long-term durability of 316L stainless steel, making it suitable for demanding applications in industries where heat and corrosion resistance are paramount.

CHAPTER - 1

INTRODUCTION
PLAN OF WORK

1.1 INTRODUCTION:

Stainless steels are among the most adaptable materials used worldwide today. Different grades of stainless steels offer a distinct mix of mechanical properties, including strength, toughness, and ductility, which make them ideal for a wide range of applications. From their role as structural components in buildings, construction projects, and housing, to more demanding uses in critical systems, stainless steels have a broad spectrum of applications. They are extensively used in fast breeder nuclear reactors, heat transport piping, boilers, reactor vessels, heat exchangers, and condenser tubes, where they are required to endure continuous thermal changes, extreme temperatures, and high thermomechanical tensile stresses.

In addition to their favorable mechanical properties, stainless steels are known for their outstanding corrosion resistance, which shields them from environmental degradation and makes them ideal for use in harsh and chemically reactive environments. The material behavior of these steels is crucial, particularly in forming processes like forging, rolling, and extrusion, where compressive forces are applied to mold metal ingots into finished products. The determination of load requirements and energy consumption in manufacturing facilities is closely tied to the tensile behavior and work-hardening characteristics of these materials under stress at varying strain rates, as well as their capacity for deformation.

Thus, it becomes essential to conduct a thorough investigation to comprehend the mechanical and corrosion characteristics of these materials under diverse conditions. This approach is crucial for determining their applicability and effectiveness in real-world scenarios. Such studies help ensure that these materials can withstand the specific demands of different environments and operating conditions, thereby guiding their optimal use in practical applications.

This study emphasizes the high-temperature tensile properties of 316L austenitic stainless steel welds, examining their behavior at both room and elevated temperatures. The investigation covers key aspects such as tensile strength, strain-hardening characteristics, ductility, and hardness. These properties are crucial for understanding how 316L stainless steel welds perform under varying temperature conditions, especially in environments where high heat resistance is necessary. The findings aim to provide insights into the mechanical behavior of the material, its ability to withstand deformation, and its overall suitability for high-temperature applications.

1.2 Plan of Work:

i**) Sample selection**: Base sample 316L austenitic stainless steel take and weld by SMAW method and prepare tensile specimen length 111 mm

ii**). Tensile test**: Tensile sample test on CFI machine INSRON 8862. Test condition is room temperature and High temperature which temperature is 600^0C. strain rate is 10^{-3}.

iii) **Sample preparation:** Sample preparation is undertaken in metallographic laboratory equipped with Sawing, automatic polishing machine through belt/cloth, Grinding, & different grade of emery paper are used for preparation of sample with required dimension and surface finish.

iv) **Optical Emission Spectroscopy:** Compositional Analysis is carried out through optical Emission Spectroscopy.

v) **Microstructure Study**: Microstructure study for the given sample tensile effect on the surface by using Optical Microscope.

vi**) Measurement of Micro hardness: b**y using Vickers Hardness Machine (HV scale), micro Vickers hardness measurements with a load of 200 gf and an indentation holding time of 10 secs were taken at points at different locations. The average hardness values were taken.

vii) Scanning Electron Microscope (SEM): A scanning electron microscope was used to study the metallographic phases of the base material room temperature and 600^0c high temperature samples.

viii) **Field Emission Scanning Electron Microscopy coupled with Energy Dispersive X-Ray Spectroscopy (EDS/EDX):** Energy dispersive spectroscopy enables the chemical characterization/elemental analysis of materials for the given base sample and weld sample room temperature and high temperature.

ix) **XRD:** X-Ray Diffractometer was used to identify materials based on their diffraction pattern.

x**) Corrosion Potential Test:** to study Corrosion behaviour of the base material and after tensile test, in different solutions (3.5 % NaCl in 100 ml of H2O is expressed as the Corrosion Penetration Rate (CPR) in mm per year, or the thickness loss of material per unit of time

CHAPTER – 2

● LITERATURE REVIEW

Literature Review

Stainless steels are high-alloy steels known for their exceptional corrosion and oxidation resistance, coupled with strong ductility and strength. Their versatility makes them prevalent in numerous applications, including crucial roles in nuclear power plants, power generation facilities, and substations. Additionally, they are widely used in food processing plants, paper manufacturing facilities, petrochemical industries, and the automotive sector. Stainless steels are also indispensable as structural materials in the building and construction industry.

2.1 Classification of Stainless Steels

Stainless steels can be classified into four primary categories: Ferritic stainless steels, Martensitic and precipitation-hardening stainless steels, Austenitic stainless steels, and Duplex stainless steels.

i) Ferritic stainless steels: Standard ferritic grades are alloyed with 11.2–19% chromium, containing minimal or no nickel. These steels are typically more affordable than their high-nickel counterparts and are not subject to price fluctuations. Adding molybdenum can enhance corrosion resistance, while alloying with niobium and/or titanium improves weldability. Due to their ferritic microstructure, these grades are magnetic**.**

Besides the standard grades, specific ferritic stainless steels are utilized at high temperatures ranging from 800°C to 1150°C in sulphur-containing environments. These grades generally have a higher carbon content to enhance creep strength and are often alloyed with silicon and aluminum to improve oxidation resistance**.**

ii) Martensitic and Precipitation Hardening Stainless Steels: Martensitic grades have a higher carbon content compared to other stainless steels, which enhances their strength and hardenability. These grades also contain minimal amounts of nickel. While adding nitrogen can further increase strength, a significant drawback is their poor weld ability. This can be improved by adding nickel or reducing the carbon content, but this compromises strength. Adding sulfur improves machinability. These steels are air-harden able, resulting in a predominantly martensitic microstructure due to the 'nose' of the TTT diagram being shifted to longer times.

iii) Duplex Stainless Steels: Duplex stainless steels are created by expanding the narrow $\alpha+\gamma$ region surrounding the closed gamma loop shown in the Fe-Cr phase diagram in **Fig 2.1**. This is accomplished by adding various alloying elements in optimal proportions to maintain a balance between the α-stabilizing and γ-stabilizing elements. The resulting microstructure at room temperature contains equal volumes of ferrite and austenite.

Duplex grades merge many of the advantageous properties of both ferritic and austenitic stainless steels. Their high strength and significant resistance to stress corrosion cracking are due to their dual-phase microstructure. Duplex stainless steels have high chromium content (20.1–25.4%) but lower nickel content (1.4–7%) compared to austenitic grades. Molybdenum (0.3–4%) and nitrogen are often added to enhance corrosion resistance and stabilize the

microstructure. In some grades, manganese is added not only as a substitute for nickel but also to increase the solubility of nitrogen in the matrix.

Due to their dual-phase microstructure, these steels exhibit superior mechanical strength, toughness, and corrosion resistance compared to their single-phase counterparts. Despite their many advantageous properties, they have limitations. Their use is restricted to temperatures above 280°C because the precipitation of sigma and chi phases at lower temperatures significantly reduces their ductility and performance.

Duplex stainless steels, along with martensitic and ferritic stainless steels, experience a phenomenon known as 475°C embrittlement. This means that these steels undergo a significant reduction in toughness and become brittle when exposed to or heat-treated within the temperature range of 400°C to 500°C. This embrittlement is believed to result from a spinodal decomposition transformation, where fine chromium-rich precipitates of the α' phase form, adversely affecting the toughness of these steels [**2**]. The transformation is driven by the miscibility gap in the Fe-Cr system, and is facilitated by high chromium content (15-75 wt.%).

Miscibility gaps occur because a single phase is unstable at certain temperatures due to the convex-concave or undulating shape of its free energy versus composition curve. Consequently, for specific alloy compositions, the parent phase separates into two phases with different compositions.

iv) Austenitic Stainless Steels Austenitic stainless steels are the most commonly used, representing over 50% of global stainless steel production. They are categorized into five sub-groups: Cr-Mn grades, Cr-Ni grades, Cr-Ni-Mo grades, high-performance austenitic grades, and high-temperature austenitic grades. These steels offer a wide range of beneficial properties, including outstanding corrosion resistance, excellent formability, and good weld ability. They also maintain strong impact resistance at low temperatures, making them ideal for cryogenic applications **[3**]. In their solution-annealed state, these steels are non-magnetic due to their austenitic microstructure and do not undergo phase transformations with changes in temperature. Consequently, they are primarily strengthened through cold working, often followed by stress relief annealing. A notable feature of these steels is that when heated within the range of 425–870°C, chromium carbide precipitates form at the austenitic grain boundaries.

This presents several issues, particularly because the formation of chromium carbide depletes the adjacent austenite matrix of chromium, increasing its susceptibility to corrosion **[4] [5] [6] [7]**. This issue is known as sensitization, and it can be addressed or prevented through the following methods:

i) Conducting a solution annealing heat treatment at temperatures between 1050°C and 1100°C effectively dissolves the formed carbides. After holding the steel at this temperature for a set duration, it is rapidly cooled (quenched) to prevent the precipitates from re-forming during the cooling process.
ii) Using stainless steel with lower carbon content naturally reduces the likelihood of precipitate formation, thereby preventing this issue altogether.
iii) Introducing elements with a higher affinity for carbon than chromium, such as titanium or tantalum, leads to the preferential formation of carbides of these

elements, thereby reducing the likelihood of chromium carbide formation. These elements are particularly used in stabilized austenitic steel grades like 321 or 347, helping to mitigate the issue of intergranular corrosion that is commonly seen in these steels.

iv) Extending the sensitization time by incorporating elements like molybdenum can influence the reaction kinetics of $M_{23}C_6$ carbides, thereby delaying the onset of sensitization

Besides chromium carbides, Cr-rich sigma phases are also known to precipitate in duplex stainless steels within the temperature range of 700°C–900°C. These phases negatively impact the mechanical properties of the steels, leading to a significant reduction in both ductility and toughness [8][9]. In addition to significantly reducing general corrosion resistance, the most frequently observed sigma phase, the Fe-Cr phase, has a Rockwell C hardness value of 68, as noted by Griffith and Bain. This phase is extremely brittle, often causing specimens to fracture during testing. [10].

The formation of these intermetallic compounds is further encouraged by the addition of alloying elements such as silicon, titanium, and molybdenum. Therefore, stainless steels with high alloy content are more susceptible to sigma phase formation.

n AISI 300 stainless steels, sigma phase formation is known to be very slow, often requiring hundreds or even thousands of hours at the specified temperature range to occur [11].

Therefore, these steels can be utilized over a wide range of temperatures, from cryogenic conditions up to elevated temperatures of around 760°C for operational purposes.

2.2 Role of Alloying Elements in Stainless Steels: Numerous alloying elements can be present in steels, each uniquely impacting the iron-carbon equilibrium phase diagram. Some of these effects are discussed as follows:

Alloying elements can be broadly classified into two categories based on how they influence the equilibrium phase diagram:

Alloying elements that expand the austenite phase field by stabilizing the gamma phase across a wider range of temperatures and compositions are known as austenite or gamma stabilizers. Elements such as Mn, Ni, and Cu fall into this category and possess an FCC (Face Cantered Cubic) crystal structure. These elements not only shift the critical points to enlarge the gamma phase field but also lower both the eutectoid temperature and eutectoid composition. For instance, a mere 3% addition of Ni can reduce the eutectoid temperature by nearly 30°C.

The other group consists of ferrite stabilizers; whose addition reduces or shrinks the austenite phase field. These elements have a Body Cantered Cubic (BCC) crystal structure, similar to the ferritic phase of iron. Common ferrite stabilizers include W, V, Mo, Cr, and Si.

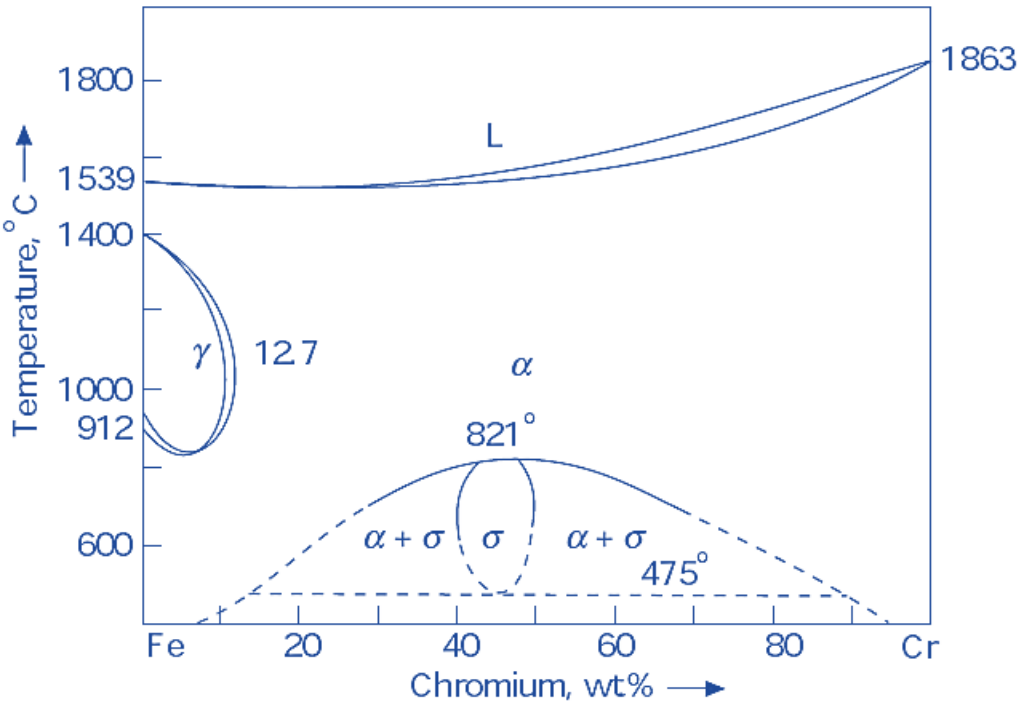

Fig 2.1 Fe Cr phase diagram showing the distinctive γ loop [12]

As illustrated in Fig. 2.1, the addition of approximately 12.7 wt.% Cr causes the austenite phase field to vanish, resulting in the ferritic phase fields of alpha and delta iron merging into a single continuous phase that remains stable from room temperature up to the melting point. Despite having higher chromium content, austenitic stainless steels maintain austenite as the stable phase due to the alloying effect of Ni, which causes the austenite phase to reappear. For example, alloying 18% Cr with 2% Ni makes the steel heat-treatable, and at even higher percentages, austenite becomes the only stable phase.

The role of individual alloying elements is briefly discussed as follow:

Chromium: Chromium is a primary alloying element that imparts corrosion resistance in stainless steels. To resist corrosion and enhance oxidation resistance at elevated temperatures, all stainless steels contain a minimum of 10.5 wt.% Cr.

Nickel: Nickel imparts ductility and toughness to stainless steels, enhances weld ability in martensitic grades, and forms intermetallic compounds in precipitation-hardening grades, significantly increasing strength. However, a drawback of adding nickel is its tendency to reduce resistance to Stress Corrosion Cracking (SCC), as demonstrated by Copson [13] for an Fe-20Cr alloy in a Cl environment. Nickel also lowers the Ductile to Brittle Transition Temperature (DBTT) in high-chromium ferritic stainless steels. [14]

Molybdenum: Molybdenum enhances both uniform and localized corrosion resistance in stainless steels. In austenitic stainless steels, molybdenum increases resistance to pitting corrosion. [15], especially in seawater and chloride solutions. Molybdenum also promotes the formation of sigma (σ) phase. [16]. and chi (χ) phases in ferritic, austenitic, and duplex stainless steels. Molybdenum significantly enhances the room temperature yield strength and tensile strength of steels, while also improving stress rupture and creep properties at high temperatures.

Manganese: Enhances hot ductility in stainless steels and increases the solubility of nitrogen in both duplex and austenitic stainless steels**. [17], [1],** Functions as an austenite stabilizer. Manganese additions help prevent hot shortness, a type of solidification cracking caused by iron sulfide constituents with low melting points or eutectics. Manganese, with a higher affinity for sulfur than iron, addresses this issue by forming stable Manganese Sulfide (MnS).

Titanium: Titanium enhances resistance to intergranular corrosion in austenitic stainless steels, and improves toughness, formability, and corrosion resistance in ferritic grades. Additionally, it increases resistance to tempering and reduces the hardness of the martensite phase in martensitic stainless steels.

Silicon: Silicon enhances oxidation resistance at high temperatures and in highly oxidizing solutions at lower temperatures. It also improves the fluidity of molten steels, addressing sluggish flow rates in certain steel grades [3]. Additionally, at concentrations above 1 wt.%, silicon acts as a ferrite former.

Cobalt: Cobalt functions as a solid solution strengthener in steels. It is also known to raise the Martensite Start Temperature (Ms), which is why it is included in martensitic grades to promote martensite formation. [18]

Sulphur: Adding sulfur, along with lead and selenium, enhances the machinability of steel grades. This allows for higher machining speeds and extends tool life.

Carbon: Carbon, an interstitial element in all steels, plays a role in expanding the closed γ loop typically observed with alloying elements like chromium. Therefore, carbon, similar to nitrogen, acts as an austenite stabilizer. For commonly used stainless steels containing 18 wt.% Cr, a fully austenitic microstructure can be achieved at room temperature when carbon exceeds 0.4 wt.%. Additionally, carbon is significant for the formation of carbides [19], Higher carbon levels greatly enhance strength but decrease ductility and toughness in both ferritic and martensitic stainless steels. Additionally, elevated carbon content increases the risk of intergranular corrosion.

The Schaeffler diagram can be created based on how various key alloying elements affect the formation of different phases in stainless steels. This diagram shows the stable phase(s) present at room temperature for a stainless steel with a specific composition.

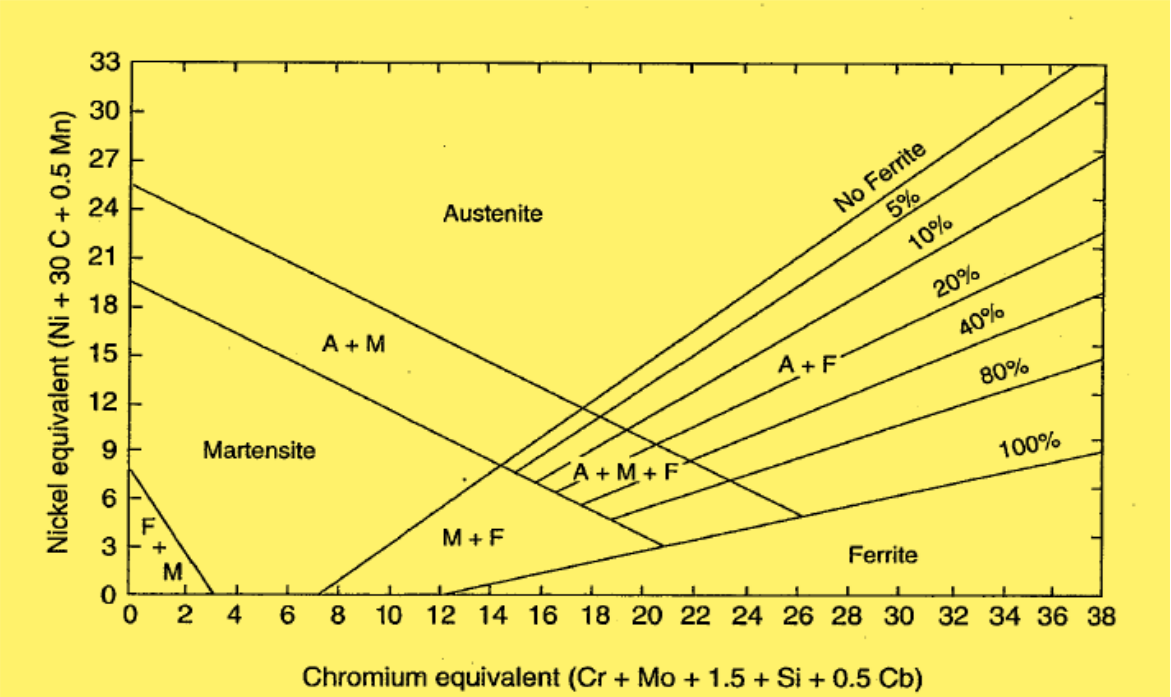

Fig 2.2 *Schaeffer diagram* (1949) [19]

Other elements: Elements like tungsten in duplex stainless grades provide resistance to pitting corrosion. Aluminum may be included in some low chromium ferritic grades to enhance overall corrosion resistance.

2.3 Character of Austenitic Stainless Steels:

Stainless steels are iron-based alloys comprising over 12% chromium, essential for passivity. They may include nickel and molybdenum as major alloying elements for specific purposes, alongside minor elements for specialized properties. The five primary groups are Ferritic, Austenitic, Martensitic, Duplex, and Precipitation Hardenable Stainless Steels. Each group offers distinct characteristics and applications within various industries.

Typical stainless steels exhibit compositions of 18-25% chromium (Cr), 8-20% nickel (Ni), and trace amounts of carbon. Within the Austenitic Stainless Steel (ASS) series, two well-established structural materials for high-temperature applications are types 304 SS and 316 SS. AISI 304 SS, with a minimum of 18% Cr and 8% Ni, provides excellent corrosion resistance. Type 316 SS is similar to 304 SS but incorporates 2-3% molybdenum (Mo) for enhanced resistance to pitting and crevice corrosion in chloride environments. The addition of Mo also improves high-temperature strength. As a ferrite stabilizer, Mo prompts 316 SS to contain higher levels of Ni than 304 SS, stabilizing austenite at low temperatures (R.S. Parmer)[20]. These alloys find extensive use in various industries due to their corrosion resistance and structural integrity under elevated temperatures.

Austenitic stainless steels are characterized by low stacking fault energy, rendering them generally non-magnetic. Unlike ferritic steels, they do not undergo a ductile-brittle transition at low temperatures. However, they exhibit lower thermal conductivity and a higher coefficient of thermal expansion compared to ferritic steels, leading to elevated thermal stresses during service [21].

These steels are favoured as major structural materials due to their satisfactory high-temperature mechanical properties, compatibility with liquid sodium coolant, weld ability, availability of design data, good irradiation resistance, and extensive operational experience in sodium-cooled reactors. In high-temperature sodium environments, austenitic stainless steels demonstrate excellent resistance to both general and localized corrosion. Fast reactors and sodium loops have operated successfully for numerous years, attesting to the long-term compatibility of austenitic stainless steels with sodium at elevated temperatures. Their selection reflects a balance of mechanical, thermal, and corrosion properties essential for demanding applications in nuclear and other industries.

2.3.1. Nitrogen Alloyed Austenitic Stainless Steels:

In nuclear-grade Austenitic Stainless Steels (ASS), carbon content is deliberately kept low to prevent sensitization, a process where chromium carbides precipitate at grain boundaries, reducing corrosion resistance. However, the reduction in strength due to decreased carbon content is compensated by nitrogen addition. Steels designated as 316L feature optimized nitrogen levels, typically around 0.14 wt.%. Nitrogen, acting as an austenitic stabilizer, offers several advantages. It improves mechanical properties and corrosion resistance, delays intergranular carbide formation, thus reducing sensitization susceptibility (Reddy). Furthermore, nitrogen addition presents an opportunity to replace costly nickel in ASS. However, excessive nitrogen levels can lead to the precipitation of brittle Cr_2N, diminishing mechanical properties and increasing susceptibility to cracking. Achieving the delicate balance between carbon reduction and nitrogen enhancement is critical for maintaining the desired properties of nuclear-grade ASS.This emphasis on nitrogen addition underscores its pivotal role in enhancing the performance and longevity of stainless steels in nuclear applications. Through careful control of nitrogen content, manufacturers strive to optimize the material's corrosion resistance, mechanical strength, and overall reliability in demanding nuclear environments.

2.3.2 Reduce Carbon Content Necessity:

During cooling, carbon precipitates as Cr-carbides at grain boundaries in the γ-phase (austenitic) between 425°C-845°C, causing sensitization. This process creates a chromium concentration gradient, reducing chromium near the grain boundary below the 12% threshold necessary for corrosion resistance, rendering the steel prone to intergranular corrosion**.**

Three main methods to avoid this issue include: -

Utilize Extra Low Carbon Content: Low carbon content reduces corrosion carbide formation probability. Austenitic stainless steel (<0.03% carbon) may compensate strength loss by adding small amounts of nitrogen.

Use of stabilizing elements:

In austenitic stainless steel, we incorporate Nb, Ti, and Ta as stabilizing elements. These elements are potent carbide formers compared to chromium. Stabilized steel forms carbides primarily with Nb and Ti instead of chromium. Consequently, chromium remains in the solid solution, preserving the steel's corrosion resistance properties. This strategy enhances the alloy's ability to resist sensitization and maintain its structural integrity in corrosive environments. The use of Nb, Ti, and Ta as stabilizing elements represents a proactive approach to enhance the performance and longevity of austenitic stainless steel components [22].

Solution annealing: -

Reheat weldment above 1040°C to dissolve Cr-carbides, then rapidly cool through sensitization range (425°C-845°C) to prevent Cr-carbide formation. This process ensures chromium doesn't have sufficient time to react with carbon, preserving the steel's corrosion resistance. Such controlled thermal treatment mitigates sensitization effects, maintaining the integrity of the weldment in corrosive environments [22].

2.4 Mechanical Properties of Austenitic Stainless Steels

Austenitic stainless steels exhibit excellent work hardening properties and significant ductility, often with elongations surpassing 50%. These steels typically have yield strengths of approximately 250 MPa (0.3% proof strength) and tensile strengths ranging from 500 to 600 MPa, depending on their specific compositional variations.

2.4.1 Nitrogen's Impact On Material Properties;

In 316LN steel, the carbon content is minimized to prevent issues related to stress corrosion cracking (SCC) and sensitization at high temperatures. However, reducing carbon content also diminishes the strength of these stainless steels. This strength loss is offset by the addition of nitrogen. Nitrogen acts as a strong austenitic stabilizer and enhances solid solution strengthening, thus maintaining the material's strength. Fatigue crack growth is essentially the degradation of material due to slippage in the cyclic plastic strain zone. Dislocations in 316LN stainless steel exhibit a planar structure. The dislocation configuration in austenitic stainless steel is influenced by the ease of cross-slip. A planar arrangement of dislocations in the slip plane occurs when (1) the stacking fault energy of the material is low, and (2) there is a short-range order phase in the alloys. It has been reported that [23] Nitrogen induces a planar arrangement of dislocations (meaning nitrogen introduces planar slip in the material), while carbon promotes a cellular arrangement of dislocations in austenitic stainless steel with added nitrogen or carbon. It has been observed that as the dislocation arrangement transitions to a planar structure, the fatigue crack growth rate decreases. [24].

The planar arrangement of dislocations implies that cross-slip is more challenging in 316LN stainless steel. Therefore, it is believed that the difficulty of cross-slip in 316LN stainless steel enhances its resistance to fatigue crack growth more effectively than in 316L stainless steel. While cross-slip facilitates the formation of coarse slip bands and large plastic zones at the

crack tip, thereby accelerating fatigue crack initiation and growth, planar slip promotes slip reversibility. This slip reversibility improves fatigue endurance by limiting the localization of cyclic strain [25] . At elevated nitrogen levels in austenitic stainless steels, nitrogen forms Cr2N clusters (short-range order, SRO) as a result of strong Cr-N interactions. These SROs, when interacting with dislocations, encourage planar slip and result in a high-stress response [26]. Dynamic strain aging (DSA) in austenitic stainless steels occurs within the temperature range of 673-873 K, significantly reducing low cycle fatigue (LCF) life due to highly localized deformation. Chromium atoms are identified as the primary contributors to DSA. Nitrogen increases the time required for carbide precipitation by slowing the diffusion of chromium. Consequently, nitrogen mitigates DSA by reducing chromium diffusivity and encourages the formation of short-range order (SRO) between chromium and nitrogen. Thus, the crack propagation rate decreases with the addition of nitrogen, and the fatigue crack growth rate diminishes with increased grain size and planar dislocation structures. The presence of ordered Cr2N zones also supports slip planarity. Enhanced slip planarity improves the reversibility of fatigue deformation, reducing the tendency for fatigue crack initiation and propagation, which leads to an extended fatigue life.

The addition of elements like phosphorus and boron can enhance irradiation stability and creep properties (Maziasz 1989), leading to a minimum specified content of phosphorus for this purpose. However, impurity elements such as sulfur and phosphorus, along with minor alloying elements like boron, silicon, titanium, and niobium, can promote hot cracking, especially in fully austenitic steels. [27]

2.5 Problems in Austenitic Steel Weld at Elevated temperature

Weld joints are crucial in high-temperature component fabrication, like thermal and nuclear power plants. Service failures in elevated temperature components are often linked to welds. Hence, extensive studies focus on the deformation, fracture, and crack growth resistance of weld materials from various perspectives.

During weld bead deposition, the molten weld pool is surrounded by already solidified beads and base material. As distance from the molten pool increases, the temperature profile decreases. Repeated thermal cycling affects the base material and solidified material adjacent to the fusion boundary, forming the heat-affected zone (HAZ). Microstructure changes in the HAZ depend on material thickness, composition, heat input, welding speed, and potential environmental interactions. While the microstructure of base metal far from the weld pool remains largely unaffected, the HAZ microstructure undergoes considerable modification due to the intense thermal gradients experienced during welding [28 RS Parmer]

In materials like aluminum or copper, lacking polymorphic transformation, the heat-affected zone (HAZ) undergoes grain growth. In mainly ferritic steels like steel, diverse microstructure bands may form, resulting in a complex weldment microstructure. This microstructural gradient affects local deformation and fracture resistance, shaping the macroscopic mechanical response of weld joints. Austenitic stainless steel serves as an example [28 RS Parmer]

2.5.1Austenitic Stainless Steel:

Austenitic stainless steel typically comprises a combined total chromium (Cr), nickel (Ni), and manganese (Mn) content of 24% or more, with Cr content usually above 16% and Ni often exceeding 7%. Chromium provides oxidation resistance and corrosion resistance, while Ni and Mn stabilize the austenitic phase, preserving it even during rapid cooling to room temperature. Austenitic stainless steels are notably ductile, with higher thermal coefficient of expansion, greater electrical resistance, and lower thermal conductivity. However, their low thermal conductivity leads to significant thermal gradients and high distortion during welding. Welding austenitic steel poses numerous challenges, particularly regarding defects during elevated temperature processing. These issues may include weld cracking, distortion, and the formation of undesirable microstructures, all of which can compromise the integrity and performance of the welded components. Understanding and mitigating these problems is crucial for ensuring the reliability and longevity of welded austenitic stainless steel structures, especially in applications where elevated temperatures are encountered.

2.5.2 Hot cracking exacerbated by the presence of δ and σ phases.

During welding, γ-phase transforms to bcc δ-ferrite at high temperatures; chemistry ensures some δ-ferrite retention upon rapid cooling. Impurities like S and P, having low solubility in γ-phase, segregate to γ-phase boundaries, forming low melting grain boundary films prone to cracking. S and P exhibit high solubility in bcc δ-ferrite, mitigating hot cracking risks. Welds are designed to retain 3%-10% γ-ferrite, but an upper limit on δ-ferrite content is set to prevent σ phase formation. At elevated temperatures (480°C-900°C), δ-ferrite transforms into the intermetallic σ phase, nucleating at the γ-δ interphase and growing inward. σ phase is brittle, increasing hardness and reducing ductility and toughness. Controlling δ-ferrite content is critical to prevent σ phase formation and maintain weld integrity [REF-5-problem of weld].

This phase redissolves when heated above 900°C.

Hot cracks occur primarily in the weld bead or occasionally in the HAZ. In the weld metal, they're termed solidification cracks, while in the HAZ, liquation cracks. These cracks typically trace the random path of grain boundaries. Hot cracks exhibit color on their inner surfaces due to oxide film formation.

1. Segregation	2. High stress in the weld metal
3. Material thickness	4. Material composition
5. Preheating	6. Weld procedure.

Excessive stress should be avoided in the solidifying metal to prevent crack formation. Thicker work pieces cool faster after welding, increasing the likelihood of hard phase formation and crack initiation. Elevated carbon content in steel raises hardenability, potentially leading to weld cracking. Similarly, high welding speeds can induce crack development.

2.5.3 HIC

Cracking can also occur in the presence of hydrogen. Hydrogen-induced cracking (HIC) transpires when specific factors are present-

I. Hydrogen in the weld metal ii. High stress iii. Existence of hard phase

The main source of hydrogen in welding is water vapour. Atomic hydrogen can easily penetrate steel, causing cracking, blistering, and loss of ductility. It diffuses through the steel lattice and recombines to form molecular hydrogen in voids, creating pressure that can lead to cracks in regions such as the heat-affected zone and weld metals.

The most effective solution to prevent hydrogen-induced cracking is to remove hydrogen by preheating the material before welding and applying post-weld heat treatment (PWHT) to reduce hardness and residual stress, thus minimizing the risk of cracking

2.5.4 Sensitization-

During cooling from elevated temperatures, the γ phase of steel experiences sensitization, typically occurring between 425°C to 845°C. Carbon precipitates at grain boundaries as chromium carbides, forming a chromium-depleted zone near the grain boundary. This reduction in chromium concentration below the critical level (12%) compromises the steel's corrosion resistance, making it prone to intergranular corrosion.

There are primarily three ways to mitigate this issue------

Remedy annealing:

We need to reheat the entire weldment to a temperature exceeding 1040°C and maintain it there to ensure the chromium carbides dissolve back into the solution. Subsequently, rapid cooling through the sensitization temperature range (425°C-845°C) prevents chromium from reacting with carbon to form chromium carbides.

Use of extra low carbon:

If the carbon content is low, the likelihood of corrosion carbide formation decreases. In austenitic stainless steel with carbon content <0.03%, the resulting strength loss can be compensated by adding a small quantity of nitrogen (N).

N is an austenitic stabilizer that provides solid solution strengthening, precipitation strengthening, and order strengthening. It generally shifts the precipitation of carbides to longer durations and delays the diffusivity of chromium, thereby prolonging the formation of chromium carbides.

Use of stabilizing elements

In austenitic stainless steel, stabilizing elements like Nb, Ti, and Mo are used. These elements are strong carbide formers compared to chromium. Consequently, in stabilized steel, Nb and Ti carbides are formed rather than chromium carbides. This allows chromium to remain in solid solution, preserving the steel's corrosion resistance [28]

2.5.5 Knife Line Attack:

Welds of stabilized austenitic stainless steel (containing Ti, Nb, etc.) may be susceptible to knife line attack. This attack occurs in a narrow band adjacent to the weld metal, where high temperatures during the heating cycle dissolve TiC and NbC. Upon rapid cooling, TiC and NbC do not have sufficient time to precipitate, leaving free carbon atoms. During reheating, chromium carbides can easily form at grain boundaries, leading to intergranular corrosion.

To avoid this problem, stabilized steel is heated within the temperature range of 1000°C to 1100°C, allowing chromium carbides to dissolve and promoting the formation of TiC and NbC. Additionally, rare earth metals such as La and Ce are effective in preventing this issue.

2.5.6 Stress Corrosion Cracking (SCC):

Austenitic stainless steels are susceptible to stress corrosion cracking (SCC) when exposed to stress and corrosive environments like chloride-ion-containing media. SCC in the heat-affected zone (HAZ) of austenitic stainless steel typically manifests as trans granular cracking. SCC can occur in components during storage, especially in environments like seaside locations, before they are put into service.

SCC during storage can be mitigated by stress-relief annealing to reduce residual stresses to safe levels

The presence of porosity and slag inclusions in welds can lead to defects, as slag can inhibit the metal from reaching its fusion temperature.

Welding induces localized heating and subsequent cooling, leading to solidification shrinkage in the metal. This creates residual stresses, which persist in the structure even after external loads are removed. These stresses generate a field around cracks, increasing the risk of cracking, with some regions experiencing stress levels nearing the material's yield strength [29].

2.6 Tensile Deformation Behaviour of ASS:

Tensile flow and work hardening behavior remain of significant scientific and technological interest due to their impact on optimizing material processing conditions and ensuring reliable performance in service. The tensile deformation behavior of austenitic stainless steel is influenced by various factors, including its chemical composition, temperature, grain size, stress state, strain, and strain rate. The monotonic deformation behavior of face-centered cubic (FCC) metals, such as austenitic stainless steel, is particularly sensitive to the strain rate and the temperature at which the deformation occurs. Understanding these dependencies is crucial for improving material performance and processing techniques.

The tensile behaviour of austenitic stainless steel is affected by the strain rate, prior cold work history, and the testing temperature. Parameters such as Ultimate Tensile Strength (UTS), percentage elongation (%EL), and percentage reduction in area (%RA) are influenced by these

factors to varying degrees. Although tensile tests are typically conducted at strain rates ranging from $1x10^{-5}$ to $1x10^{-1}$ s^{-1}, which are low enough to be considered quasi-static as noted by many researchers, the poor thermal conductivity of austenitic stainless steels means that a significant amount of the deformation heat is retained within the material, resulting in similar outcomes. [30]

2.6.1 Stages of Tensile Flow Behaviour:

Tensile flow in single crystal FCC metals unfolds in three distinct stages. Stage I is characterized by easy glide, where the material experiences minimal strain hardening. During this phase, dislocations can travel considerable distances without significant barriers, leading to slip occurring predominantly on a single slip system, a process known as laminar flow. In Stage II, strain hardening intensifies rapidly with increased strain. Here, slip occurs across multiple slip systems, leading to the formation of Lomer-Cottrell barriers and the development of dislocation tangles, eventually forming a distinct cell structure with high dislocation density. In Stage III, the strain hardening rate diminishes with further strain due to dynamic recovery processes. At this stage, the stress is sufficient to enable dislocations to engage in mechanisms that are inactive at lower stresses, such as cross slip, which reduces the internal stress fields. The flow stress in this stage is highly temperature-dependent. This three-stage tensile flow behavior is influenced mainly by the metal's purity, the testing temperature, and the strain rate of deformation

2.6.2 Effect of Strain Rate:

It is well established that the stress needed to sustain deformation rises with an increase in strain rate, a phenomenon commonly referred to as the strain rate effect. Numerous researchers have documented the influence of strain rate on the material's flow behaviour [31]. It has been reported that the tensile flow stress of Fe-Al alloy is highly dependent on the deformation strain rate and the testing temperature. The study examined the effect of strain rate in FCC metals using the Hopkinson bar test and explained the findings through dislocation theories. It suggested that the strain rate effects were likely due to dislocation glide and interactions among dislocations. The influence of strain rate on flow behaviour can be characterized by strain rate sensitivity. Strain rate sensitivity is the increase in stress needed to produce a specific rise in plastic strain rate at a given strain and temperature [30]. The strain rate sensitivity (SRS) of a material varies with testing temperature; it is lower at room temperature and rises as the testing temperature increases. Numerous researchers have explored the strain rate sensitivity of various materials [32]. The strain rate sensitivity (m) of metals is typically minimal (< 0.1) at room temperature but escalates with rising temperatures. For most superplastic materials, m ranges between 0.4 and 0.8 [30].

2.6.3 Effect of Temperature:

Typically, as the test temperature rises, strength tends to decrease while ductility increases. [30]. It has been observed that for BCC metals, the yield stress increases notably as temperature decreases, whereas for FCC metals like nickel, the yield stress exhibits only slight dependence

on temperature [30]. In FCC metals, while flow stress shows little dependence on temperature, the strain hardening exponent tends to decrease as temperature increases [30].

It proposed that at elevated temperatures, dynamic strain ageing (DSA) often manifests as serrations in the stress-strain curve. This phenomenon arises from the viscous behavior of mobile dislocations and increased diffusivity of solute atoms, resulting in vacancy generation during plastic deformation. The observed serrated flow behavior is attributed to the dynamic interaction between solute atoms and dislocations, termed as dynamic strain aging (DSA) [33].

Observed that the yield strength (YS) experiences a slight decline with temperature up to 300°C. Beyond this point, there is a peak in YS at 400°C, accompanied by a reduction in elongation percentage. Additionally, the strain hardening rate reaches its maximum at 400°C [34].

It has been shown that for austenitic stainless steels, the shape of the stress-strain curve changes as the test temperature varies from room temperature down to cryogenic levels. At room temperature, tensile tests produce parabolic curves, but as the temperature decreases, the curves gradually become sigmoidal (S-shaped) [35] . These curves feature a plateau region, indicating easy deformation at low strain values. According to Gunter and Reed [36] , this behavior is associated with ε-martensite formation. Bearing an orientation relationship of (111) γ/ (00.1) ε, ε-martensite forms in this region due to the low stacking fault energy of the austenitic matrix. In contrast, at higher strains, there is a rapid increase in strain hardening, which is attributed to the formation of α-martensite.

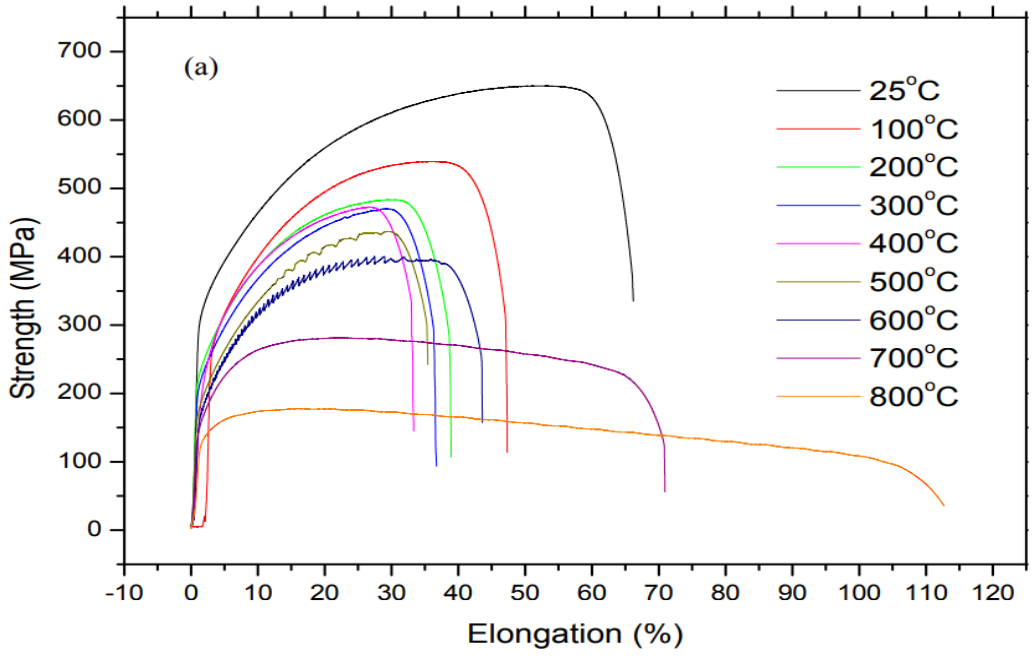

Fig 2.3 Tensile curves of 316L austenitic stainless steel showing DSA phenomenon (serrated flow behaviour) at 500℃ and 600℃ [37]

2.6.4 Dynamic Strain Aging in Stainless Steels:

Dynamic Strain Aging (DSA) describes the occurrence of serrations in the tensile curves of various metals or alloys at elevated temperatures, such as plain carbon steels, HSLA steels, and notably 316 and 304 stainless steels.

Serrated flow at elevated temperatures results from the interaction between solute atoms and dislocations. At sufficiently high temperatures, solute atoms like carbon and nitrogen, due to their increased diffusivity and relatively small size, can catch up with moving dislocations. When these atoms encounter a dislocation, they effectively "pin" it by condensing into the high-energy core of the dislocation. [38]. The 'pinning' of dislocations is overcome when the local shear stress exceeds the barrier, allowing the dislocations to be pulled away from the obstructing solute atoms. This process repeats, leading to the pinning and unpinning of dislocations, which is essentially what causes the local peaks or humps observed in the flow curves.

2.7. Work Hardening Behaviour of Austenitic Stainless Steels:

Work hardening refers to the increase in flow stress with plastic deformation due to various interactions that impede dislocation movement, such as the cutting through dislocation forests, formation of jogs and kinks in dislocation lines, heightened friction stress against glissile dislocations, dislocation pileups, and the development of dislocation cell structures. This indicates that plastic deformation induces multiple changes in the material's microstructure, and the material's response evolves accordingly. Several models have been proposed to describe material behavior during plastic deformation. A few of these models are discussed below:

2.7.1 Holloman Relationship

He Holloman relationship, formulated by J.H. Holloman, is used to characterize the general work hardening behavior of metals. This relationship can be mathematically expressed as

$\sigma=(\varepsilon p)n$ 2.1

Here, K represents the strength coefficient, σ denotes the true stress, $\boldsymbol{\varepsilon_p}$ stands for the true plastic strain, and n is the strain hardening exponent.

When this power law relationship is plotted on a double logarithmic scale, it produces a straight line. The slope and intercept of this line (when extended) correspond to the values of n and K, respectively.

Although this relation is straightforward, it can predict the plastic flow behavior of 18-8 stainless steels with considerable accuracy. Low and Garofalo [40] It has been suggested that deviations from this behavior are probably due to phase changes occurring during deformation. It is well established that for FCC metals and alloys, such as austenitic stainless steels with

relatively low stacking fault energy (SFE), the Holloman relationship is accurate at high levels of plastic strain. However, significant deviations from linearity are noted at lower strain values.

Numerous researchers [41, 42**]** have observed that the tensile deformation of various austenitic stainless steels occurs in distinct stages. They reported that the transition strain, which marks the shift from one stage to another, is heavily influenced by the strain rate of deformation. Furthermore, the minimum work hardening parameter (n_1) decreases with increasing strain rate, suggesting that multiple slip and cross slip activities occur to accommodate the higher strain rate.

2.7.2 Ludwik Analysis:

Another empirical relation introduced by Ludwik aims to describe the plastic flow behavior of metals. While preserving the same power-law relationship as the Holloman model and using the same parameters n and K, Ludwik's equation includes an additional term that represents the true yield stress. Consequently, the Ludwik relation is expressed as follows:

$\sigma = \sigma_0 + (\varepsilon p)n$ 2.2

Direct parallels can be drawn between the Ludwigson relation and the Ludwik relation, as both include an additional term that pertains to the stress at which the material begins to yield. In the Ludwigson relation, the stress value at which ϵ=0 corresponds to the proportional limit and is denoted by eK_2. Comparisons of experimental $eK2$ values with test records for stainless steels have demonstrated good agreement between the two.

After taking logarithmic on both sides [Eq. 2.2] following expression can be obtained.

$n(\sigma - \sigma_0) = \ln(\acute{K}) + \acute{n}.ln(\varepsilon p)$. …….. 2.3

Similar to the Holloman relationship, plotting ($\sigma - \sigma 0$) against εp on a double logarithmic scale should produce a single straight line. Jadav et al. [34] observed a two-stage behavior in Nimonic C-263 alloy at 300°C and 650°C. They proposed that planar slip is the primary mechanism in the lower strain range, whereas cross slip becomes more dominant at higher strains.

2.7.3 Kocks-Mecking Analysis:

Using the K–M approach, the work hardening behavior in metals and alloys can be effectively described by examining the variations in the instantaneous work hardening rate ($\theta = d\sigma/d\varepsilon$) in relation to the flow stresses. However, Kocks and Mecking [44] noted that the different stages of work hardening can be more effectively understood by multiplying the true stress by the work hardening rate (θ).

The flow stress, τ, is comprised of two components: τ_S and τ_G. The component τ_S accounts for the stress due to dislocation cutting processes and is sensitive to temperature, while τ_G represents the stress resulting from elastic interactions between dislocations. Extensive experiments have shown that τ_G is directly proportional to the square root of the dislocation

density and can be expressed as $\tau_G = \alpha G b\sqrt{N}$, where G is the shear modulus, b is the Burger's vector, N is the dislocation density in cm^{-2}, and α is a constant approximately equal to 10^{-1}.

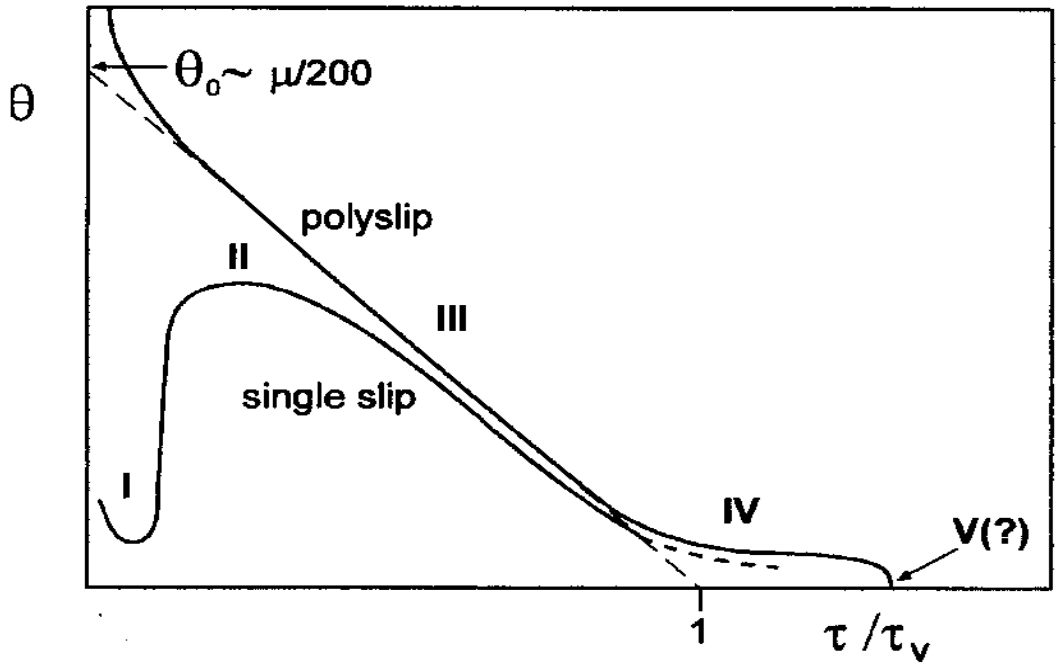

Fig 2.4 Illustration of the different work hardening stages in a polycrystal (upper curve) vs a single crystal (lower curve) **[45 page 219]**

For polycrystals, a similar analogy can be made, but additional factors such as grain size and texture (preferred orientation) must be considered. Stage II is absent in polycrystals, and stage III is followed by stage IV, which is characterized by a sharp kink in the Θ-σ curve. According to Rollet [46], this is a distinctive feature of two-phase alloys, where the hardening rate decreases further before eventually reaching zero. While this is generally true, some researchers describe stage IV as linear, attributing any negative deviations from linearity to a new stage V. This type of hardening behavior is observed in steels. Consequently, a Θ-σ plot (Kocks-Mecking plot) effectively captures the general hardening behavior of fcc metals.

2.8 Ductile Fracture Under Monotonic Deformation:

It is widely recognized that fcc metals, including austenitic stainless steels, experience ductile fracture over a broad range of temperatures, including ambient conditions. Ductile fracture comprises three distinct stages: the nucleation of micro voids, the growth of these voids, and their coalescence to form a crack, ultimately culminating in fracture [47]. Voids are known to nucleate at precipitates, inclusions, second-phase particles, shear bands, or even at dislocation pileups. The mechanism of void nucleation can involve either the decohesion of second-phase

particles or the shearing of these particles, depending on factors such as particle size, volume fraction, and interfacial bond strength. [48].

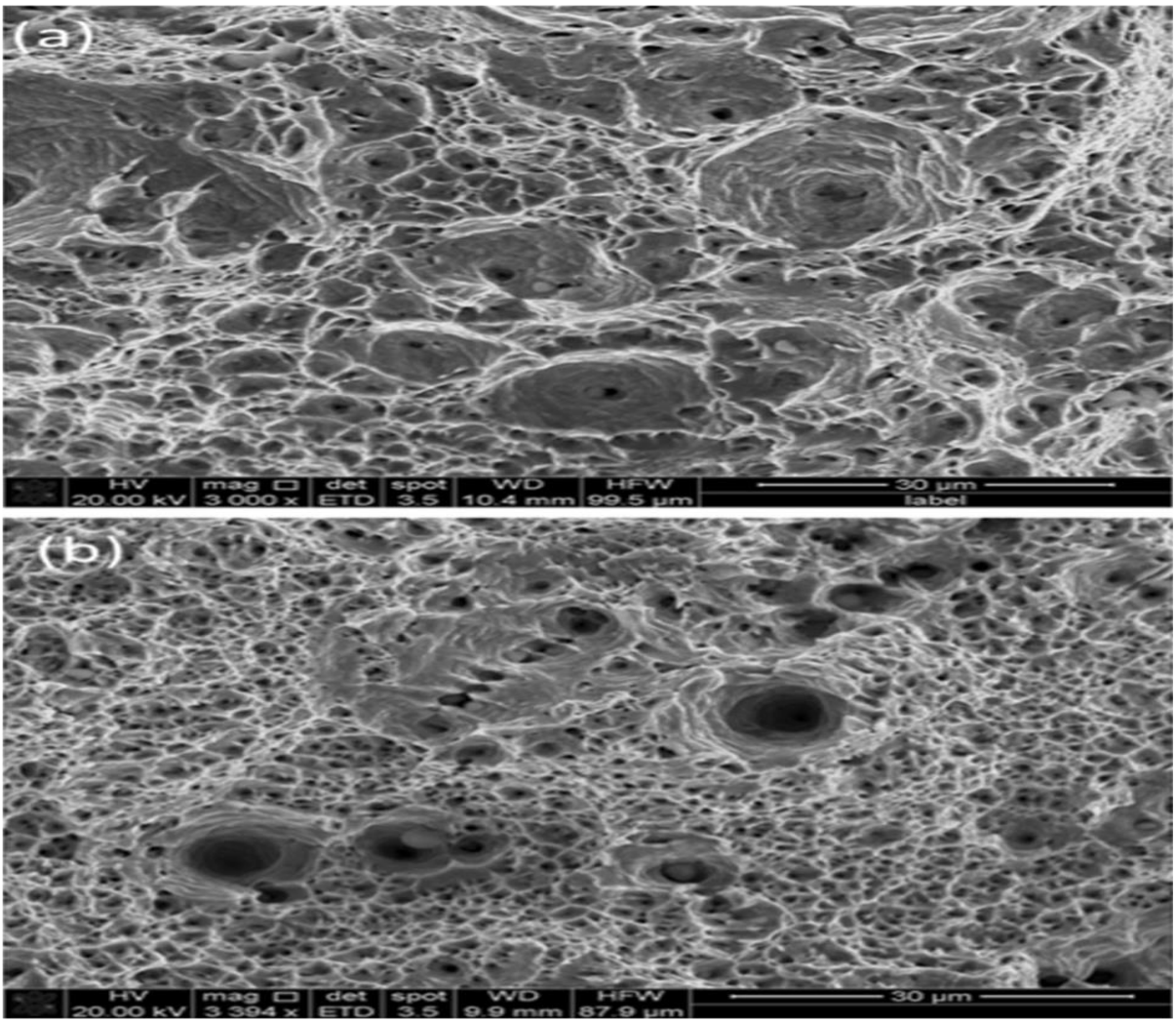

Fig 2.5 Tensile fracture surface of ASS 316L tested at a strain rate of 10^{-3} [49]

2.9 Types Of Corrosion & Corrosion Behavior Of Stainless Steels

Corrosion refers to the deterioration of a metal due to electrochemical reactions with its environment. While it's impossible to completely eliminate corrosion, it can be controlled through different methods. The harmful impacts of corrosion, such as reduced component efficiency, financial losses, contamination, and more, can lead to disastrous outcomes if left unchecked, potentially causing loss of life [50] .

Corrosion is fundamentally an electrochemical process, involving the transfer of electronic charge between the metal surface undergoing corrosion and its surrounding environment.

The different types of corrosion are briefly outlined as follows:

i) Uniform corrosion: Uniform corrosion involves the even removal of metal across its surface. It is a frequently observed form of corrosion, but it necessitates a metal with consistent composition and an environment that can reach the entire surface of the metal. However, in real-world situations, there is typically some level of non-uniformity present.
ii) Galvanic corrosion: Galvanic corrosion takes place when two different metals are in contact with each other in the presence of an electrolyte. The metal with a higher position in the galvanic series (having a more positive electrode potential) is safeguarded, while the metal with a lower reduction potential is more susceptible to corrosion. This concept is applied in underground pipelines, where stainless steels are used to shield them from corrosion damage.

iii) Crevice corrosion: Crevice corrosion is a type of localized corrosion that typically occurs at the interface between two different metals, concentrating on a small contact area. This phenomenon often arises in riveted joints, where the area between the bolt and the surrounding base metal plate becomes prone to corrosion. Stainless steels are particularly susceptible to crevice corrosion when exposed to aerated salt solutions.

iv) Pitting corrosion : This is another form of localized corrosion, marked by the development of pits. In stainless steels, this type of corrosion is quite common since the corrosion resistance of these steels relies on a stable, passivating oxide layer (usually composed of Chromium or Aluminum) that forms on the metal surface. These oxide films are particularly vulnerable in chloride-rich environments, where any localized attack can cause the breakdown of this protective layer, leading to the formation of pits.

v) Intergranular corrosion: This form of corrosion arises from chemical segregation or the depletion of elements like chromium at the grain boundaries. As a result, there is a lack of passivating elements such as chromium in these areas, rendering the grain boundaries and adjacent regions susceptible to environmental corrosion. This issue is particularly significant in steels with less than 10 wt. % chromium and is exacerbated by the precipitation of chromium carbides within the temperature range of 425°C to 815°C.

vi) Environmental Induced Cracking: In addition to the various common types of corrosion, the damage caused by corrosion can become significantly worse when a material is subjected to stress in a corrosive environment. There are three specific forms of failure that arise from the combined effects of stress and environmental interaction, which are outlined below.

vii) Stress Corrosion Cracking: Stress corrosion cracking (SCC) happens in metals exposed to static tensile stresses under specific environmental conditions. Alloys are particularly vulnerable to SCC, while pure metals generally show less susceptibility to this type of damage [50]. Stress corrosion cracking (SCC) necessitates specific environmental conditions, such as hot chloride solutions for stainless steels and the presence of nitrates for carbon steels. Dissolved oxygen levels and halide ion concentrations are critical factors in SCC. The issue worsens with higher temperatures, although a definitive temperature threshold below which SCC susceptibility diminishes is not yet established. Practically, pitting and crevice corrosion are more prevalent at lower temperatures, particularly with low chloride ion concentrations. Ultimately, SCC leads to brittle fracture in metals.

viii) Hydrogen Induced Cracking: Hydrogen-induced cracking (HIC) arises from the diffusion of atomic hydrogen into the metal lattice even without an external stress field. Cracks begin to propagate when the internal pressure increases beyond the hydrogen solubility limit, leading to the formation of molecular hydrogen at potential crack initiation sites such as inclusions or defects. This issue is exacerbated in environments containing H_2S, which provides a source of hydrogen and inhibits the recombination of atomic hydrogen into diatomic molecules, allowing easier diffusion into the metal lattice. HIC is particularly problematic for non-austenitic steels.

Hydrogen embrittlement, closely related to hydrogen-induced cracking (HIC), involves the reduction in ductility of metals due to the absorption of atomic hydrogen into the metal lattice. Although HIC and hydrogen embrittlement share similarities, they differ in key aspects. Hydrogen embrittlement is detectable only under applied stress, whereas HIC can occur without external stress. Additionally, hydrogen embrittlement is reversible: removing or expelling the trapped hydrogen can restore the metal's ductility, unlike HIC, which is often more permanent [51] .

2.10 Mechanism of Pitting Corrosion：

The resistance of an alloy to pitting corrosion is influenced by factors such as pH and temperature, with higher pitting potentials indicating greater resistance to pitting. Chloride ions (Cl-) decrease the alloy's pitting potential, accelerating the pitting process. In the absence of Cl- ions, the breakdown of the passive layer is a slow process where the hydrated oxide layer disintegrates over time, producing ferric ions. Chloride ions expedite this breakdown by interacting with and replacing the hydrated passive film ($FeOOH$) to form an intermediate $FeOCl$ complex. This complex readily decomposes into ferric ions, leading to selective thinning of the oxide film at sites of heterogeneity or inclusions. Consequently, the oxide layer is progressively removed, exposing the bare metal. This exposed metal then dissolves anodically, generating Fe2+ ions and initiating a local pit [50] .

Pits typically begin at specific locations with inhomogeneities or inclusions, frequently sulphide inclusions. In sensitized stainless steel, grain boundaries commonly act as starting points for the formation and expansion of pits.

2.11 Role of Alloying Elements in Corrosion Of Steels:

Chromium: Chromium enhances the corrosion resistance of stainless steels across a wide range of potentials and pH levels. Consequently, duplex stainless steel grades exhibit significantly improved corrosion resistance due to their higher chromium content, typically exceeding 20%.

Nitrogen: Nitrogen improves the resistance to localized corrosion, including pitting and crevice corrosion. Osozawa and Okato [52] proposed a mechanism where ammonium ions form locally around pits, buffering and controlling the pH within acceptable levels. The inclusion of nitrogen has been shown to extend the passivity range in steels, thus postponing

the initiation of pitting. Stainless steels with nitrogen, such as 316LN, exhibit higher pitting potentials across all temperatures compared to 316 or 316L grades, which lack nitrogen.

Molybdenum: The inclusion of Mo slows the expansion of pits. This has been experimentally demonstrated by Tomashov [53a] in 18Cr-14Ni steels, showing that in steels with Mo, the increase in both the diameter and depth of pits occurs at significantly slower rates compared to those without Mo.

Other elements: The inclusion of elements such as V, Si, and Re has been shown to enhance the corrosion resistance of steels by stabilizing the passive oxide layer. Elements like Boron and Carbon can influence corrosion resistance differently depending on their form; Boron, when in solid solution, improves corrosion resistance, whereas Carbon generally has minimal effect. Carbides, however, tend to have detrimental effects and reduce corrosion resistance. Rare earth metals, as well as Te and Se, can lead to the formation of harmful telluride and selenide precipitates. On the other hand, Re additions are beneficial for strengthening resistance to pitting corrosion.

The impact of key alloying elements like Cr, Mo, and N on the corrosion resistance of stainless steels is often quantified by the Pitting Resistance Equivalent Number (PREN)[54]. This number is calculated using the formula %Cr + 3.3%Mo + (16% or 30%)N. The coefficient for Nitrogen is 30 for austenitic stainless steels and 16 for steels with a duplex microstructure.

Titanium: Incorporating small amounts of Ti enhances the pitting potential of alloys, making them more resistant to pitting compared to Ti-free alloys and steels[55]. This improvement is attributed to Ti's strong affinity for carbon and nitrogen, which allows it to bind with these elements. By doing so, Ti prevents the formation of detrimental chromium carbides and nitrides, which otherwise deplete chromium from the base matrix and weaken its resistance to corrosion.

Copper: The effect of copper on the pitting corrosion resistance of stainless steels remains debated. Research on SS 301 steels has shown that small amounts of copper, such as increasing its weight percentage from 0.2% to 0.5%, can be beneficial[55]. However, adding more than 1% copper did not show significant improvement. Subsequent studies have suggested that exceeding 1.5% copper is detrimental, while concentrations below 0.8% tend to produce mixed results, leading to the formation and repassivation of small or metastable pits.

Silicon: The inclusion of silicon enhances the pitting corrosion resistance of stainless steels. Research by Wilde [56] on 18Cr-8Ni stainless steels has shown that silicon elevates the Critical Breakdown Potential (Ec), which is the potential at which the material transitions into a transpassive state characterized by rising anodic current densities following the breakdown of passivity and onset of pitting. Higher Ec values indicate an extended passive region where the current density remains nearly constant, thereby reflecting improved corrosion resistance of the material.

2.12 Corrosion Test Parameters and Their Measurements :

Corrosion of a conductive surface, such as a metal dissolving in an acidic solution, indicates that both the metal oxidation and the reduction of $H+$ ions to $H2$ occur on the same surface. These processes are represented by two half-cell reactions. However, different electrode potentials for these reactions cannot coexist on a conductive surface. Assuming there is no charge buildup, both reactions must occur at a unified potential known as the corrosion potential ($Ecorr$). The resulting current associated with this potential is termed the corrosion current ($Icorr$).

The values of $Ecorr$ and $Icorr$ can be measured through linear polarization tests, which may be galvanostatic, potentiostatic, or potentiodynamic, depending on whether the current or potential is controlled during the experiment. Potentiodynamic or potentiostatic tests are carried out using a potentiostat connected to three electrodes submerged in an electrolytic cell. An external overvoltage is applied between a reference electrode and the test metal (acting as the anode), while the current passing through the counter electrode (cathode) and the test metal is recorded. The intersection of the linear cathodic and anodic branches on the polarization curve, known as Tafel plots, provides the desired parameters.

The corrosion current density $icorr$ is related to the rate of corrosion (or metal loss) as

$$r = \frac{0.129\ a\ j\ corr}{n\rho}$$

where r is the corrosion rate in mils per year (1 mil=0.001 inch), ρ is the density of the material in g/cm3, icorr is the corrosion current density in μA/cm2 and a is the atomic weight in g. Implying that materials possessing low $jcorr$ values along with high $Ecorr$ values have higher corrosion resistance.

A notable phenomenon observed in materials like SS 316L , which are prone to pitting corrosion, is seen during cyclic polarization tests. When these materials are polarized into the transpassive region and then the polarization direction is reversed, they follow a different path than the initial curve, exhibiting hysteresis. The point where the reversed polarization curve intersects the original one is known as the protection potential ($Eprot$). Below this potential, existing pits cannot expand, effectively halting pitting corrosion. Between the initial polarization and $Eprot$, existing pits may continue to grow, but the initiation of new pits stops. [50]

2.13. Weld Ability of Stainless Steels:

i) Austenitic Stainless Steels :

Austenitic stainless steels are known for their good weldability, but factors such as impurity levels of sulfur and phosphorus, as well as the composition of the base and filler materials, play a crucial role during the solidification of weldments. Issues such as weld solidification cracking can occur in these steels. Elevated levels of sulfur and phosphorus increase the risk

of solidification cracking, while the composition of the base metal, particularly the $Creq/Nieq$ ratio, significantly influences this phenomenon [3]. Research has shown that when austenite is the primary solidifying phase, the susceptibility to solidification cracking is at its highest. Conversely, when ferrite is the primary solidifying phase, the occurrence of solidification cracking is largely mitigated.

ii) Ferritic Stainless Steels:

Ferritic stainless steels are typically less susceptible to solidification cracking. However, the presence of alloying elements like Ti and Nb can promote solidification cracking in these steels. A significant issue during the welding of ferritic stainless steels is High Temperature Embrittlement (HTE) in the Heat Affected Zone (HAZ). High levels of interstitial elements such as carbon and nitrogen, along with coarse grain sizes, increase the likelihood of HTE.[3]

HTE leads to a reduction in tensile ductility and toughness due to the formation of intragranular precipitates of chromium carbides, nitrides, or carbonitrides during the cooling of weldments.

iii) Martensitic Stainless Steels

Martensitic stainless steels are susceptible to Hydrogen Induced Cracking (HIC) due to the presence of untempered martensite. Consequently, welding of these steels often requires pre- or post-weld heat treatments. Another common issue is reheat cracking, which can arise from cyclic heating caused by multiple weld passes or post-weld heat treatments. The presence of molybdenum, along with impurities such as sulfur, lead, antimony, tin, boron, and copper, has been linked to this type of cracking.

iv) Duplex Stainless Steels

Duplex stainless steels are generally resistant to both Hydrogen Induced Cracking (HIC) and solidification cracking. However, high levels of chromium and molybdenum can lead to the formation of intermetallic compounds (such as sigma and chi phases) in the temperature range of 570°C to 1000°C, which significantly reduces the ductility and toughness of the weld metal. During welding, cooling, and reheating cycles, parts of the weld metal and the Heat Affected Zone (HAZ) are exposed to this temperature range. To address this issue, a step annealing post-weld heat treatment (PWHT) procedure has been implemented.[50]

Chapter 3

Experimental Details

3.1 Shielded Metal Arc Welding Process (SMAW):

Shielded metal arc welding (SMAW), commonly known as manual metal arc (MMA) welding or stick welding, is a manual arc welding process utilized for joining metals. In SMAW, a consumable electrode coated with flux is employed to create the weld joint. This process is widely favoured for its versatility and suitability across various welding applications. The SMAW process involves several key components and steps to achieve successful welds. Firstly, an electrical circuit is established using a welding machine, which generates the necessary electricity for welding. The setup includes a welding cable with an electrode holder to secure the electrode and a ground cable with a clamp to connect to the work piece, completing the circuit. To initiate the welding process, the electrode is brought into contact with the work piece, effectively closing the electrical circuit. The electric current flows through the circuit, causing the electrode to heat up and melt. As the electrode melts, its metal core is deposited onto the work piece, forming the weld bead. One of the distinctive features of SMAW is the presence of flux coating on the electrode. The flux serves multiple purposes during the welding operation. Firstly, it acts as a protective barrier, preventing atmospheric contamination of the weld pool. When the electrode melts, the flux coating decomposes, releasing gases that form a shield around the molten weld puddle. This shielding gas prevents the ingress of oxygen and nitrogen from the surrounding air, which could otherwise lead to weld defects such as brittleness or porosity. Furthermore, the flux coating facilitates the removal of impurities and oxides from the weld zone, ensuring the formation of a clean and sound weld joint. Additionally, the flux contributes to the stability of the arc during welding, promoting smooth and consistent metal transfer from the electrode to the work piece. The choice of electrode and flux composition depends on the specific welding application and the material being welded. Different types of electrodes are available, each designed for particular welding tasks and metal types. For example, electrodes with rutile or cellulose-based flux coatings are commonly used for general-purpose welding of mild steel, while low-hydrogen electrodes are preferred for welding high-strength steels and critical applications where weld quality is paramount.

Electric current, whether in the form of alternating current (AC) or direct current (DC) sourced from a welding power supply, serves as the catalyst for creating an electric arc between the electrode and the metals slated for joining. During the welding operation, the flux coating of the electrode undergoes decomposition, emitting vapers that function as a shielding gas. Simultaneously, a layer of slag is formed, serving as additional protection for the weld area against atmospheric contamination. Shielded metal arc welding (SMAW) stands out due to its adaptability and the straightforwardness of its equipment and procedures, making it one of the most widely used welding processes globally. Its prevalence is particularly notable in the maintenance and repair sector, where it outperforms other welding methods. Despite the rising popularity of flux-cored arc welding, SMAW retains its prominence, especially in the construction of steel structures and industrial fabrication settings. Although its primary application revolves around welding iron and various grades of steel, including stainless steel, shielded metal arc welding can also accommodate other metals such as aluminum, nickel, and copper alloys. Its versatility and effectiveness across a range of materials contribute to its enduring relevance in diverse industrial sectors.

3.1.1 Development –

Following the initial discovery of the electric arc by Humphry Davy in 1800 [29], progress in electrical welding remained stagnant until Auguste de Méritens introduced a carbon arc torch, which he patented in 1881. Subsequent advancements came from Nikolay Benardos, who

developed carbon arc welding and secured patents in 1887, showcasing an early version of the electrode holder. Nikolay Saviano's [30] invention of the consumable metal electrode in 1888 marked another significant milestone in welding technology. Further innovations emerged in 1890 when C. L. Coffin received a U.S. patent for his arc welding method, which involved utilizing a metal electrode. Similar to shielded metal arc welding (SMAW), this process involved melting the electrode metal, which then acted as filler material deposited into the weld. These developments laid the groundwork for modern welding techniques and played a pivotal role in shaping the evolution of welding technology.

In the early 1900s, A. P. Strohmenger and Oscar Kjellberg made significant advancements in welding technology by introducing the first coated electrodes. Strohmenger utilized a coating of clay and lime to stabilize the arc, while Kjellberg coated iron wire with mixtures of carbonates and silicates for electrode coating. Despite these innovations, the initial electrodes faced challenges due to their high cost and complex production methods. However, in 1912, Strohmenger introduced heavily coated electrodes, although their adoption was limited due to cost and production complexities. The situation improved in 1927 with the development of an extrusion process, which reduced coating costs and enabled manufacturers to create more intricate coating mixtures tailored for specific welding applications. Further advancements came in the 1950s when manufacturers began incorporating iron powder into the flux coating. This innovation facilitated an increase in welding speed, enhancing efficiency and productivity in the welding process. These developments marked significant milestones in electrode technology, laying the foundation for modern welding practices.

3.1.2 Operation: ---

Shielded Metal Arc Welding (SMAW), commonly known as stick welding, is a widely used arc welding process known for its simplicity and versatility. In SMAW, an electric current, typically either alternating current (AC) or direct current (DC), is used to create an electric arc between a consumable electrode and the metals being joined. The process involves several key steps, starting with the setup of the welding equipment and preparation of the work piece. Firstly, the welding equipment is set up, consisting of a welding power supply, a welding cable with an electrode holder, and a ground cable with a clamp. The power supply generates the electric current required for welding, while the electrode holder securely holds the consumable electrode. The ground cable is attached to the work piece to complete the electrical circuit. Next, the work piece is prepared for welding by cleaning and prepping the surface to ensure proper adhesion and quality of the weld. This may involve removing any debris, rust, or contaminants from the surface using a wire brush or grinder. Once the work piece is prepared, the welder selects the appropriate electrode based on factors such as the type of metal being welded, the welding position, and the desired weld characteristics. The electrode consists of a metal core coated with a flux material, which plays a crucial role in shielding the weld from atmospheric contamination. With the electrode securely held in the electrode holder, the welder strikes an arc by bringing the electrode into contact with the work piece and quickly withdrawing it to create a gap. This action initiates the electric arc, which generates intense heat, melting both the electrode and the base metals. As the electrode melts, the flux coating decomposes, releasing gases that form a protective shield around the weld area, preventing atmospheric contamination and ensuring the integrity of the weld. The flux also forms a layer of slag, which helps to trap impurities and improve the quality of the weld. The welder moves the electrode along the joint, carefully controlling the arc length, travel speed, and angle to achieve the desired weld bead size, shape, and penetration. Proper technique and consistent

movement are essential to ensure uniform weld quality and prevent defects such as undercutting, porosity, or incomplete fusion. Once the weld is completed, the electrode is removed from the work piece, and the slag is removed using a wire brush or chipping hammer. The weld area is then inspected visually or using non-destructive testing methods to ensure compliance with welding standards and specifications.

The welding technique employed in Shielded Metal Arc Welding (SMAW) varies depending on factors such as the type of electrode, the composition of the workpiece, and the position of the joint being welded. These factors also influence the welding speed, with different techniques required for flat, sloped, vertical, or upside-down welding positions. For flat welds, which require minimal operator skill, electrodes that melt quickly but solidify slowly are often used. This allows for higher welding speeds since the electrode can be deposited rapidly without compromising the integrity of the weld. In contrast, welding in sloped, vertical, or upside-down positions demands greater operator skill and precision. In these scenarios, electrodes that solidify quickly are preferred to prevent the molten metal from flowing out of the weld pool. However, such electrodes tend to melt more slowly, necessitating a slower welding speed to ensure proper fusion and penetration. Despite the slower welding speed, the use of quick-solidifying electrodes is essential for maintaining the structural integrity of the weld in challenging positions.

3.1.3 Equipment: -

Ultimately, the selection of the appropriate welding technique, electrode type, and welding speed is critical to achieving high-quality welds with SMAW across various welding positions and work piece compositions. It requires careful consideration of factors such as weld joint configuration, material thickness, and desired weld characteristics to ensure optimal welding performance and weld integrity. Top of Form

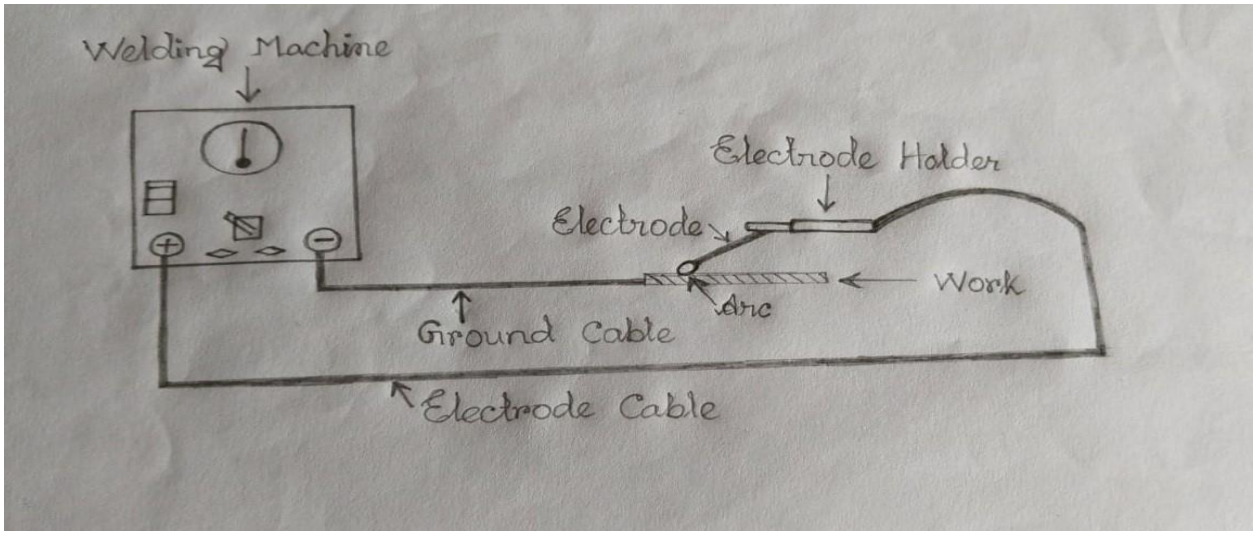

Fig 3.1: SMAW system setup

Shielded Metal Arc Welding (SMAW) equipment typically comprises a constant current welding power supply, an electrode holder, a ground clamp, and welding cables, also referred to as welding leads

i) Power supply:

Fig 3.2- Power supply

The power supply utilized in Shielded Metal Arc Welding (SMAW) typically features a constant current output, ensuring that the current level, and consequently the heat generated, remains relatively stable even if there are variations in arc distance and voltage. This consistency is crucial, especially in manual welding applications where the operator directly controls the welding torch. By maintaining a constant current output, the power supply helps to stabilize the welding arc, making it easier for the operator to maintain a consistent arc length and achieve uniform weld bead characteristics. This is particularly advantageous in SMAW, where the welding electrode is consumed as it melts into the weld pool. Using a constant current power source is preferred over a constant voltage source in SMAW because it minimizes fluctuations in heat output, ensuring more predictable and controlled welding conditions. With a constant voltage power supply, changes in arc length can lead to significant variations in heat input, making it challenging for welders to maintain weld quality and consistency. While the current output in SMAW power supplies is generally constant, skilled welders can manipulate the arc length slightly to introduce minor fluctuations in current, allowing for finer control over the welding process. This level of precision is beneficial when executing complex welds or when adjusting for variations in work piece geometry.

In Shielded Metal Arc Welding (SMAW), the choice of polarity—whether it's direct current electrode negative (DCEN), direct current electrode positive (DCEP), or alternating current (AC)—plays a crucial role in controlling the welding process and influencing weld characteristics. When using DCEN, where the electrode is negatively charged, heat accumulates primarily on the electrode. This leads to faster electrode melting but results in shallower weld penetration. Conversely, switching to DCEP, with the electrode positively charged, directs more heat into the work piece, promoting deeper weld penetration. Alternating current (AC) offers a balance between electrode melting rate and weld penetration by continuously changing polarity. With AC, the electrode alternates between positive and negative charges, effectively distributing heat evenly between the electrode and the work piece.

This rapid polarity reversal, occurring hundreds of times per second, ensures a more uniform heat distribution, enhancing weld quality and consistency.

Shielded Metal Arc Welding (SMAW) equipment typically comprises a step-down transformer and a rectifier, crucial components for converting high-voltage alternating current (AC) into lower-voltage direct current (DC) suitable for welding. The welding transformer is integral in this process, as it steps down the voltage from the mains supply to a level conducive for welding. This transformation is essential because the high-voltage AC power from the mains is unsuitable for welding applications. By reducing the voltage and increasing the current, the transformer ensures that the welding process operates within the desired parameters. For instance, whereas the mains supply may deliver electricity at 220 volts and 50 amps, the transformer modifies these values to a more suitable range, typically around 17–45 volts and currents of up to 600 amps. This adjustment is crucial for achieving the necessary heat output and weld quality during the SMAW process.

ii) Electrode:

Fig 3.3- Electrode

The selection of the electrode in Shielded Metal Arc Welding (SMAW) is influenced by various factors, such as the material being welded, the welding position, and the desired characteristics of the weld. Each electrode is enveloped in a metal compound known as flux, which serves multiple functions during the welding process. Primarily, the flux coating undergoes decomposition when exposed to the heat of the arc, emitting gases that establish a shielding environment around the weld. This shield effectively prevents atmospheric impurities, like oxygen and nitrogen, from infiltrating the weld zone, thereby preserving the integrity of the weld joint. Secondly, the flux comprises deoxidizing agents that aid in eliminating impurities from the weld metal, resulting in a cleaner and stronger weld. By removing oxides and other undesirable elements, these deoxidizers contribute to the overall quality and robustness of the weld. Additionally, the flux coating facilitates the creation of a protective slag layer on the surface of the weld bead. This slag acts as a barrier, shielding the molten weld pool from external factors and preventing oxidation or contamination. Moreover, the slag helps regulate the cooling rate of the weld, promoting proper solidification and reducing the likelihood of defects. Furthermore, the flux coating enhances the stability of the welding arc, ensuring consistent performance and improved control over the welding process. A stable arc is essential for achieving precise weld deposits and minimizing spatter, resulting in cleaner and more uniform welds. Lastly, the flux may contain alloying elements that are incorporated to enhance specific properties of the weld, such as increased strength, corrosion

resistance, or improved mechanical properties. These alloying components tailor the weld composition to meet the specific requirements of the application, enhancing the overall performance and durability of the welded joint.

Electrodes in Shielded Metal Arc Welding (SMAW) are categorized based on their melting and solidification characteristics. "Fast-fill" electrodes melt quickly, enabling high welding speeds. Conversely, "fast-freeze" electrodes solidify rapidly, stabilizing the weld pool and facilitating welding in various positions. Intermediate electrodes, known as "fill-freeze" or "fast-follow" electrodes, offer a balance between melting and solidification rates, accommodating different welding conditions.

Electrodes in Shielded Metal Arc Welding (SMAW) often have cores resembling the base material, but occasionally differ significantly for specific applications. For instance, stainless steel electrodes may be employed to weld carbon steel pieces or to join stainless steel with carbon steel components.

Electrode coatings can comprise various compounds like rutile, calcium fluoride, cellulose, and iron powder. Calcium fluoride (CaF2) electrodes, termed basic or low-hydrogen, are hygroscopic and require dry storage. They create robust welds, albeit with a coarse, convex joint surface. Cellulose-coated electrodes, especially when combined with rutile, offer deep weld penetration. However, due to their high moisture content, special precautions are necessary to prevent excessive cracking risks. Additionally, iron powder is commonly added to coatings to enhance electrode productivity, potentially doubling the yield.

iii) The Electrode Holder: -

Fig-3.4 - The electrode holder

An electrode holder, also known as an electrode clamp or electrode tong, is an essential component in shielded metal arc welding (SMAW) and other welding processes. Its primary function is to securely hold the welding electrode while allowing the welder to manipulate it during the welding operation. The electrode holder consists of several key parts, each serving a specific purpose. At its core is a durable metal body, often made of copper alloy or other heat-resistant materials, designed to withstand the high temperatures generated during welding. This

body houses a spring-loaded mechanism that applies pressure to grip the welding electrode firmly in place. The front end of the electrode holder features a jaw or clamp mechanism that securely grips the electrode. This mechanism can typically be adjusted to accommodate electrodes of different diameters, ensuring compatibility with various welding applications. The jaws are usually serrated to provide a better grip on the electrode, minimizing the risk of slippage during welding. The rear end of the electrode holder is equipped with an insulated handle, often made of heat-resistant materials such as rubber or fiberglass. This handle provides a comfortable and secure grip for the welder while also insulating them from electric shocks. Additionally, the handle may feature ergonomic designs or contours to reduce hand fatigue during prolonged welding sessions. To ensure electrical conductivity, the electrode holder contains internal wiring that connects the electrode to the welding machine via a flexible welding cable. This cable is typically attached to the rear of the electrode holder and secured with sturdy connectors or terminals. Proper electrical connections are crucial for maintaining a stable arc during welding and ensuring consistent weld quality. Some electrode holders also incorporate safety features such as heat-resistant shields or insulation to protect the welder from burns and electric shocks. These additional features enhance operator safety and comfort, particularly when welding at high temperatures or in challenging environments.

iv) The Ground Clamp: -

The ground clamp, also known as the earth clamp or grounding clamp, is an essential component in welding operations, particularly in shielded metal arc welding (SMAW) and other processes where a complete electrical circuit is necessary for welding to occur. Its primary function is to establish a secure electrical connection between the welding work piece and the welding machine's power source, thereby completing the electrical circuit required for welding. The ground clamp consists of a sturdy metal body, typically made of copper or brass, which serves as the conductor for the electrical current. It features a clamp mechanism at one end, designed to securely attach to the work piece being welded. The clamp mechanism often includes serrated jaws or teeth to provide a firm grip on the work piece, ensuring good electrical contact and minimizing the risk of slippage during welding. The other end of the ground clamp is equipped with a terminal or connector that allows it to be attached to the welding machine's ground cable. This cable, usually made of flexible copper wire covered in insulation, carries the electrical current from the welding machine to the ground clamp and ultimately to the work piece. Proper connection between the ground clamp and the welding machine is essential for maintaining a stable electrical circuit and ensuring the success of the welding operation. In addition to providing electrical conductivity, the ground clamp also serves an important safety function. By establishing a reliable electrical ground, it helps prevent the build-up of electrical charges on the work piece and reduces the risk of electric shock to the welder or damage to the welding equipment. Proper grounding is crucial for safe and effective welding, especially when working with high currents or in environments where electrical hazards may be present. Overall, the ground clamp is a critical component in welding operations, facilitating the flow of electrical current necessary for welding while also ensuring the safety of the welder and the integrity of the welding equipment. Its robust construction, secure clamp mechanism, and reliable electrical conductivity make it an indispensable tool in the welding process.

v) Welding Cables-

Fig-3.5. Welding Cable

Welding cable is a specialized type of electrical cable designed for use in welding applications, where it serves as the primary conductor for delivering electrical current from the welding machine to the welding electrode or torch. It plays a crucial role in maintaining a stable and efficient electrical circuit during welding operations.

Welding cables are constructed to withstand the harsh conditions typically encountered in welding environments, including exposure to heat, sparks, oil, grease, and mechanical stress. They are often subjected to bending, twisting, and abrasion during use, so they must be highly durable and flexible to withstand these demands

The construction of welding cables typically consists of several components:

Conductor: The conductor is the central core of the cable through which electrical current flows. Welding cables are usually made of highly conductive copper strands to minimize electrical resistance and heat build-up.

Insulation: The conductor is surrounded by a layer of insulation, typically made of synthetic rubber or thermoplastic materials. The insulation provides electrical insulation to prevent short circuits and electrical shocks while also protecting the conductor from physical damage and environmental hazards

Jacket: The outer layer of the welding cable is called the jacket, which provides additional protection to the cable and insulation layers. The jacket is usually made of durable and flame-resistant materials to withstand the heat and sparks generated during welding.

Welding cables come in various sizes (gauges) and lengths to accommodate different welding applications and power requirements. Thicker cables with larger conductor sizes are used for higher current welding processes, while thinner cables are suitable for lighter-duty welding tasks.

3.1.4 Quality: -

Common quality issues encountered in SMAW include porosity, inadequate fusion, insufficient penetration, and weld cracking. Although weld spatter does not compromise the

weld's integrity, it detracts from its visual appearance and necessitates additional cleaning efforts.

Common issues such as porosity, inadequate fusion, insufficient penetration, and weld cracking can arise from various factors. Excessive current, prolonged arc length, and arc blow—caused by magnetic forces deflecting the electric arc—can induce porosity. Joint contamination, rapid welding speed, and long arc length, particularly with low-hydrogen electrodes, can also contribute to porosity. While not always visible, porosity poses a significant risk to weld strength. Inadequate fusion, often visible, results from low current, contaminated joint surfaces, or improper electrode selection. Shallow penetration, which weakens weld strength, may necessitate adjustments to welding speed, current, or electrode size. Additionally, factors like high carbon, alloy, or sulfur content in the base material increase the likelihood of cracking, especially in the absence of low-hydrogen electrodes and preheating.

Moreover, it's crucial to avoid over-restraining the work pieces during welding, as this can lead to the accumulation of residual stresses within the weld. As the weld cools and contracts, these residual stresses can promote cracking, compromising the integrity of the weld.

3.1.5 Safety:

Shielded Metal Arc Welding (SMAW) poses potential hazards if safety measures aren't observed. The process involves an exposed electric arc, increasing the risk of burns, which can be mitigated with appropriate personal protective gear like heavy-duty leather gloves and long-sleeved jackets. Moreover, the intense brightness of the welding area can cause arc eye, an eye condition resulting from UV light exposure that inflames the cornea and damages the retinas. Welders use specialized helmets with dark face plates to shield their eyes from this harmful light, with newer models featuring self-darkening face plates for added convenience. Transparent welding curtains are also commonly used to enclose the welding area, protecting nearby workers from UV exposure. However, it's important to note that these curtains should not replace the filter glass in welding helmets.

Moreover, the vaporization of metal and flux materials during SMAW exposes welders to hazardous gases and particulate matter. The smoke generated contains oxide particles of varying types, with the size of these particles influencing the toxicity of the fumes. Smaller particles pose a higher risk. Additionally, gases such as carbon dioxide and ozone may form, posing dangers if proper ventilation is lacking. To address this, some modern welding masks feature an electric-powered fan designed to aid in the dispersal of harmful fumes.

3.1.6 Application and Materials: -

Due to its adaptability and straightforwardness, shielded metal arc welding (SMAW) has been particularly prevalent in the maintenance and repair sector, as well as extensively utilized in erecting steel structures and industrial fabrication. While its usage has seen a decline with the emergence of flux-cored arc welding in construction and the growing popularity of gas metal arc welding in industrial settings, SMAW's affordability and versatility ensure its continued relevance. This is especially true for hobbyists and small businesses, where specialized welding methods may not be financially viable or essential. The thickness of the material suitable for SMAW is primarily determined by the skill level of the welder, typically not dropping below 1.5 mm.

There are some advantages and disadvantages of this welding process is discussing below: -

Merits: -

Portability: SMAW equipment is relatively compact and portable, allowing for welding in various locations, including remote or outdoor settings.

Versatility: It can be used to weld a wide range of materials, including carbon steel, stainless steel, cast iron, and non-ferrous metals like aluminum and copper.

Simple Equipment: SMAW equipment is straightforward and requires minimal setup, making it accessible to beginners and professionals alike.

Cost-Effectiveness: Compared to some other welding methods, SMAW is relatively inexpensive in terms of equipment and consumables, making it suitable for budget-conscious projects.

High Penetration: SMAW can achieve deep weld penetration, making it suitable for welding thick materials and creating strong, durable welds.

Suitable for Outdoor Use: The flux coating on SMAW electrodes provides a protective shield against atmospheric contamination, making it ideal for outdoor welding where wind and other environmental factors may affect the weld.

No External Shielding Gas Required: SMAW electrodes contain flux, which generates a shielding gas when heated, eliminating the need for external shielding gas cylinders.

Less Sensitivity to Surface Cleanliness: SMAW can tolerate some degree of surface contamination, making it more forgiving in less-than-ideal welding conditions.

Demerits: -

Low Productivity: SMAW typically has lower deposition rates compared to other welding processes, resulting in slower welding speeds and lower productivity, especially for larger projects.

Limited Welding Positions: SMAW is less suitable for welding in overhead or vertical positions, particularly for novice welders, as controlling the weld pool can be challenging.

Slag Removal: The flux coating on SMAW electrodes produces slag, which must be removed after each pass. Slag removal can be time-consuming and labour-intensive, particularly for large welds.

High Skill Requirement: SMAW requires a high level of skill and experience to produce quality welds consistently. Novice welders may struggle with maintaining arc length, controlling weld bead shape, and managing slag effectively**.**

Limited Joint Access: SMAW electrodes are relatively short, limiting access to tight or confined spaces. This can make welding in complex or restricted areas challenging.

Potential Porosity: Improper welding technique, such as excessive moisture in the electrode flux or inadequate cleaning of the base metal, can result in weld porosity, reducing the weld's strength and integrity.

Health and Safety Risks: Like all welding processes, SMAW generates fumes, gases, and ultraviolet radiation, posing health and safety risks to welders. Proper ventilation, personal protective equipment, and safety training are essential to mitigate these risks.

Environmental Impact: The flux coatings used in SMAW electrodes contain various compounds, some of which may be harmful to the environment if not disposed of properly. Waste management and recycling of electrode packaging and slag are essential to minimize environmental impact.

Arc blow can occur during stick welding when using Direct Current (DC) due to the magnetic

Field generated around the electrode and base metal. This magnetic field can disrupt the arc, leading to an unstable weld puddle and excessive spatter. However, this issue can be mitigated by utilizing Alternating Current (AC) or adjusting the positioning of the ground

Clamp. With AC, the constantly changing direction of current prevents the build-up of a strong magnetic field, reducing the likelihood of arc blow and ensuring a more stable weld.

Chapter 4

Experimental Procedure

4. Experimental Procedure:

4.1 Introduction: - This section focuses on the experimental procedures conducted and methodologies employed in the current investigation. Specifically, it covers the procedures involved in fabricating tensile specimens, assessing the performance of 316L austenitic stainless steel (ASS) tensile specimens, and analysing the mechanical properties of the weld zone in the tensile specimens. By outlining these steps, the chapter provides a comprehensive overview of the experimental setup and methodology utilized in the study. Through these experiments and evaluations, researchers aim to gain insights into the behavior and characteristics of the materials under investigation, thereby contributing to the broader understanding of their mechanical properties and performance.

4.2 Core Wire of 316L Electrode: -

In this research, the rimming wires utilized for welding the 316L austenitic stainless steel (ASS) electrode, measuring 3.15 mm in diameter and 450 mm in length, were procured from commercial sources. The core wires were meticulously inspected to ensure they were devoid of any impurities such as dirt, oil, rust, or other forms of contamination. This meticulous examination was crucial to maintain the integrity and purity of the welding materials, thereby facilitating accurate and reliable experimental results.

4.2.1- Composition Of 316 L Electrode:

Elements	C	Si	Mn	Cr	Mo	Ni	Al	Cb	Cu
Wt.%	0.028	0.282	1.24	16.62	2.14	10.2	0.008	0.063	0.3

4.3 Backing Oven:

A backing oven is a piece of equipment used in welding processes, particularly in the field of shielded metal arc welding (SMAW). It is essentially an oven used to preheat welding electrodes before they are used in welding operations. Preheating the electrodes helps to remove any moisture that may have been absorbed, ensuring that they burn cleanly and consistently during the welding process. Additionally, preheating can help to reduce the risk of hydrogen-induced cracking in the weld metal.

The backing oven typically maintains a controlled temperature suitable 2500c and For 2 hours welding electrode being used. This temperature 2500 c is designed to effectively remove moisture without damaging the electrodes. By keeping the electrodes dry and at the optimal temperature, the backing oven contributes to the overall quality and integrity of the welds produced during welding operations.

4.4 Welding Procedure and Grooving Design: -

Welds were applied to a 316L ASS plate with a thickness of 22 mm, where a groove was prepared according to the groove design illustrated in Fig. 4.1. The groove was created by joining two plates with a backing strip. Additional steel pieces were welded on both sides of the joint groove to allow for the initiation and termination of the arc. This facilitated the extraction of more specimens from the weld deposits. The welding parameters specified in

Table 4.2 were employed in accordance with the standard AWS SFA - 5.1. The electrode was positioned at approximately a 45-degree angle along the welding direction using DC (+), and a total of 10 passes were necessary to completely fill the groove**.**

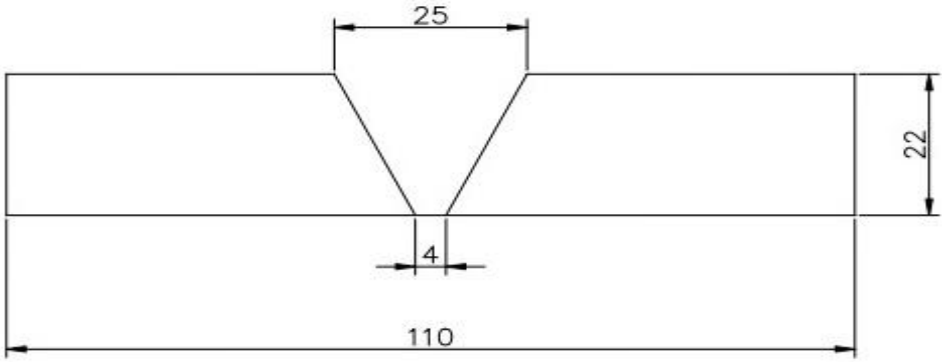

Fig 4.1- groove design

Table 4.1- Base metal and groove angle for test assembly

Plate length (mm)	Plate Width (mm)	Plate thickness (T) (mm)	Backing strip width (mm)	Root opening (mm)	Groove angle (mm)
300	120	22	60	5	30

4.5 Test Assembly and Location of Test Specimen: -

For each test weld assembly, tensile specimens, transverse V-notch Charpy specimens, and metallography specimens were extracted. The specific locations for each type of specimen are illustrated in Fig. 4.2. All-weld tensile specimens were prepared to evaluate the tensile strength of the weld metal. Transverse V-notch Charpy specimens were used to assess the impact toughness across the weld. Metallography specimens were collected to examine the microstructure and phase distribution within the weld zone. This approach ensured a comprehensive analysis of the mechanical and structural properties of the welds, facilitating a thorough evaluation of the welding process and its effects on the material.

Figure 4.2 - Test assembly and location of the test specimen and groove design

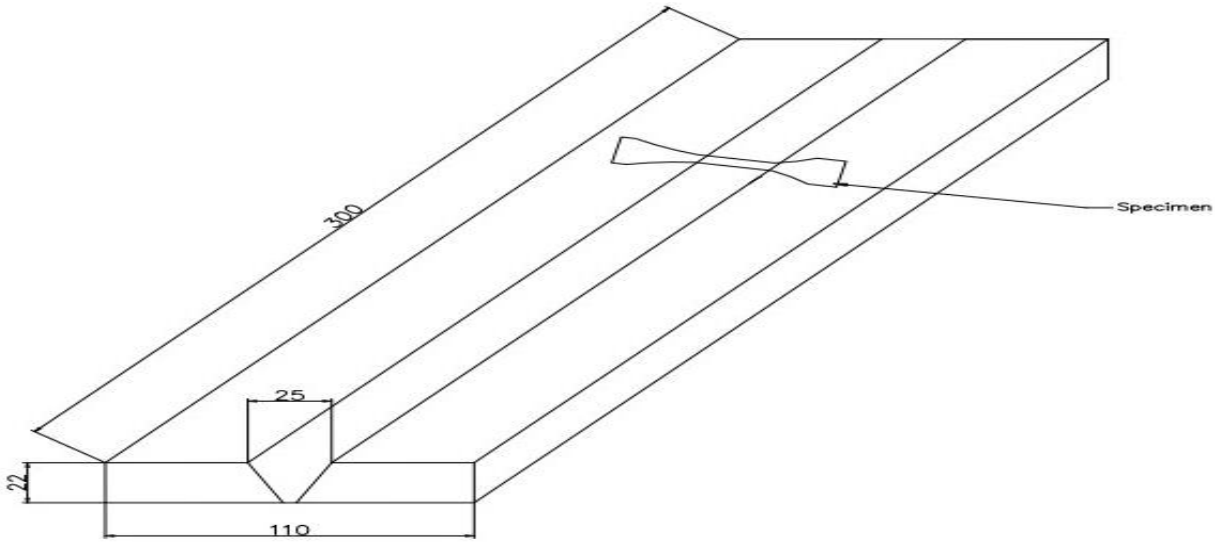

Fig- 4.3 - Prepared test assembly

4.6 Welding Parameter Used for Experimental Electrode on 316L ASS:

Table 4.2 - Welding parameter

Current type	DC (+)
Welding current	90 amp
Open circuit voltage	68
Welding voltage	28 (average)
Welding speed	
Interpass temperature	150 ^{0}C -250 ^{0}C

4.7 Preparation of Weld Pad:

The weld pad prepared for chemical analysis is illustrated in Fig. 4.4. To obtain undiluted weld metal, the filler metal was deposited on 316L ASS in the flat position using multiple layers. The preheat temperature and the interpass temperature were maintained below 150 °C, and the slag was carefully removed after each pass. The dimensions of the completed pad are provided in Table 4.3. This method ensured the production of high-quality weld metal, suitable for accurate chemical analysis. By adhering to these parameters, the integrity and purity of the weld metal were maintained, facilitating precise assessment of its chemical composition.

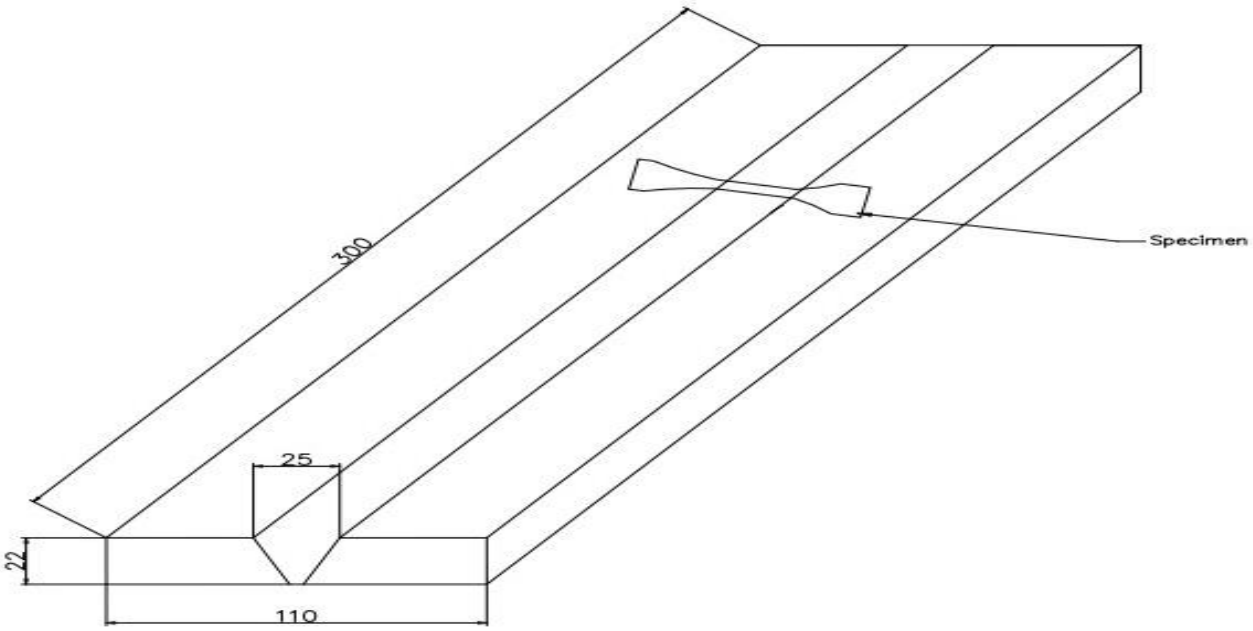

Fig 4.4- weld pad preparation for chemical analysis

Table 4.3- The dimension of weld pad on 316L ASS

Number of layer in height	10
Height of the layer	22 mm
Length of the deposited weld metal at surface	300 mm
Width of the deposited weld metal at surface	110 mm

Fig-4.5- Before Welding

Fig-4.6- After Welding

4.8 Chemical composition of 316 L ASS:

Table 4.4: Chemical composition of the 316 L stainless steel

Element	C	Mn	Si	S	P	Ni	Cr	Mo	N
Wt. %	0.016	0.94	0.404	0.0020	0.044	10.023	16.36	2.02	0.031

4.9 Chemical composition of 316 L ASS in Weld Zone

Table 4.5: Chemical composition of the 316 L Austenitic stainless steel in Weld Zone

Element	C	Si	Mn	S	P	Ni	Cr	Mo	N
Wt. %	0.022	1.06	0.62	0.016	0.045	11.82	17.23	2.57	0.103

4.10 Sample Preparation for Tension test:

The dimensions of the all-weld tensile specimens were prepared according to the AWS SFA 5.1 standard. The gauge length (G), gauge diameter (D), fillet radius (F), and grip diameter (B) are specified in Fig 4.7. Tensile tests were performed using a Servo-Electric (Instron 8862 M-1(CFI-625) type universal testing machine with a 100 KN capacity, applying a strain rate of 0.5 mm/min. The tensile specimens were securely gripped axially, and the load was steadily increased by the actuator. During the tests, load and displacement histories were simultaneously recorded. The tests concluded when the specimen fractured completely into two separate pieces. Key tensile test data, including yield strength (YS), ultimate tensile strength (UTS), and percent elongation, were documented.

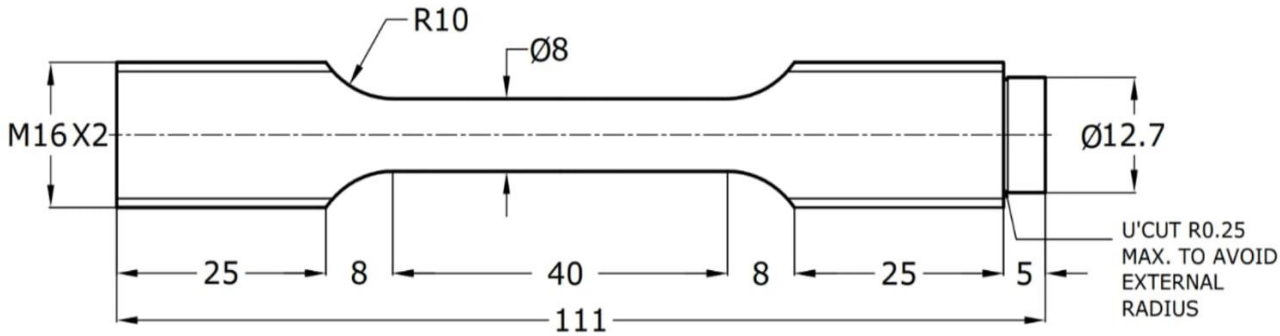

Fig-4.7 - Tensile test specimen geometry

Fig-4.8 a = Tensile test specimen

4.11 Tensile Test:

The dimensions of the all-weld tensile specimens were prepared in accordance with the AWS SFA 5.1 standard, with the gauge length (G), gauge diameter (D), fillet radius (F), and grip diameter (B). Tensile tests were carried out using a Servo-Electric (Instron 8862) universal testing machine, which has a capacity of 100 KN, applying a strain rate of 0.5 mm/min. The specimens were held securely in place axially, and the actuator gradually increased the load. Throughout the tests, the load and displacement data were recorded simultaneously. The tests were concluded when the specimen fully fractured into two separate pieces. Key tensile test results, such as yield strength (YS), ultimate tensile strength (UTS), and percent elongation, were documented. We have test sample in room temperature and high temperature.

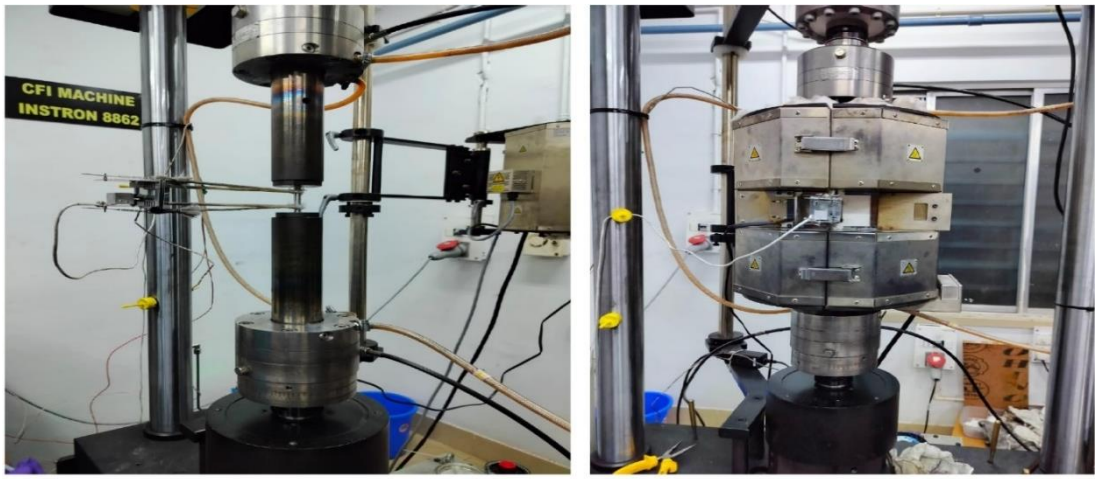

Fig- 4.9 – Pre-test Tensile Specimen

Room temperature after test sample

High temperature After test sample

Fig – 4.10- After testing Tensile Specimen

4.12 Fracture Analysis of Samples Subjected to Monotonic Deformation:

SEM micrographs were obtained from the fracture surfaces of the specimens which had failed under monotonic tensile loading at different temperature.

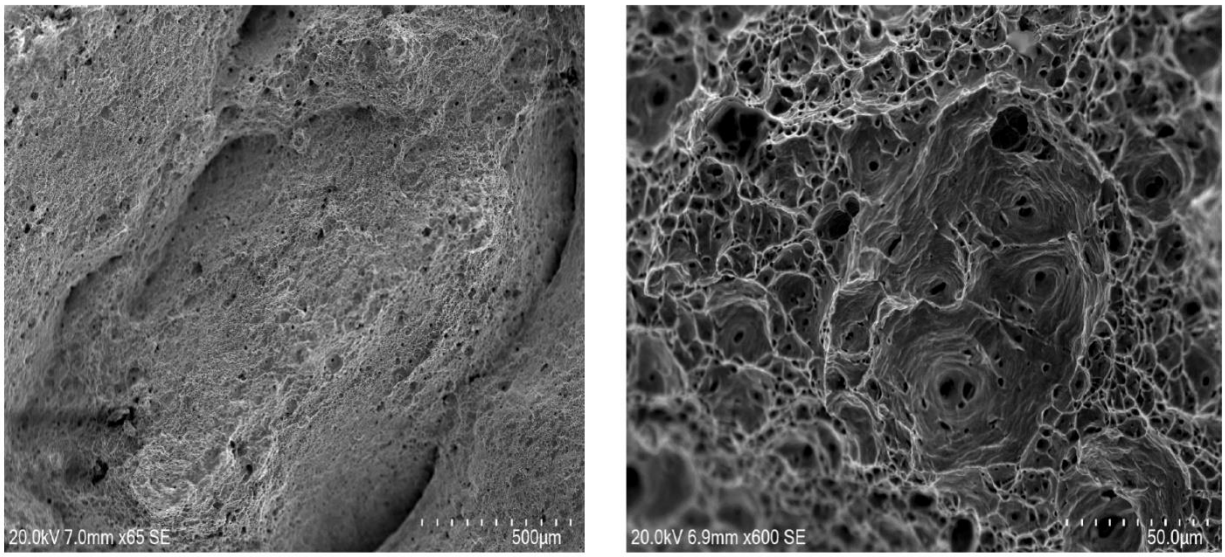

Room Temperature fracture

Figure 4.11: Room temperature fractographic images

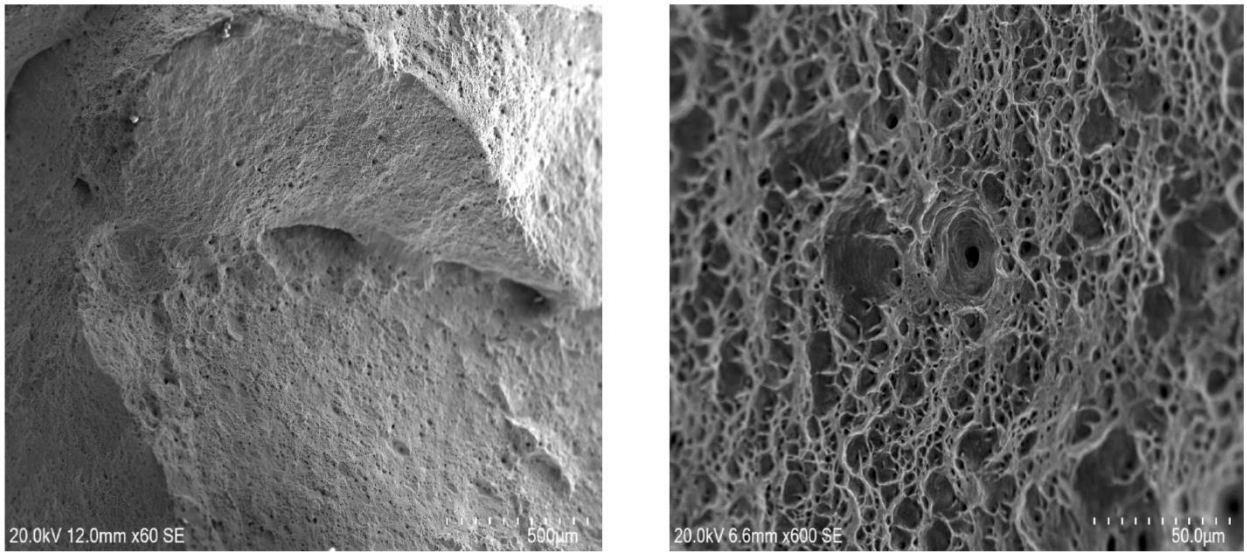

Figure 4.12: High temperature fractographic images

4.13 Sample Preparation for Microstructure:

The preparation of samples for optical microscopy involved several stages. It was crucial to ensure that the specimen's surface was mirror-polished, free of unevenness or scratches, to obtain a clear microstructural image. Variations in the material's surface could influence the microstructure of a sample, making the preparation process for microscopy a critical aspect. Achieving a true surface was challenging, especially when manual polishing was required, as soft or ductile materials could deform during mechanical polishing. To address this, various abrasion procedures were employed to prepare the samples in different orientations, followed by cloth polishing and etching.

4.13.1 Grinding:

To develop the microstructures of various weld metals, the sample preparation begins with flattening the surface using a grinding wheel, followed by a belt grinder. Surface layers damaged by cutting and excessive surface roughness were removed through grinding. The specimens were ground using a belt conveyor equipped with emery paper of 60 grit, while an appropriate coolant (water) was applied to remove debris and dissipate heat

4.13.2 Paper Polishing:

For surface polishing of the samples, silicon carbide paper was used, and the polishing was carried out manually on a wooden table. The coarseness of the paper is indicated by a number, representing the number of silicon carbide grains per square inch. A lower number indicates coarser paper, while a higher number signifies finer emery paper; for example, 1200-grit paper is finer than 400-grit. The grinding process involves multiple stages, with each successive stage using finer paper (a higher number). Each stage removes the scratches left by the previous one.

This is done by orienting the specimen perpendicular to the direction of the previous scratches and ensuring these earlier scratches are completely removed. Between each grade of paper, the specimen was thoroughly washed with soapy water to prevent contamination by coarse grit on the surface. Typically, the grades of paper used progressively, from coarsest to finest, were 120, 180, 400, 800, 1200, 1500, 2000, 2500, and 3000. Paraffin was applied to the paper to ensure smooth polishing, acting as a lubricant to reduce heat and prevent debris build up on the surface. Finally, the specimens were thoroughly rinsed with water, followed by alcohol, and then left to dry.

4.13.3 Cloth Polishing:

Polishing discs were covered with a soft cloth embedded with abrasive diamond particles. Two different grades of particles were used: a coarser grade, typically with micron-sized particles, which removed scratches from the final grinding stage, and a finer grade, typically with diamond particles of 1 micron in diameter, to achieve an extremely smooth surface. Before switching to a finer polishing wheel, the specimen was thoroughly cleaned with warm soapy water followed by alcohol to prevent disc contamination, as debris could become embedded in the surface. Alumina (Al2O3) paste with a grit size of 0.25 μm was applied during polishing to achieve a scratch-free, mirror-like finish, with water being continuously fed over the specimen during the process. Cloth polishing continued until all scratches were completely removed, which was verified by viewing the surface under an optical microscope.

Figure - 4.11 - Cloth Polishing machine

4.13.4 Etching:

Etching was performed to reveal the prominent microstructure of the metal surface by selectively chemically attacking the high-energy sites, as well as to remove the thin deformed layer introduced during polishing. In alloys containing more than one phase, etching creates contrast between different regions due to variations in topography or reflectivity**.**

The polished surface was etched using an etchant prepared by carefully mixing 70% HCl and 30% HNO_3 in a 100 ml solution, which was kept in a small glass container. The etchant was applied using a cotton bud, gently wiped over the surface a few times. The specimen was then immediately rinsed with distilled water, washed in alcohol, and dried using a dryer. Care was

taken to avoid over-etching, as this could obscure the key features intended for observation. To prevent hand contamination and further scratching, the surface of the specimen was always covered with a small piece of paper or cloth. After these steps, the samples were ready for microstructural imaging under an optical microscope.

4.14 Microstructure Observation Using an Optical Microscope:

The specimens for the test were polished metallographically and etched prior to microscopic examination. A metallurgical optical microscope equipped with accessories was used to capture optical micrographs at various magnifications. **The Machine used Model LEICA DM2700 M coupled with a digital camera interfaced with a personal computer using a software LASV 12.4.**

Ideally, the surface to be examined optically was kept flat and level by embedding the specimen in plastic clay, which was placed on a microscope glass slide beneath the lens. The slide was levelled by adjusting the levelling wheels, ensuring that the entire field of view was in focus for clear imaging.

Fig 4.12: Optical Microscope

4.15 Micro Hardness Measurement:

After capturing images with optical microscopy, samples were subjected to micro-hardness testing using a Vickers hardness tester. The hardness values were obtained on the HV scale, with 10 measurements taken along the horizontal axis of the polished surface. The test was

performed in the micro-force range, applying a load of 200 gmf with a dwell time of 15 seconds.

4.16 SEM & EDX (Scanning Electron Microscopy and Energy Dispersive Spectroscopy):

Metallographic phase analysis and chemical/elemental characterization of the base sample and the four age-hardened samples were conducted using a HITACHI SU 3800 Scanning Electron Microscope in secondary electron imaging mode.

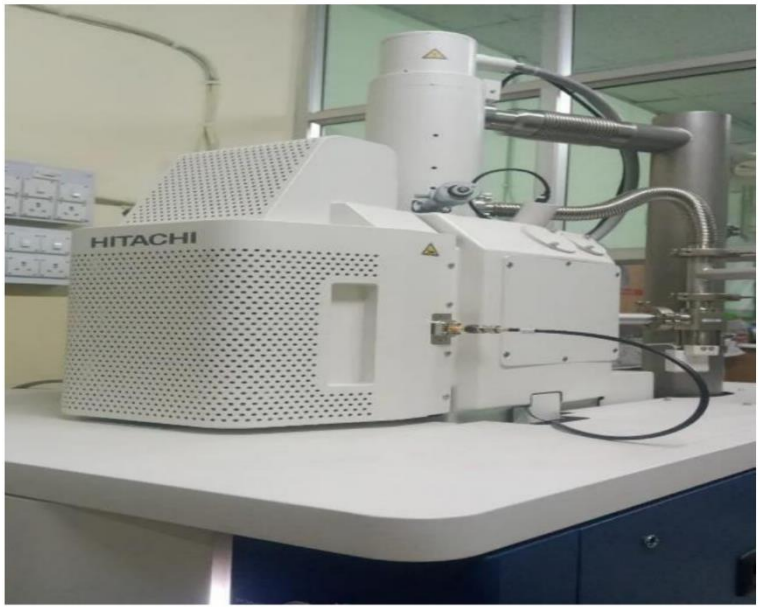

Fig - 4.13 - Scanning Electron Microscope

4.17 X-Ray Diffraction (XRD):

X-ray Diffraction was performed to examine the diffraction patterns and crystallographic phases of the samples using an X-ray diffractometer (Rigaku Smart Lab Japan), model Ultima III, operating at 40 kV and 30 mA (1.2 kW), and equipped with Smart Studio II software. The XRD instrument was set up with the necessary measurement parameters, including a copper beam target with a wavelength of 1.5406 Å, a scanning range of 10° to 100°, and a scanning rate of 2 degrees per minute.

X-ray diffraction (XRD) is a powerful analytical technique used to obtain detailed information about the chemical composition and crystallographic structure of both natural and synthetic materials. It allows for the determination of various properties such as phase, particle size, crystal defects, and grain size.

In this study, we utilized an X-ray diffractometer with Cu-Kα radiation, which has a wavelength of 1.5406 Å. The X-rays were directed at the sample mounted on a sample holder, and the intensity of the reflected X-rays was recorded as a function of the angle (2θ) at which the incident beam was deviated. Strong reflections occur when Bragg's law is satisfied:

$$2d\sin\theta=\lambda$$

Here, d represents the interplanar spacing, λ is the wavelength of the X-ray, and θ is the glancing angle.

Fig- 4.14 - XRD Machine

Depending on the crystal structure and lattice parameters, peaks appear at various 2θ values, corresponding to different sets or families of atomic planes.

Among the various XRD techniques, the powder diffraction method is particularly significant due to its applicability to all crystalline substances, including powdered samples. This method is highly convenient for obtaining diffraction data and calculating particle sizes. Powder diffraction data are used to identify single-phase or multi-phase samples by comparing the observed peaks with standard data from JCPDS (Joint Committee on Powder Diffraction Standards) files.

In summary, XRD using powder diffraction is a versatile and widely applicable method for analysing the crystallographic structure and chemical composition of materials. By examining the reflected X-rays and their corresponding angles, we can identify the material's phase composition, particle size, and other structural characteristics.

4.18 Corrosion Tests

Corrosion tests were performed to evaluate the susceptibility of the sample to localized corrosion, such as cracking or pitting, and to assess its ability to form a passive layer through alloying elements in corrosive environments. The goal of the test was to evaluate the material's corrosion resistance and its suitability for use in a line and acidic environments. The study employed an electrochemical technique known as linear polarization resistance. The corrosion potential of the alloys under investigation was analysed using the open circuit potential transient method. Potentiodynamic polarization measurements were utilized to determine key corrosion parameters, including corrosion potential (E-corr), corrosion current (I-corr), and

corrosion rate in mm/year, which indicates material loss due to corrosion in real time, as well as the alloys' capacity to form a passive layer. The corrosion behavior of Austenitic stainless steel 316L weld sample was investigated using Tafel polarization techniques and electrochemical impedance spectroscopy (EIS) with an Auto lab system.

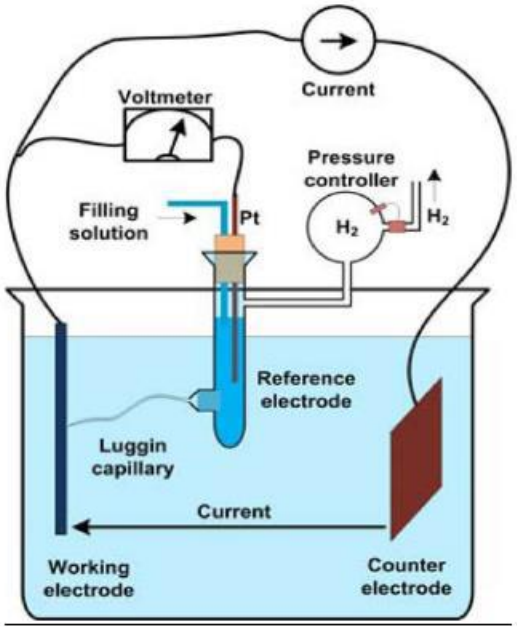

Fig – 4.15: Circuit Diagram of corrosion Test

Pitting Corrosion Test: -

Pitting corrosion occurs when the protective oxide layer on the surface of stainless steel breaks down, allowing the bare metal underneath to become susceptible to a loss of electrons through oxidation in the presence of a corrosive aqueous solution. This electrochemical reaction initiates the formation of small cavities, or "pits." Although usually detectable through thorough visual inspection, these pits can grow deep enough to perforate a tube wall entirely. Pitting corrosion can also facilitate the initiation of cracks in tensile stressed components. Environments with higher chloride concentrations, including those created by evaporation from deposited saltwater droplets, are prone to pitting corrosion—especially at high temperatures. When inspecting metal tubing for pitting corrosion, check for reddish-brown iron oxide deposits and any potential pits that might have developed on the metal surface.

In our thesis work, we are investigating the pitting corrosion on the surface of three specimens after they have undergone tensile testing in a NaCl environment. The aim is to understand the differences in corrosion rates among the three deformed specimens and to examine the corroded surfaces to gain insight into the mechanisms behind these variations. Figure 4.16 illustrates the pitting corrosion mechanism on the surface of stainless steel. Initially, a passive film forms on the stainless steel surface, with the exterior primarily covered by negative hydroxyl ions and the interior by positive iron ions, creating a capacitor-like behavior.

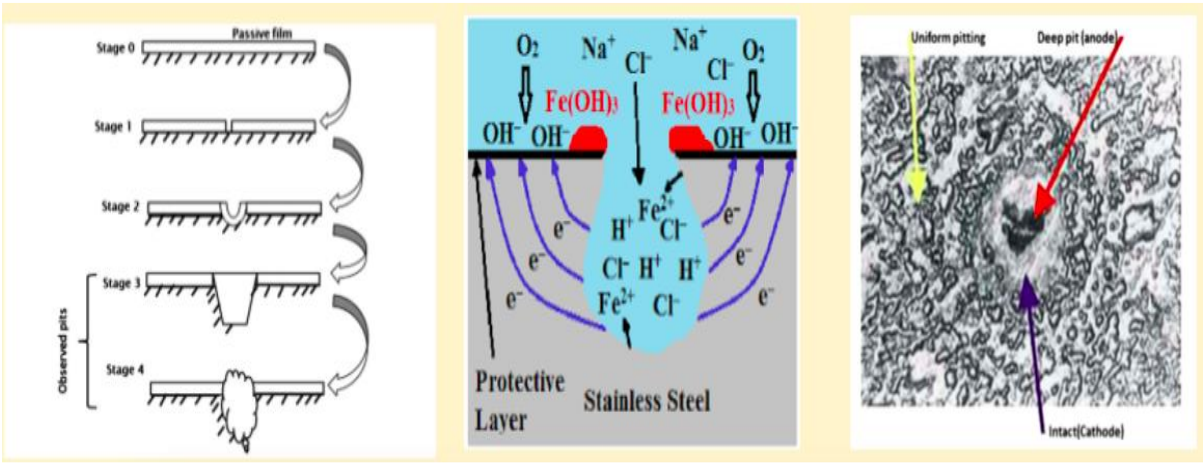

Figure 4.16 Visual aspects of the pitting corrosion on Stainless Steel

The aggressive chloride ions displace the hydroxyl ions and attack the passive film on the stainless steel surface. This interaction with the ferrous ions results in the formation of cavities or pits.

In Figure 4.17, the apparatus used for pitting corrosion testing is shown, where the deformed sample serves as the anode and is connected to the positive terminal of the potentiometer. A graphite electrode, acting as the cathode, is connected to the negative terminal. The potential difference between the working electrodes is measured by the Auto lab software, which then generates the Tafel plot on the computer. From the resulting Tafel plot data, the corrosion potential and the corrosion rate of the deformed specimen are determined

Figure 4.17: Corrosion Testing Auto lab instrument

CHAPTER 5

Result

5.1 Chemical Composition of Base Metal and Weld Metal In ASS 316L

i. Chemical Composition of 316 L ASS:

Table 5.1: Chemical composition of the 316 L stainless steel

Element	C	Mn	Si	S	P	Ni	Cr	Mo	N
Wt. %	0.016	0.94	0.404	0.0020	0.044	10.023	16.36	2.02	0.031

ii. Chemical composition of 316 L ASS in Weld Zone

Table 5.2: Chemical composition of the 316 L Austenitic stainless steel in Weld Zone.

Element	C	Si	Mn	S	P	Ni	Cr	Mo	N
Wt. %	0.022	1.06	0.62	0.016	0.045	11.82	17.23	2.57	0.103

5.2 Tensile Test:

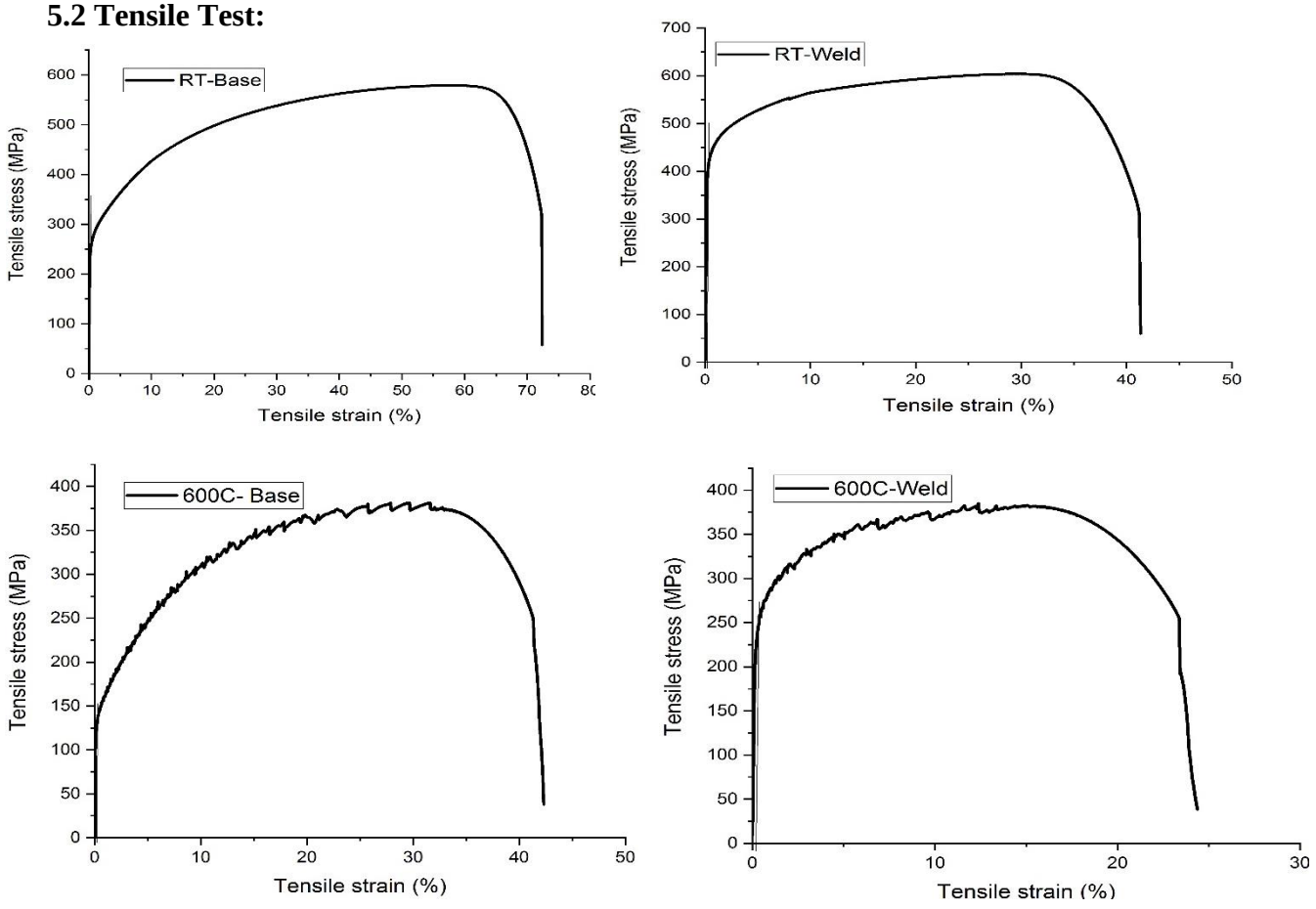

Plot –5.1- Tensile test base sample on room temperature and high temperature

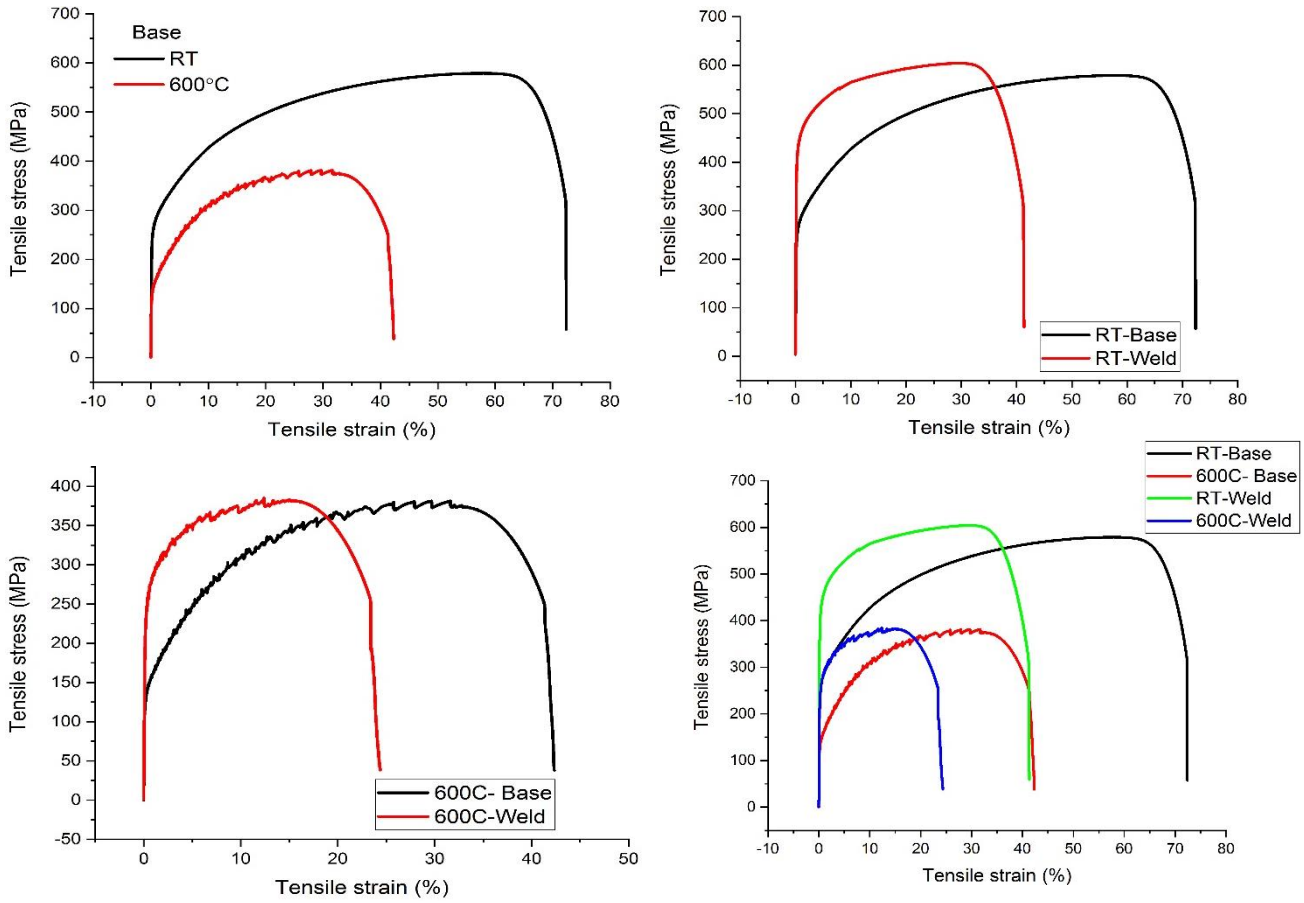

Plot –5.2- Tensile test base sample on room temperature and high temperature

These sample 316L ASS of tensile test is done on Instron M1 (CFI-625) in different condition like room temperature and high temperature and different state like base material and weld material. The engineering stress – engineering strain curve is shown in Plot 5.1 (a-d). When we test base material then we did not see DSA (dynamic strain aging), so, it can be said that DSA varies with testing parameter like temperature. From the literature [38] we got that DSA depends on strain rate and temperature of tests. DSA was observed after testing at high temperature in base material and weld condition. DSA affects the ductility severely [38] which can be seen in Plot 5.2(a). Weld material has decreased ductility and hardness simultaneously.

In plot 5.2 (a), it is observed that the ductility got reduced in case of elevated temperature, 600^0C tested specimen. It is so occurring due to Dynamic strain aging (DSA) of type A is observed at 600^0C. Strength (UTS) is lower in case of 600^0c because the flow is easy at elevated temperature test. Plot 5.2 (b) shows the engineering stress – engineering strain diagram of Base and Weld material at Room temperature. Weld material ductility is very less in comparison to base material due to the microstructural difference between base and weld .Weld material has dendrite structure (fig- 5.5) which is brittle in nature.

Plot 5.2(c) shows the engineering stress – engineering strain diagram of base and weld material tested at 600^0C. It can be observed that weld material shows lesser ductility. It is so that additional ductility reduction due to cellular microstructure (fig-5.6) the strength (UTS) is similar in both the case. Because the strength mostly depends on temperature .

5.3 Microstructure Observed Using an Optical Microscope:

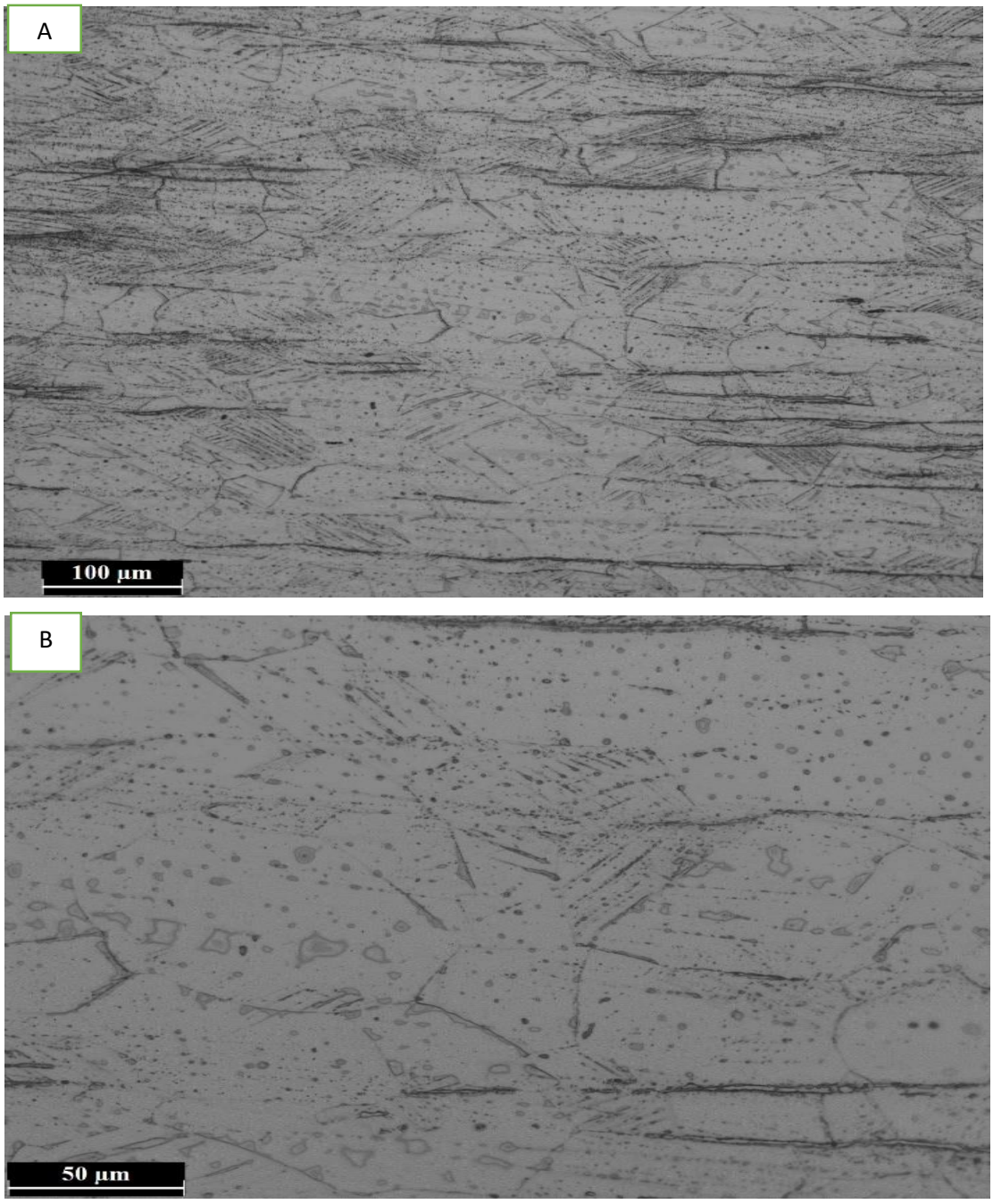

Fig 5.1: Microstructure of Base sample at Room temperature (A) 20X, (B) 50X

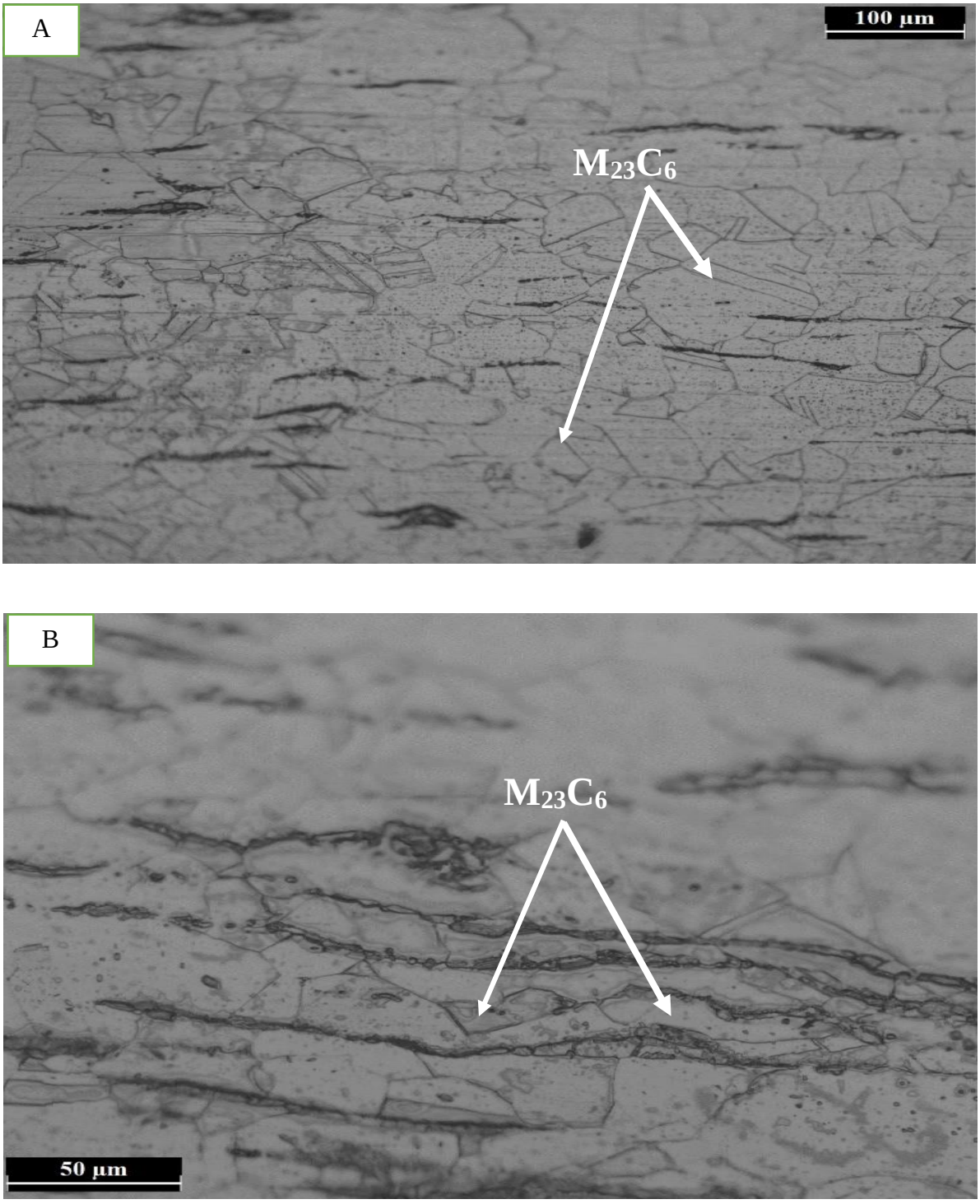

Figure 5.2: Microstructure of Base sample at High temperature (A) 20X, (B) 50X

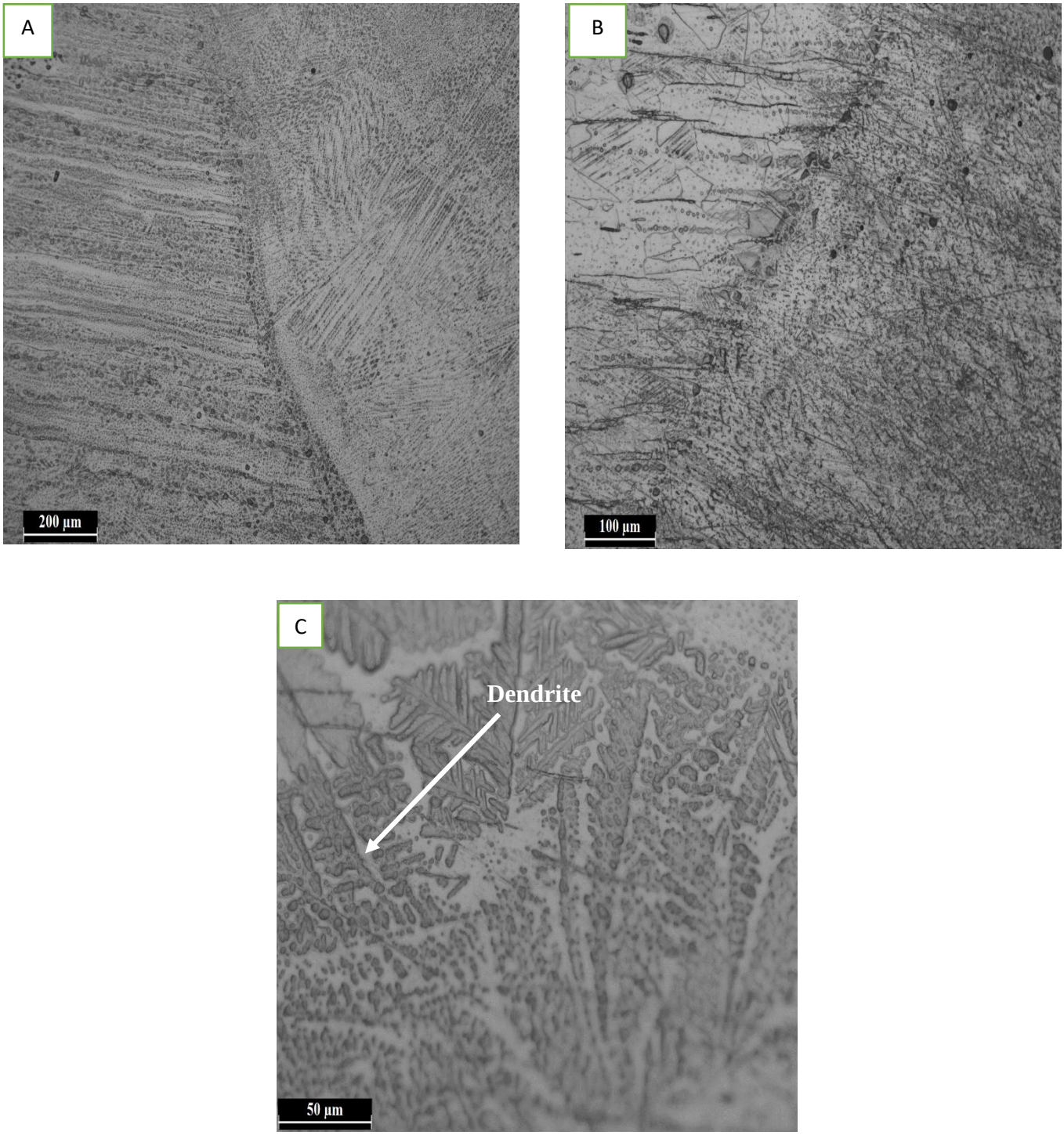

Fig 5.3: Microstructure of sample on HAZ zone at Room temperature (a) 10X, (b) 20X, (c) 50X

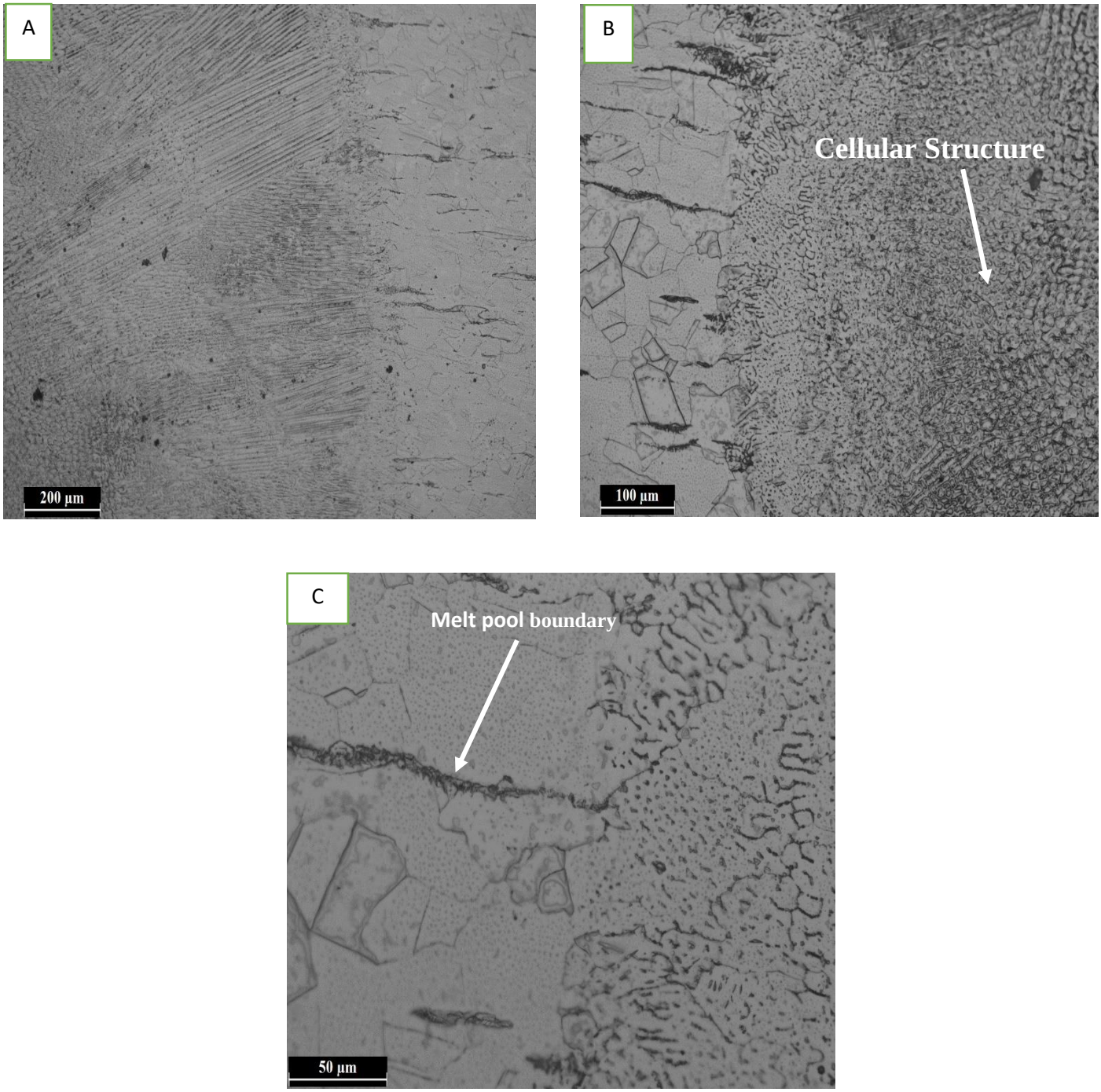

Fig- 5.4: Microstructure of sample on HAZ zone at High temperature (a) 10X, (b) 20X, (c) 50X

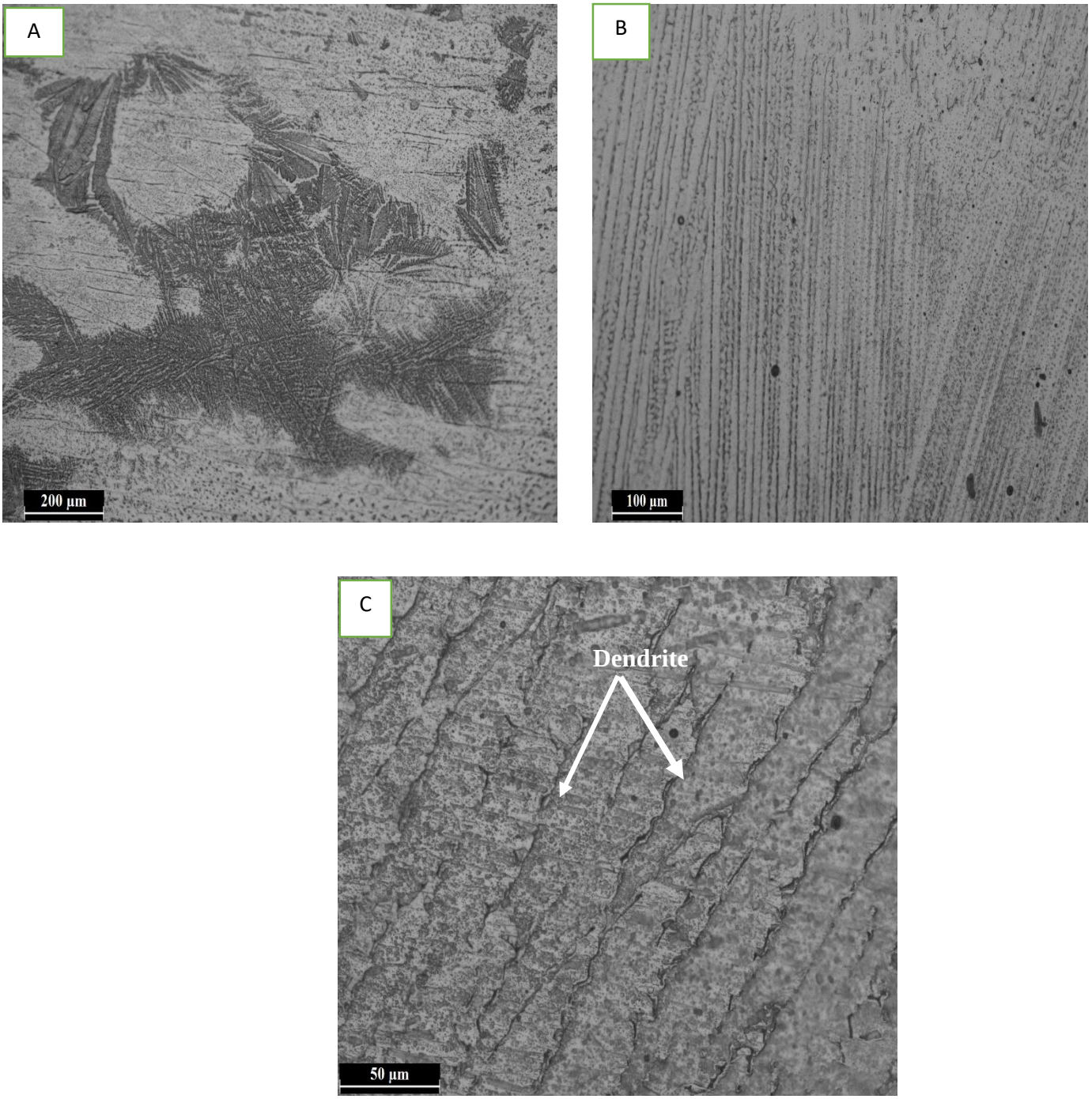

Fig- 5.5 Microstructure of sample on Weld zone at Room temperature (a) 10X, (b) 20X, (c) 50X

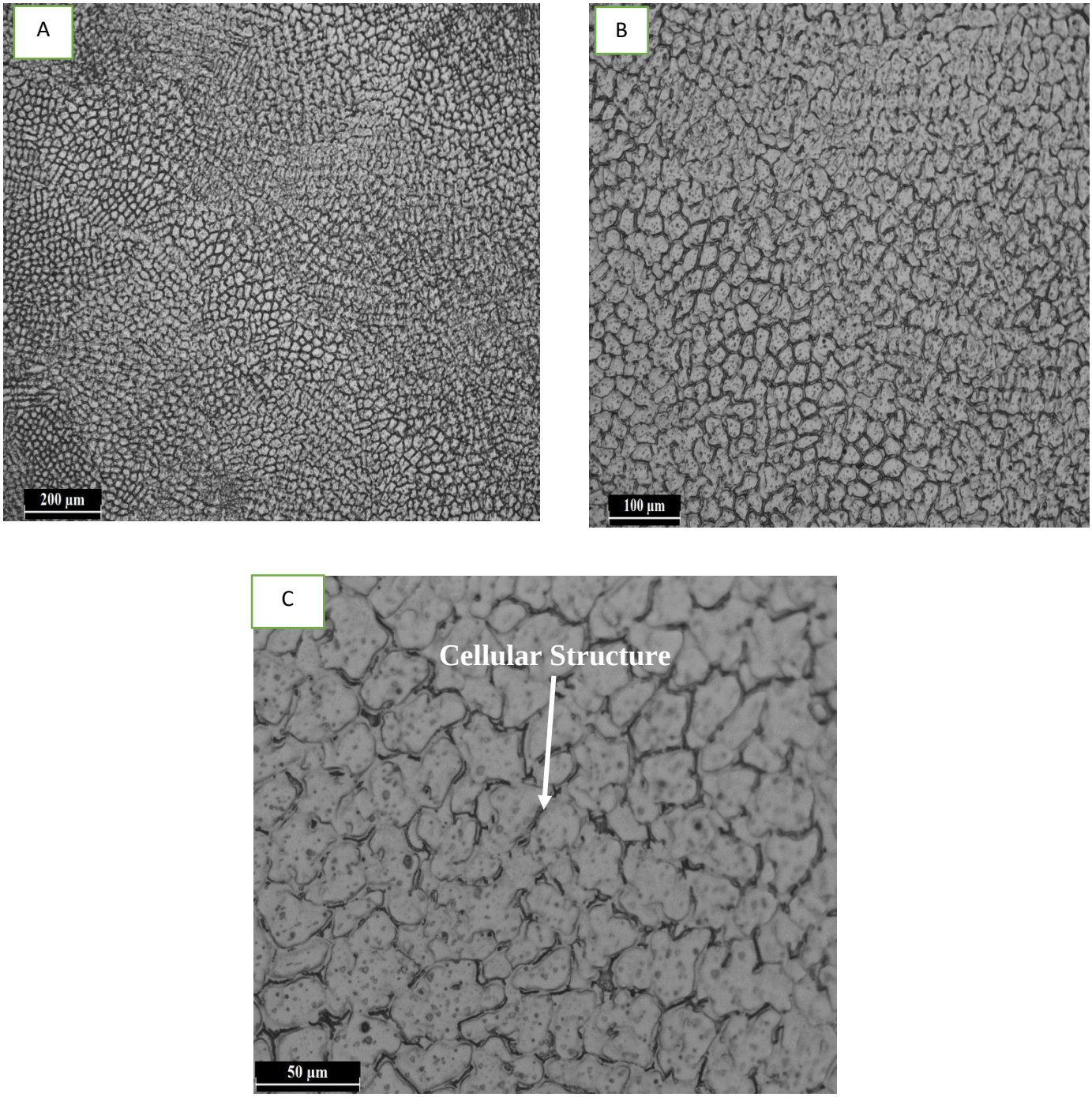

Fig – 5.6 - Microstructure of sample on Weld zone at High temperature (a)10X, (b)20X, (c)50X

The specimens of 316L Austenitic stainless steel, Room temperature and High Temperature were subjected to analysis of base zone, HAZ zone and weld zone microstructure in optical microscope. Proper polishing and etching were carried out before microscopic examination. A metallurgical optical microscope with accessories was used for capturing the images using lens with magnification of 10X, 20X, and 50 X for analysis of microstructure.

5.4 Micro Hardness Data in HV Scale, Load: 200gf, Dwell Time 10 Sec:

Table – 5.3- hardness test result before test tensile weld specimen

Sample reading				
SL	**Point**	**D1**	**D2**	**HV**
i)	X-6.019 Y-20.494	37.4	37.4	264.9
ii)	X-7.00 Y-18.006	41.5	40.7	219.2
iii)	X-7.00 Y-19.122	38.4	38.2	252.5
iv)	X-7.00 Y-15.019	39.3	38.6	244.4
v)	X- 7.00 Y-14.004	37.9	38.5	254.3
vi)	X-7.00 Y-12.548	38.7	40.9	234.1
vii)	X-7.00 Y-12.289	39.3	38.8	243.5
viii)	X-7.00 Y-11.260	36.2	36.8	278.3
ix)	X-7.00 Y-10.743	37	36.1	275.1
x)	X-7.00 Y-4.676	35.2	37.5	280.5
xi)	X-7.00 Y- 6.333	39.1	38.2	247
xii)	X-7.00 Y-7.305	38.4	38.2	252
	Average	38.2	38.325	**262.15**

Table – 5.4- hardness test result after tensile test weld specimen in room temperature

Sample reading -1				
SL	Point	D1	D2	HV
i)	X-1.029 Y-10.061	36.5	36.5	278.3
ii)	X-1.029 Y-9.923	35.8	35.7	290.4
iii)	X-1.029 Y-9.208	35.8	35.8	289.3
iv)	X-1.029 Y-7.208	35.8	36.1	288.2
v)	X- 1.029 Y-5.227	37.2	36.8	271.0
vi)	X-1.029 Y- -0.734	36.9	36.7	274.1
vii)	X-1.029 Y- -5.217	36.3	34.7	293.9
viii)	X-1.029 Y- -6.907	36.9	38.6	260.0
ix)	X-1.029 Y- -13.769	36.7	36.5	276.2
	Average	36.43	36.15	**280.15**

Table – 5.5- hardness test result after tensile test weld specimen in high temperature

Sample reading -2					
SL	Point	D1	D2	HV	
i)	X-0.397 Y-13.769	41.1	39.9	226.1	
ii)	X-0.464 Y- - 13.475	39.3	38.6	244.4	
iii)	X-0.464 Y- -10.224	39.0	38.6	246.1	
iv)	X-0.464 Y- - 9.856	38.6	37.1	259	
v)	X- 0.464 Y- - 9.413	40.7	40.3	226.1	
vi)	X- 0.464 Y- -8.886	39.3	40.2	235	
vii)	X-0.464 Y- -1.560	38.4	34.6	278.3	
viii)	X- 464 Y- -5.966	40	36.8	251	
	Average	**39.55**	**38.26**	**245.75**	

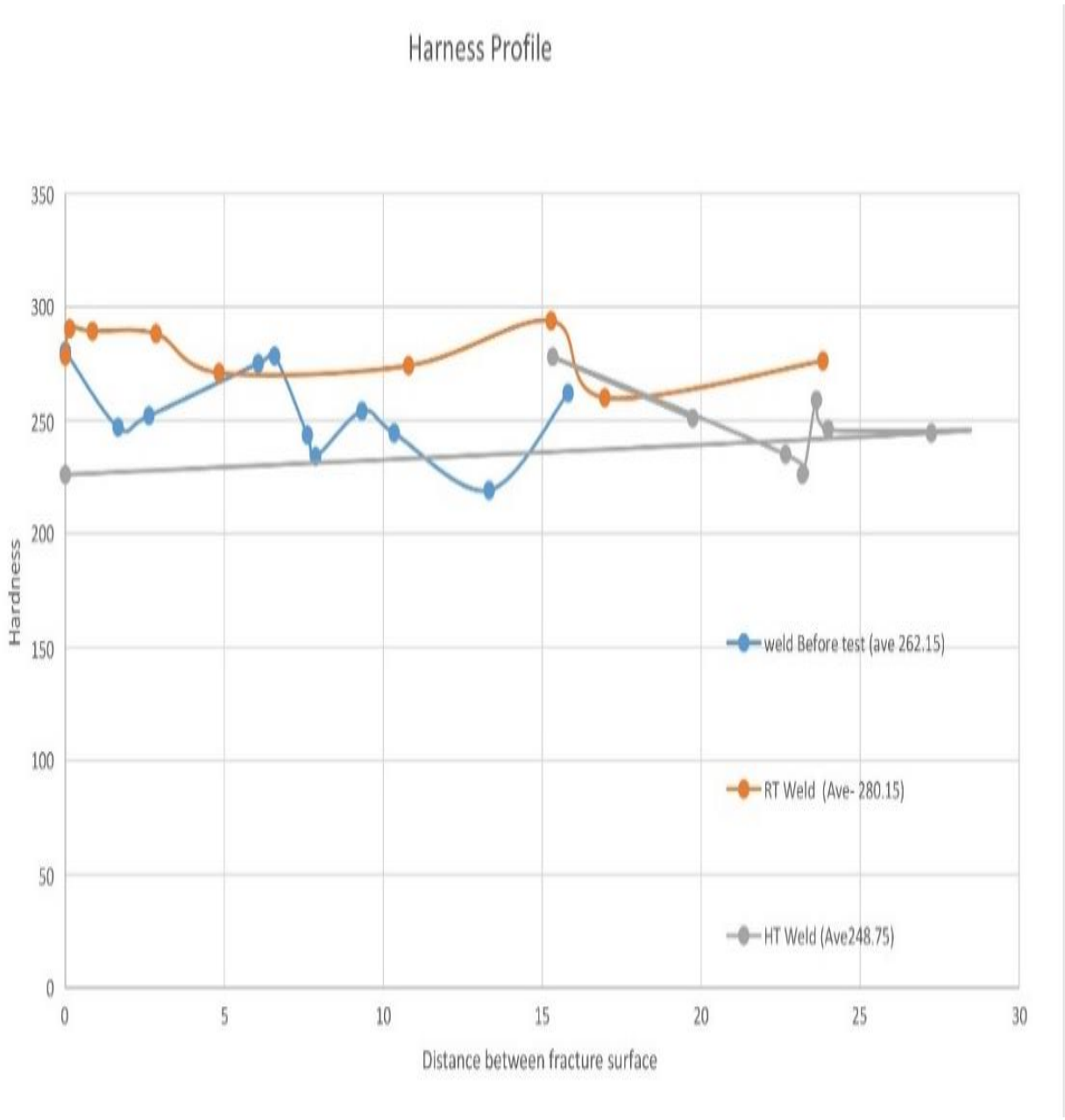

Fig-5.3 Hardness profile Weld before test sample , Room temperature weld and High temperature weld

We have test this three type of sample in microhardness testing method , we see this sample result before the tensile speciment has hardness is modarate then when we test in tensile test in room temperature then hardness is increases than before test speciment . After when we have tensile test in High temperature then Hardness is reduce than other type of speciment condition .we get the hardness is more in tensile test in room temperature ave. value is 280.15. then we get hardness is medium in normal condition without tensile test ,ave hardnes value is 262.15 . and last we get the hardness is much low in high temperature test ave hardness value is 245.75.

5.5 - SEM Image of the Sample: -

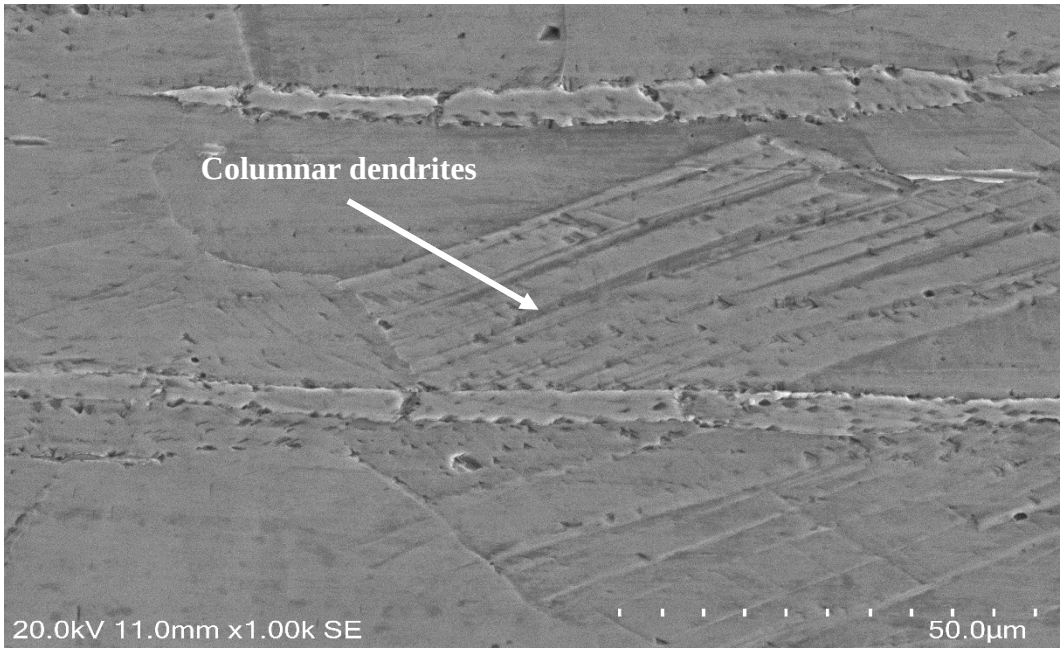

Fig-5.7- SEM image of Base Zone in Room Temperature Sample

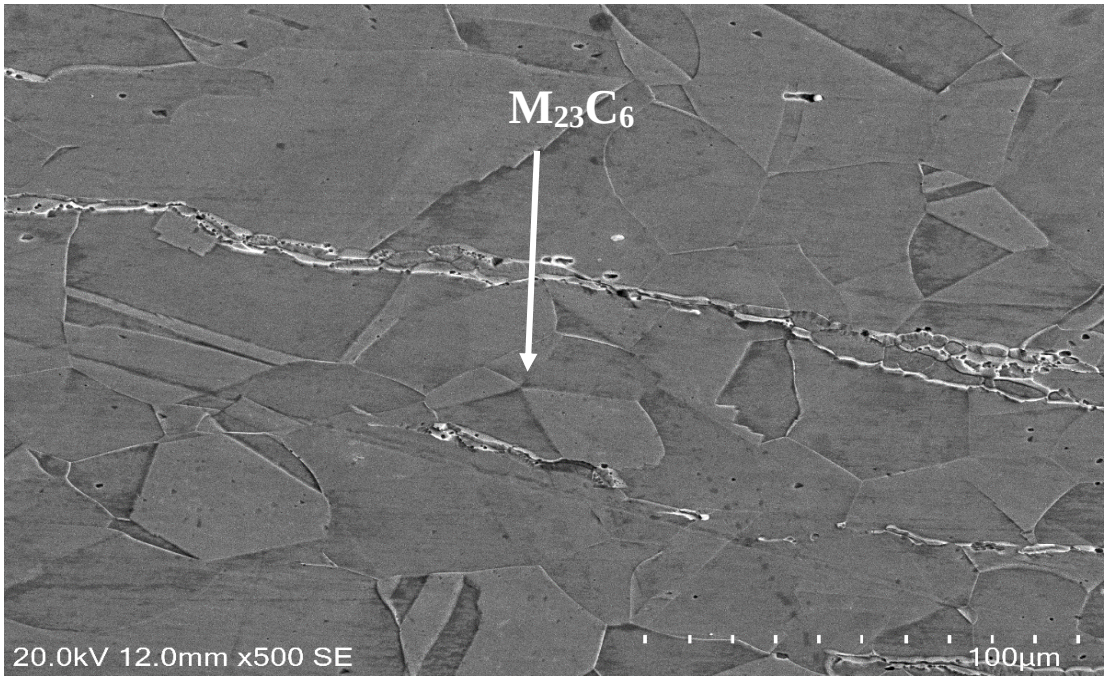

Fig-5.8- SEM image of Base Zone in High temperature Sample

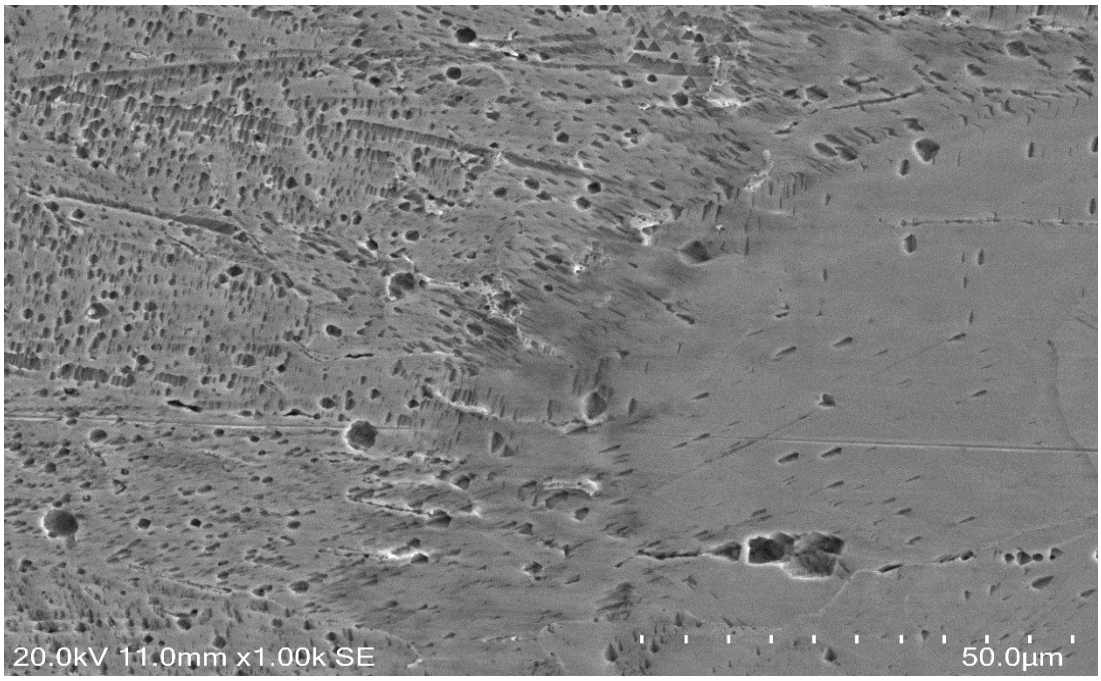

Fig-5.9- SEM image of HAZ Zone in Room Temperature Sample

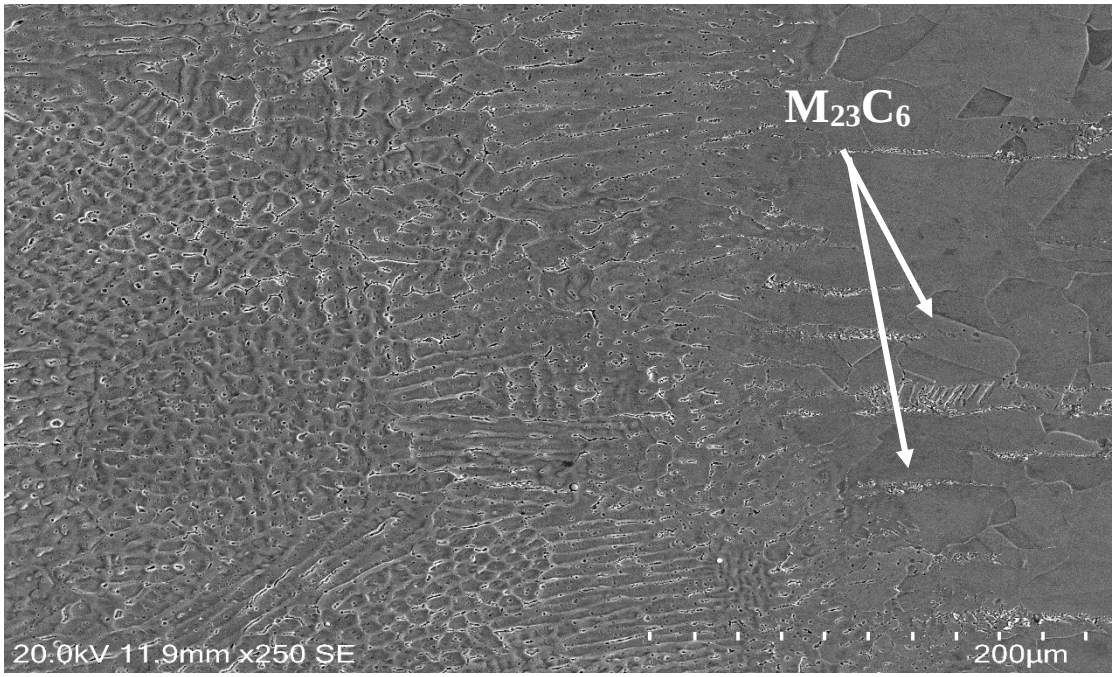

Fig-5.10- SEM image of HAZ Zone in High temperature Sample

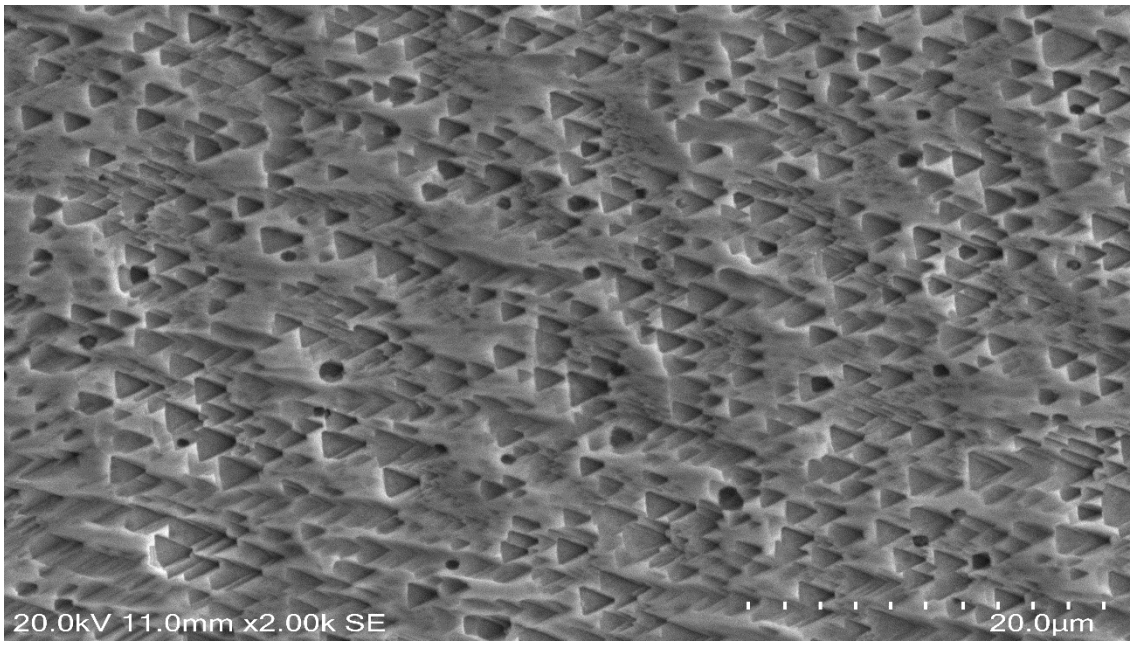

Fig-5.11- SEM image of Weld Zone in Room Temperature Sample

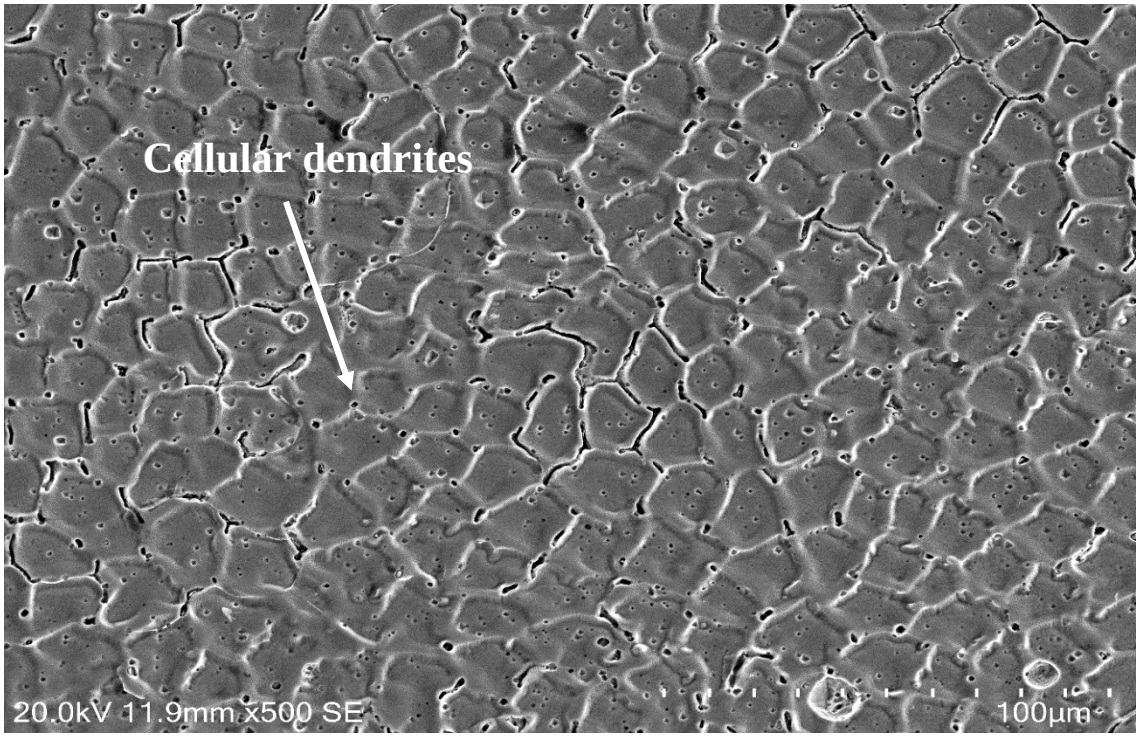

Fig-5.12- SEM image of Weld Zone in High temperature Sample

The samples were characterized by using Field Emission scanning Electron microscope (SEM), before that samples were prepared with suitable method. Micrographs images were captured with different magnifications. Base sample and weld samples images are shown above. As observed by various re-earchers, the cellular structure varied both in size and shape, with some grains showing very elongated cells. [55, 56]. However, most of the published literature focused on the cellular structure developed in as-printed material.

5.6 Energy Dispersive Spectroscopy (EDS) Result of The Room Temperature And High Temperature Sample: -

Sample Name: Room Temperature

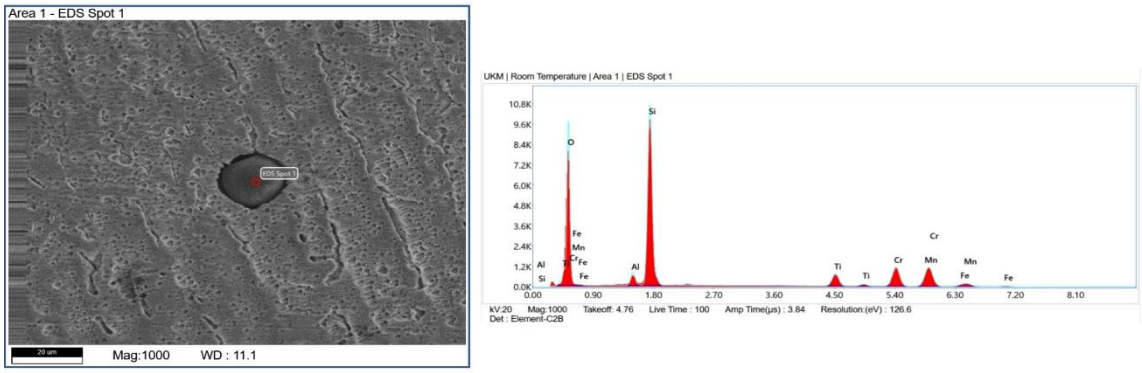

Element	Weight %	Atomic %	Error %	Net Int.	R	A	F
O K	57.88	74.24	10.67	506.21	0.9056	0.0708	1.0000
Al K	2.34	1.78	10.80	57.93	0.9265	0.2227	1.0139
Si K	24.80	18.12	8.17	837.21	0.9300	0.3183	1.0044
Ti K	2.58	1.11	5.13	86.11	0.9537	0.8413	1.0825
Cr K	5.67	2.24	3.83	148.11	0.9589	0.8916	1.0483
Mn K	6.02	2.25	3.80	138.46	0.9614	0.9129	1.0437
Fe K	0.70	0.26	11.68	14.46	0.9639	0.9078	1.0515

Fig – 5.12 .i

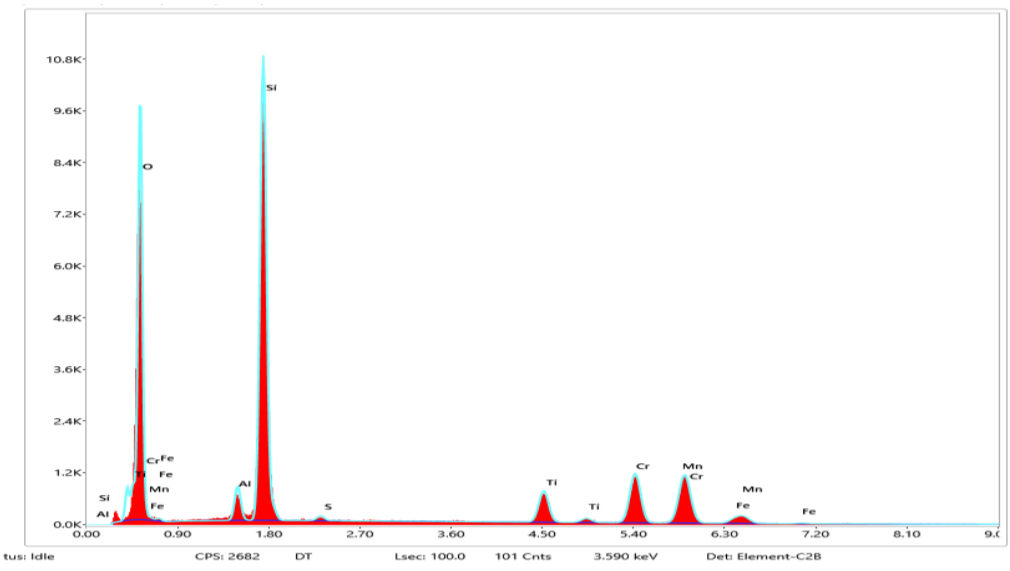

Fig – 5.12.ii- EDS spectrum of Base Sample in Room Temperature

Author: Apex User

Creation: 5/23/2024 4:03:24 PM

Sample Name: High Teperature

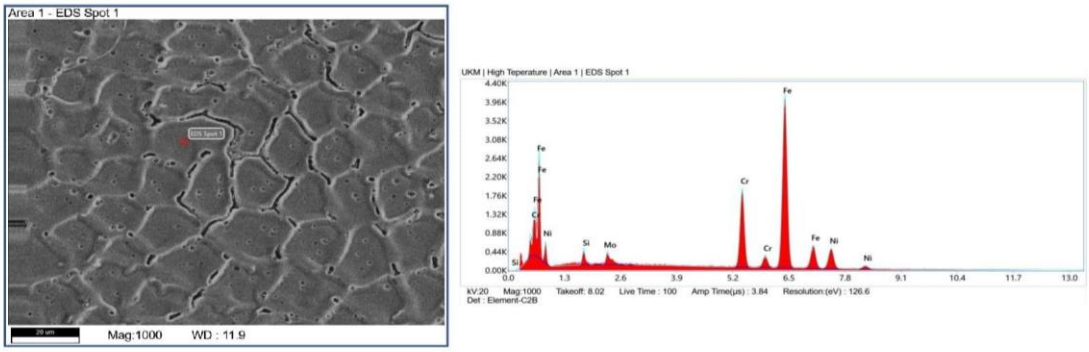

Element	Weight %	Atomic %	Error %	Net Int.	R	A	F
Si K	3.86	7.47	13.11	31.54	0.8402	0.1604	1.0083
Cr K	17.28	18.08	4.56	241.18	0.8904	0.8600	1.1983
Fe K	62.77	61.15	3.67	574.60	0.9006	0.8390	1.0419
Ni K	11.61	10.76	6.62	71.93	0.9115	0.7345	1.0378
Mo L	4.48	2.54	17.55	27.21	0.8524	0.3238	1.0079

Fig – 5.13.i

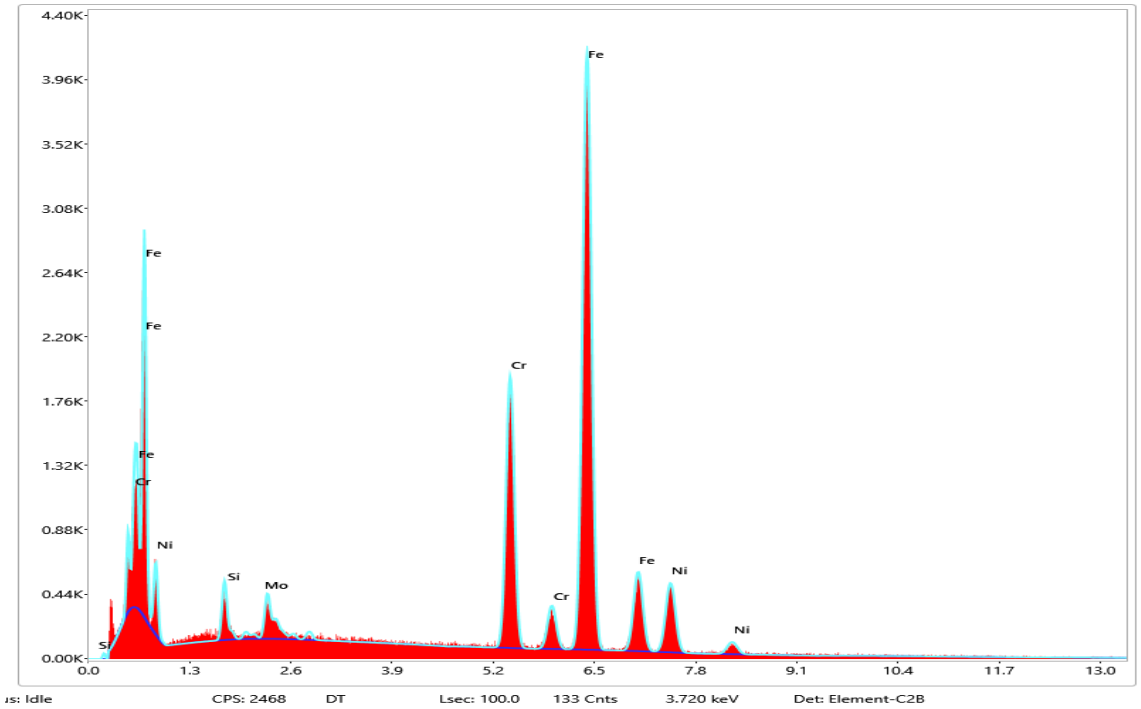

Fig – 5.13.ii - EDS spectrum of Base Sample in High temperature

Author: Apex User

Creation: 5/23/2024 3:16:59 PM

Sample Name: Room Temperature

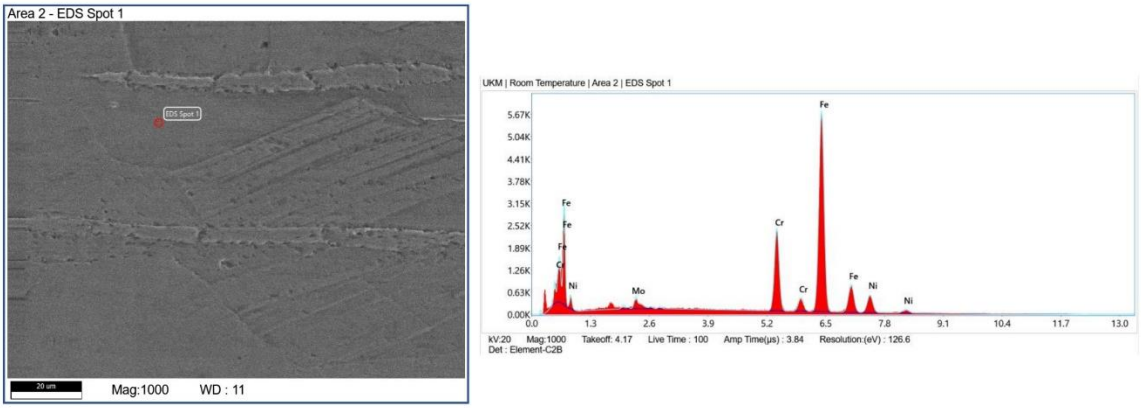

Element	Weight %	Atomic %	Error %	Net Int.	R	A	F
Cr K	16.98	18.39	4.50	304.84	0.8882	0.8653	1.2181
Fe K	69.49	70.07	3.51	800.92	0.8985	0.8432	1.0379
Ni K	9.64	9.25	6.83	73.77	0.9097	0.7214	1.0372
Mo L	3.90	2.29	13.52	30.59	0.8499	0.3329	1.0085

Fig – 5.14.i

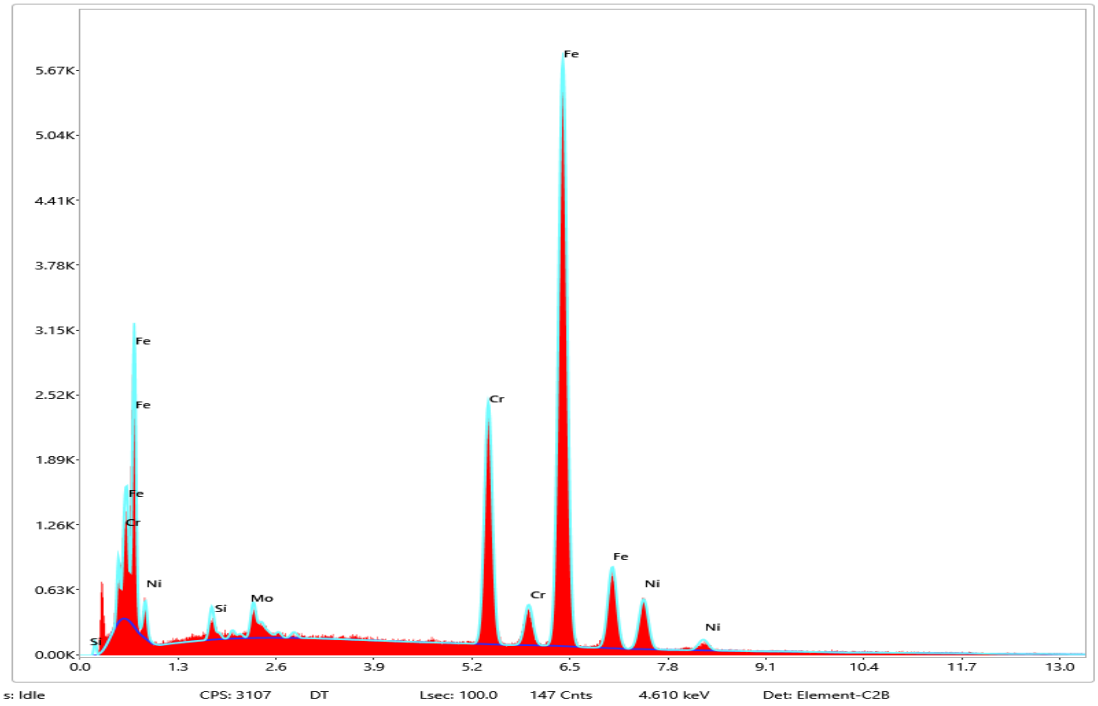

Fig – 5.14.ii- EDS spectrum of HAZ zone in Room temperature

Author: Apex User

Creation: 5/23/2024 4:15:41 PM

Sample Name: High Teperature

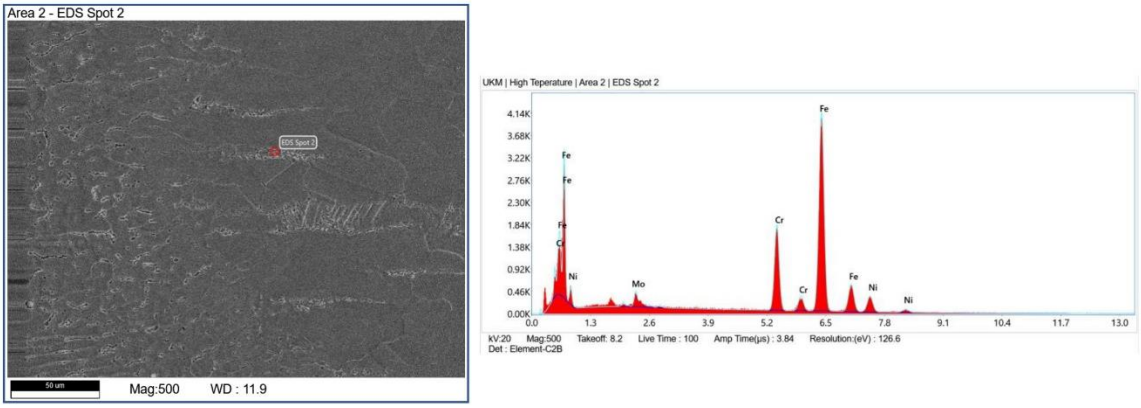

Element	Weight %	Atomic %	Error %	Net Int.	R	A	F
Cr K	17.66	19.19	4.62	230.30	0.8877	0.8624	1.2092
Fe K	68.76	69.57	3.63	578.37	0.8981	0.8387	1.0370
Ni K	8.67	8.35	7.51	48.71	0.9092	0.7207	1.0376
Mo L	4.91	2.89	17.60	28.46	0.8493	0.3350	1.0084

Fig – 5.15.i

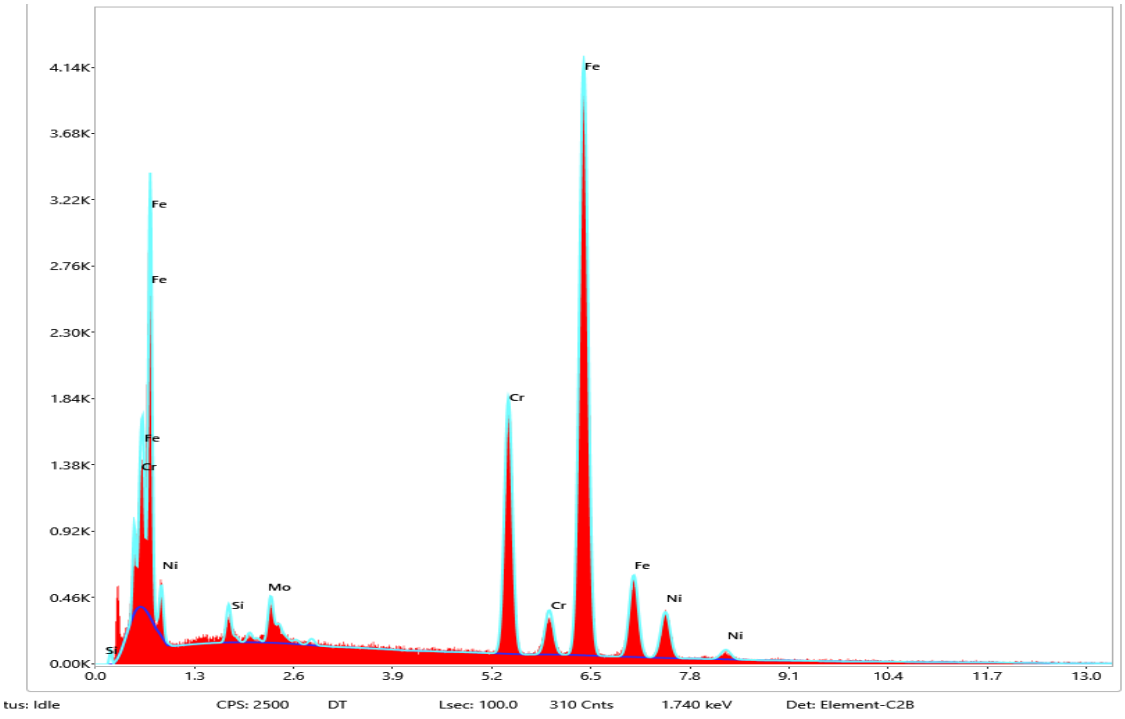

Fig – 5.15.ii - EDS spectrum of HAZ zone in High Temperature

Author: Apex User
Creation: 5/23/2024 3:27:48 PM
Sample Name: Room Temperature

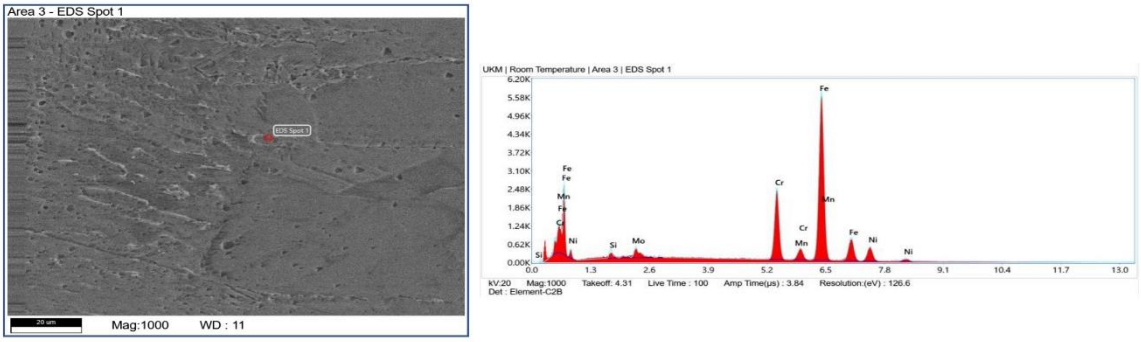

Element	Weight %	Atomic %	Error %	Net Int.	R	A	F
Si K	2.36	4.62	13.69	25.21	0.8396	0.1589	1.0085
Cr K	16.90	17.89	4.49	315.21	0.8898	0.8631	1.2094
Mn K	1.23	1.23	19.16	18.08	0.8949	0.8822	1.0817
Fe K	66.33	65.38	3.53	800.43	0.9001	0.8418	1.0377
Ni K	9.11	8.54	6.77	73.56	0.9111	0.7256	1.0376
Mo L	4.08	2.34	13.76	33.17	0.8518	0.3284	1.0083

Fig – 5.16.i

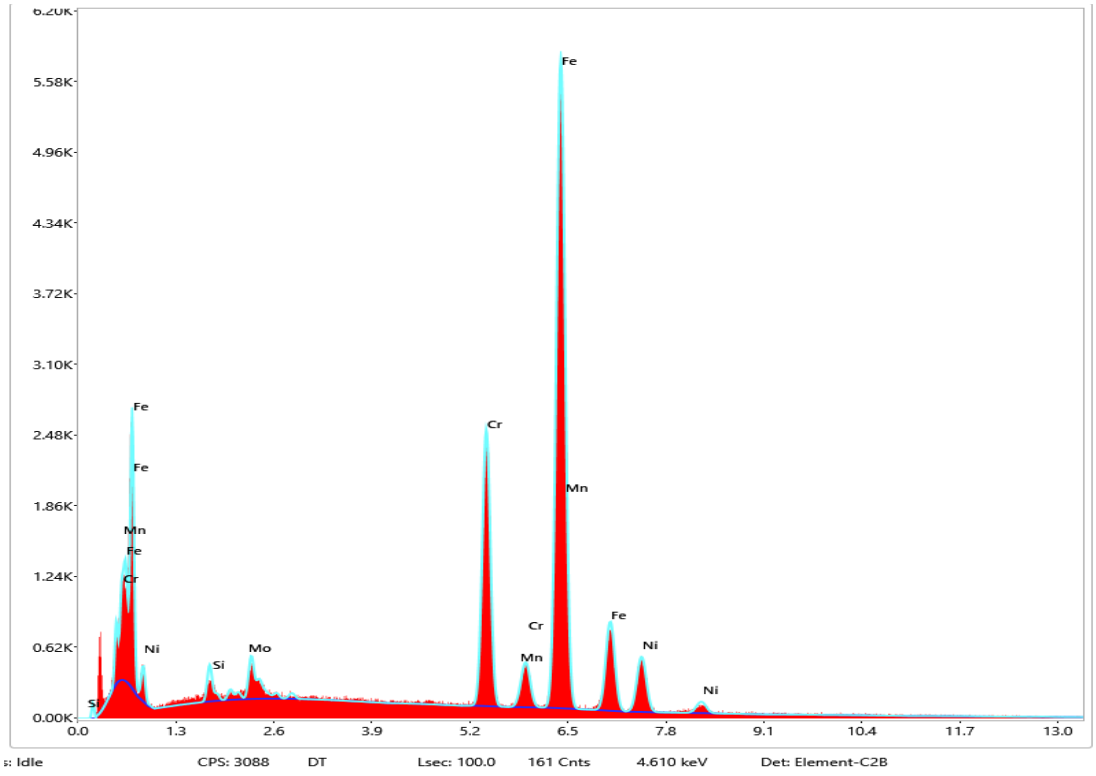

Fig – 5.16.ii - EDS spectrum of Weld zone in Room Temperature

Author: Apex User

Creation: 5/23/2024 4:22:24 PM

Sample Name: High Teperature

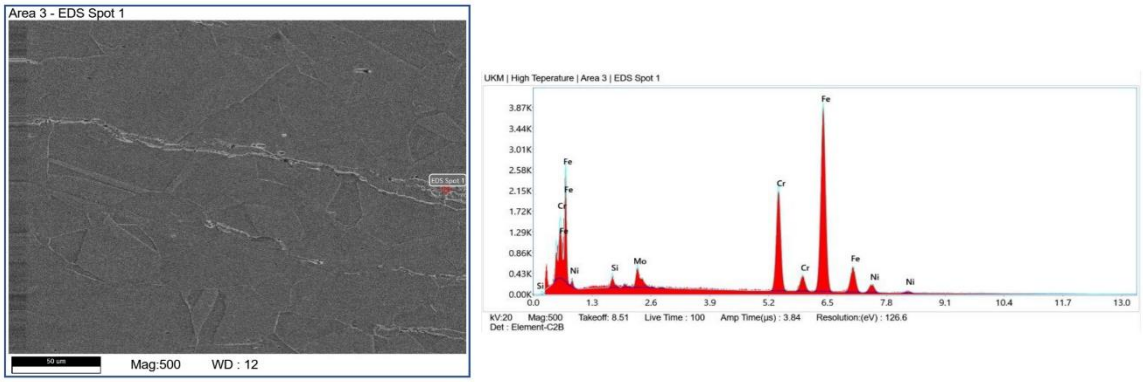

Element	Weight %	Atomic %	Error %	Net Int.	R	A	F
Si K	2.80	5.48	13.65	22.70	0.8391	0.1650	1.0088
Cr K	21.69	22.98	4.38	285.08	0.8894	0.8567	1.1744
Fe K	64.18	63.31	3.85	548.71	0.8997	0.8197	1.0329
Ni K	4.69	4.41	9.27	27.57	0.9107	0.7211	1.0392
Mo L	6.64	3.81	16.12	40.25	0.8513	0.3352	1.0081

Fig – 5.17.i

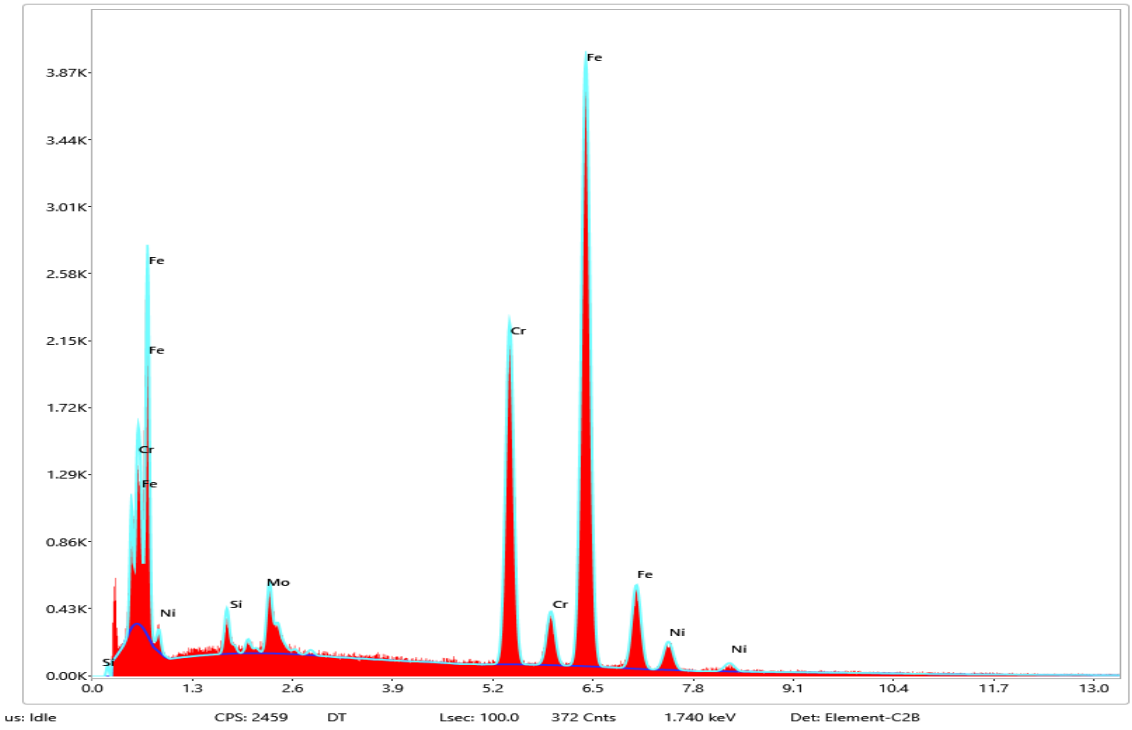

Fig – 5.17.ii - EDS spectrum of Weld zone in High Temperature

It sounds like the FESEM and EDS characterization of both your base sample and weld sample revealed similar compositions. The elements Fe, Cr, Mo, Si, and Ni were prominently detected in both samples, with smaller amounts of Al, S, and Ti. Since no changes were observed between the base sample and the weld sample, this suggests that the welding process did not significantly alter the elemental composition.

5.7 X-Ray Diffraction (XRD)

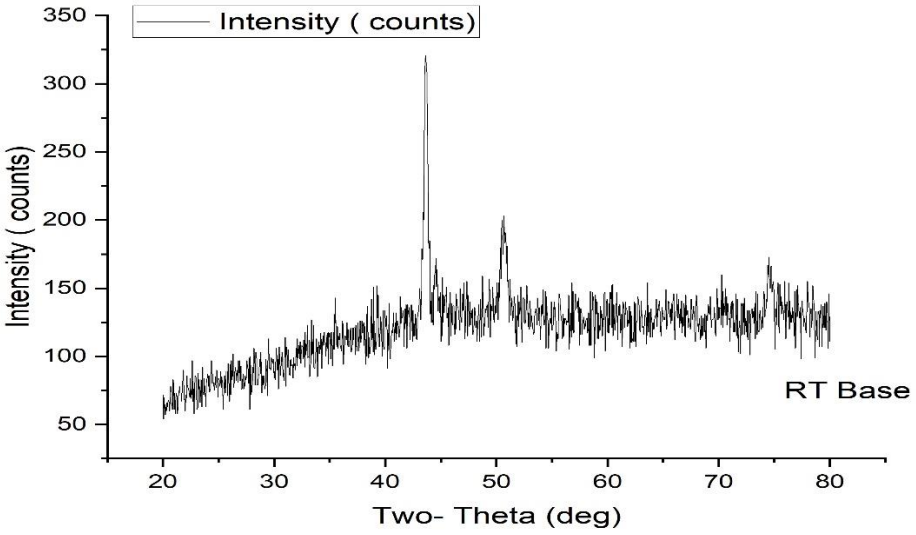

Fig- RT Base

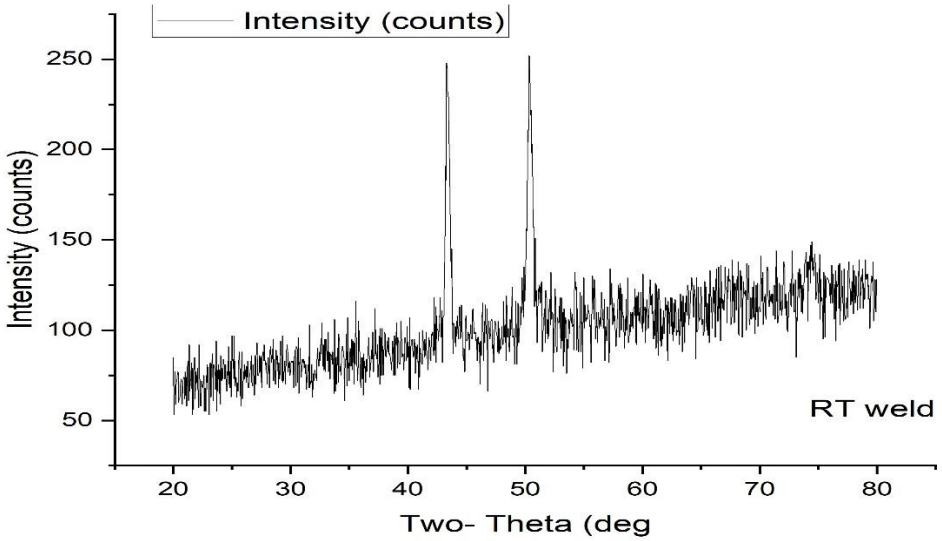

Fig- RT weld

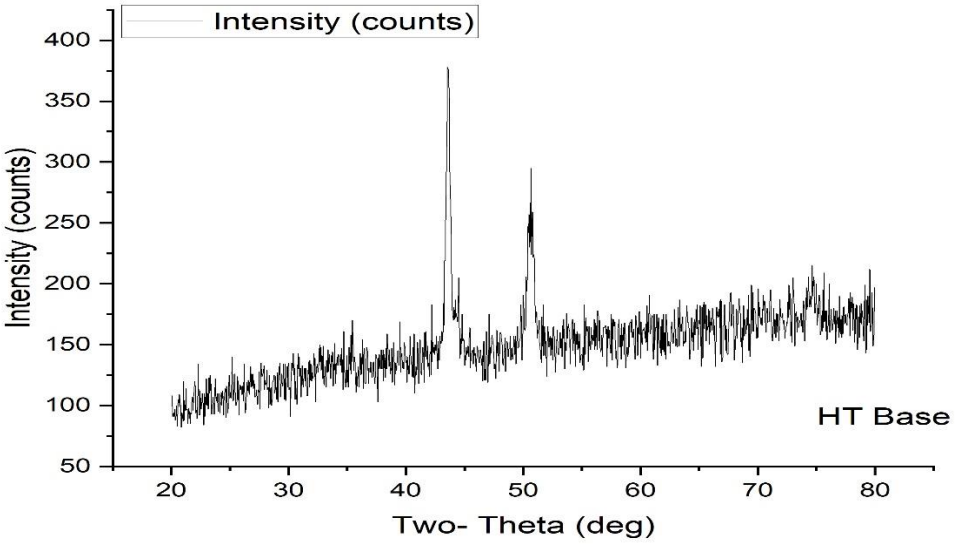

Fig- HT Base

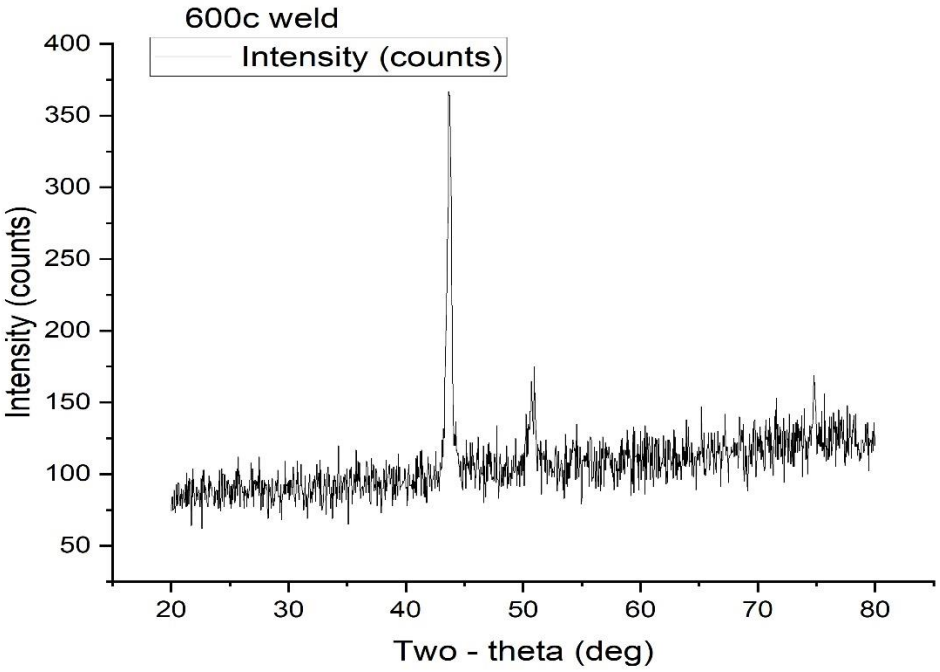

Fig – HT Weld

In XRD analysis we get some different pick in different sample, like we get intensity in room temperature base material 319, room temperature weld material has 248 and 252, High temperature base material has 376 and high temperature weld material has 364. we have concluded that high temperature non weld specimen has high intensity than other material, then high temperature weld material has intensity less than base material intensity. Room temperature weld material has low intensity than other sample.

5.8 Corrosion –

Pitting Corrosion Analysis-

In this section we shall discuss about the effect of pitting corrosion on the specimens after tensile deformation, which we have used as the part of the study-

Experimental Parameters:

Scan rate: 0.005 V/s.

Initial potential: -0.8 V.

Final potential: 1 V.

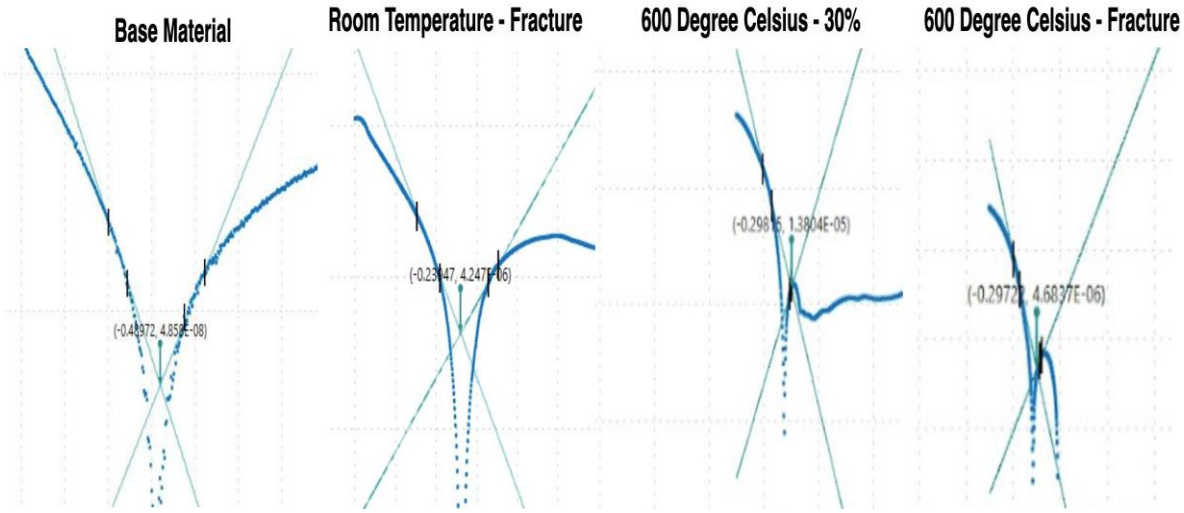

Figure 5.18 - Tafel's Plot of ASS 316L under four different deformation situations

Table 5.3: Value of ECorr, ICorr and the corrosion rate of ASS 316L under four different conditions which is extracted from the Tafel's Plot in Figure 5.18

Sample Type	**Base**	**Room Temp/Frac**	**600^0 C/30%**	**600^0C / Frac**
I Corr (A/cm^2)	1.73E-07	2.65E-05	8.62E – 05	2.92E-05
E Corr (Volts)	-0.489	-0.23321	-0.32365	-0.31228
Corrosion rate (mm/year	0.0020161	0.30844	1.0025	0.34015

In Table 5.3, it is observed that the corrosion rate is the lowest for the base material, primarily due to the presence of a passive film layer on the surface of the austenitic stainless steel (ASS) 316L. This passive film, composed mainly of chromium oxide, acts as a protective barrier, significantly reducing the material's susceptibility to corrosive attacks. The integrity and

stability of this passive layer are crucial in maintaining the low corrosion rate of the base material under no stressed conditions.

Mechanical deformation significantly increases the corrosion rate at room temperature. This is due to micro cracks and defects in the passive film caused by tensile stress, which expose the metal to corrosive agents. The strain also heightens the material's susceptibility to localized corrosion, such as pitting and crevice corrosion.

When tensile tests are performed at 600°C with 30% strain, corrosion rates peak. The high temperature accelerates the breakdown of the passive film, creating more corrosion nucleation sites and enhancing the diffusion of corrosive species into the metal. This environment, combined with stress, promotes stress corrosion cracking (SCC), a dangerous form of localized corrosion that leads to crack propagation and potential material failure.

The application of tensile load significantly increases the corrosion rate by disrupting the passive layer and promoting stress corrosion cracking (SCC). At high temperatures, stress accelerates pitting corrosion by creating additional nucleation sites. Pitting, which forms deep, localized pits, can cause severe material loss and compromise structural integrity without obvious surface damage.

CHAPTER – 6

CONCLUSIONS

6.1 CONCLUSION

In this work, microstructure and corrosion behaviour of weld 316 L austenitic stainless steel was studied in details. Austenitic stainless steel 316L weld metal and base material sample tensile test room temperature and high temperature. After characterization of sample by various test such tensile test, optical microscope, micro hardness, SEM, XRD, and pitting corrosion test following conclusion are below...

Material's tensile properties varies with temperature and with welding condition. We observed that weld material sample's ductility is lesser than the un-weld (base) material. High temperature weld material has lesser hardness and ductility than base material. DSA (dynamic strain aging) of **type A** was observed during the elevated temperature tensile test, 600°C.

The microstructures of 316L ASS Room temperature and high temperature samples changes with increase in temperature during tensile test process. The cellular structure varied both in size and shape, with some grains showing very elongated cells.

The micro hardness value observed highest 280.15 HV room temperature and was identified as peak room temperature condition, High temperature condition also identified, high temperature condition hardness is low, however optimization of two parameters temperature and time is important to obtain reasonable strength.

In present work, it is observed that the corrosion behaviour is significantly influenced by the type of corrosive medium. Based on the result obtained by Tafel polarization test, for performing this pitting corrosion test the corrosive environment needs to be prepared. For our study, we have prepared a medium containing 3.5 % NaCl in 100 ml of H2O. 316L Austenitic stainless steel in weld is best preferable while using in corrosive environment in salt and acid medium due to susceptibility to pitting corrosion or localized corrosion attack.

References—

[1]. Handbook of Stainless Steels (Outokumpu)
[2]. SOLOMON H. D., LEVINSON L. M. "Mossbauer effect study of 475º embrittlement of duplex and ferritic stainless steels", Act Metallurgical, vol. 26, no. 3, p.429-442, 1978.
[3]. Welding Metallurgy and Weldability of Stainless Steels (John C. Lippold, Damien J. Kotecki
[4]. A. Pardo *, M.C. Merino, A.E. Coy, F. Viejo, M. Carboneras, R. Arrabal: Influence of Ti, C and N concentration on the intergranular corrosion behaviour of AISI 316 Ti and 321 stainless
[5] Wasnik DN, Kain V, Samajdar I, Verlinden B, De PK. Acta Mater 2002;50:4587
[6]. Min KS, Nam SW. J Nucl Mater 2003;322:91.
[7]. Hall EL, Briant CL. Metall Trans A 1984;15:793
[8]. Hall EO, Algie SH. The sigma phase. Metallurgical reviews. 1966; 11:61-88.
[9]. Zucato, I., Moreira, M. C., Machado, I. F., Lebrão, S. M. G., (2002). Microstrucutural Characterization and the effect of phase transformations on toughness of the UNS S31803 duplex stainless steel aged treated at 850oC. Materials Research, 5, 385-389

[10]. E. C. Bain and W. E. Griffiths, Trans. Amer. Inst. Alin. Met. Eng., 1927, 75, 166
[11]. Comparative study on sigma phase precipitation of three types of stainless steels: austenitic, superferritic and duplex D. M. E. Villanueva, F. C. P. Junior, R. L. Plaut and A. F. Padilha*

[12]. Steels: Microstructure and Properties (Harry Bhadeshia, Robert Honeycombe)
[13]. Copson, H.R. 1959. Physical Metallurgy of Stress-Corrosion Fracture, Interscience, New York, p. 126

[14]. Floreen, S., and Hayden, H.W. 1968.*Transactions of the American Society for metals*, 61:489-499

[15]. R. J. BRIGHAM, E. W. TOZER; Effect of Alloying Additions on the Pitting Resistance of 18% Cr Austenitic Stainless Steel. CORROSION 1 May 1974; 30 (5): 161–166.

[16]. Effects of alloying elements on σ phase precipitation in δ-γ duplex phase stainless steels Y. Maehara, Y. Ohmori, J. Murayama, N. Fujino, and T. Kunitake

[17]. J.W. Simmons, Overview: high-nitrogen alloying of stainless steels
[18]. Microstructural evolution and mechanical properties of 316 austenitic stainless steel by CGP Rahul Singh a , Shubham Agrahari a , Surya Deo Yadav b , Abhishek Kumar a,

[19]. Schaeffler, A.L. 1949.Constitution diagram for stainless steel weld metal Metal Progress, 56(11): 680-680B

[19]. PROGRESS IN fERROUS-ALLOY DESIGN v. F. Zackay and E. R. Parke.
[20]. Development of high performance cast stainless steels for ITER shield module applications Author links open overlay panel .T. Busby ,P.J. Maziasz ,A.F. Rowcliffe ,M. Santella,M. Sokolov

[21]. DETERMINATION OF TUNGSTEN INERT GAS WELDING INPUT PARAMETERS TO ATTAIN MAXIMUM TENSILE STRENGTH OF 316L AUSTENITIC STAINLESS STEEL MOI Subhas Chandra1 , PAL Pradip Kumar2 , BANDYOPADHYAY Asish3 , RUDRAPATI Ramesh.

[22]. PROGRESS IN fERROUS-ALLOY DESIGN v. F. Zackay and E. R. Parke.
[23]. Comparative study on the fatigue crack growth behavior of 316L and 316LN stainless steels: effect of microstructure of cyclic plastic strain zone at crack tip Wan-Young Maeng *, Mun-Hwan Kim]
[24]. Development of high performance cast stainless steels for ITER shield module applications--J.T. Busby ⇑, P.J. Maziasz, A.F. Rowcliffe, M. Santella, M. Sokolo
[25]. Influence of nitrogen-induced grain refinement on mechanical properties of nitrogen alloyed type 316LN stainless steel---Dae Whan Kim].
[26]. Takemoto T., Mukai K., Hoshino K., Trans. ISIJ 26 (1986) 337-344].
[27]. TWINNING AND FRACTURE OF SINGLE CRYSTALS OF 3% SILICON IRON* D .Hull 1960).
[28]. THE BEHAVIOUR OF ADVANCED QUENCHED AND TEMPERED STEELS DURING ARC WELDING AND THERMAL CUTTING R S parmer.
[29]. STRESS-CORROSION CRACKING K. SIBRADZKI Department of Applied Science, Brookhaven National Laboratory, Upton, NY 11973, U.S.A. and R. C. NEWMAN Corrosion and Protection Centre, UMIST, P.O. Box 88, Manchester M60 IQD, England
[30]. G. E. Dieter and D. J. Bacon, Mechanical metallurgy vol. 3: McGraw-hill New York, 1986
[31]. D. Sastry, Y. Prasad, and S. Deevi, "Influence of temperature and strain rate on the flow stress of an FeAl alloy," *Materials Science and Engineering: A*, vol. 299, pp. 157-163, 2001.
[32]. A. Kundu and P. C. Chakraborti, "Effect of strain rate on quasistatic tensile flow behaviour of solution annealed 304 austenitic stainless steel at room temperature," Journal of materials science, vol. 45, pp. 5482-5489, 2010
[33]. A. Cottrell, "AH Cottrell, Philos. Mag. 44, 829 (1953)," Philos. Mag., vol. 44, p. 829, 1953
[34]. J. Jadav, K. R. V. Rajulapati, N. Eswaraprasad, and K. B. S. Rao, "Effect of Temperature on Tensile flow behaviour of Nimonic C-263 alloy," Materials Today: Proceedings, vol. 5, pp. 5475-5480, 2018
[35]. De, A.K., Speer, J.G., Matlock, D.K. *et al.* Deformation-induced phase transformation and strain hardening in type 304 austenitic stainless steel. *Metall Mater Trans A* **37**, 1875–1886 (2006)
[36]. C.J. Guntner and R.P. Reed: Trans. ASM, 1962, vol. 55, pp. 399-419
[37]. Muhamed, G.A.; Gündüz, S.; Erden, M.A.; Taştemur, D. Dynamic Strain Aging Behaviour in AISI 316L Austenitic Stainless Steel under As-Received and As-Welded Conditions. *Metals* **2017**, *7*, 362.
[38]. A.H. Cottrell, Theory of dislocations ,Progress in Metal Physics, Volume 4,1953
[39]. J. H. Hollomon, "Tensile deformation," *Aime Trans*, vol. 12, pp. 1-22, 1945
[40]. J. R. Low and F Garofalo: *Proc. Soc. Stress Anal.*, 1947, vol. 4 p. 16
[41]. K. K. Chawla and M. Meyers, Mechanical behavior of materials: Prentice Hall, 1999.
[42]. X. Xie, D. Ning, and J. Sun, "Strain-controlled fatigue behavior of cold-drawn type 316 austenitic stainless steel at room temperature," Materials Characterization, vol. 120, pp. 195-202, 2016
[43]. P. Ludwik, "Elemente der Technologischen Mechanik, Julius Springer, Berlin," CrossRef Google Scholar, p. 32, 1909

[44]. U. Kocks and H. Mecking, "Physics and phenomenology of strain hardening: the FCC case," Progress in materials science, vol. 48, pp. 171-273, 2003.

[45]. Kocks, U. F. and Heinrich Mecking. “Physics and phenomenology of strain hardening: the FCC case.” Progress in Materials Science 48 (2003): 171-273.
[46]. Rollett AD, Kocks UF, Doherthy RD. In: Sachdev AK, Embury JD, editors. Formability and metallurgical structure. The Metall. Society; 1987. p. 211
[47]. Gurson, A.L., 1977. Continuum theory of ductile rupture by void nucleation and growth: Part I – Yield criteria and flow rules for porous ductile media. ASME Journal of Engineering Materials and Technology 99, 1–15.
[48]. "Anderson, T.L., 1995. Fracture Mechanics: Fundamentals and Applications, third ed. CRC Press, Boca Raton, New York. 265
[49]. Tensile Fracture Behavior of 316L Austenitic Stainless Steel Manufactured by Hot Isostatic Pressing A.J. COOPER, W.J. BRAYSHAW, and A.H. SHERRY
[50]. Kotecki D.J. 1989. Heat treatment of duplex stainless steel weld metals, Welding Journal 68(11): 431s-441s
[51]. May L. Martin, Petros Sofronis, Hydrogen-induced cracking and blistering in steels: A review, Journal of Natural Gas Science and Engineering, Volume 101,2022
[52]. Y.C. Lu, M.B. Ives, C.R. Clayton, Synergism of alloying elements and pitting corrosion resistance of stainless steels, Corrosion Science, Volume 35, Issues 1–4,1993
[53]. N.D. Tomoshav, G.P. Chernova and O.N. Markova, Zashchita Metallov, 7(1971), p. 104
[54]. Iris Alvarez-Armas,Suzanne Degallaix-Moreuil, Duplex Stainless Steels
[55] Microstructure and high temperature tensile properties of 316L fabricated by laser powder-bed fusion , Sebastien Dryepondt , Peeyush Nandwana , Patxi Fernandez-Zelaia , Fred List III
[56] Microstructures and Creep Properties of Type 316LN Stainless Steel Weld Joints, A.R. PAVAN, T. SAKTHIVEL, B. ARIVAZHAGAN, M. VASUDEVAN, and B.R. VAISHNAVI KRUPA